Reduced-Order Modeling for Ensemble Real-time Estimation and Control

by

Binghuai Lin

B.S. Hydraulic Engineering, Tsinghua University, 2005

M.S. Hydrology, Tsinghua University, 2007

Submitted to the Department of Civil and Environmental Engineering

in partial fulfillment of the requirements for the degree of

Doctor of Philosophy

at the

MASSACHUSETTS INSTITUTE OF TECHNOLOGY

June 2012

Author .....

Department of Civil and Environmental Engineering

May 4, 2012

Certified by .....

Dennis McLaughlin

H.M. King Bhumibol Professor of Civil and Environmental Engineering

Thesis Supervisor

Accepted by .....

Heidi M. Nepf

Chair, Departmental Committee for Graduate Students

Reduced-Order Modeling for Ensemble Real-time Estimation and Control

by

Binghuai Lin

Submitted to the Department of Civil and Environmental Engineering
on May 4, 2012, in partial fulfillment of the
requirements for the Degree of Doctor of Philosophy in
the field of Civil and Environmental Engineering

Abstract

Efficient exploitation of subsurface resources requires better understanding of subsurface physical properties as well as optimization of control strategies. Advances in technology have created the possibility of providing real time measurements of subsurface conditions. These measurements can be used to reduce uncertainty in the description of subsurface conditions, and combining uncertainty quantification and control optimization leads to improved management of subsurface resources through the closed-loop control framework.

The ensemble closed-loop control utilizes an ensemble representation to describe complex probabilistic distributions of uncertain model parameters. To reduce the computational burden and make it feasible to apply the ensemble closed-loop control to large-scale problems, this thesis proposes a robust reduced-order model for subsurface solute transport that is sufficiently accurate in the ensemble closed-loop process. The reduced-order model is based on a second-order expansion of the governing equations discretized by the mixed finite element method and the upwind finite difference method. As a result, the reduced-order model can incorporate state and parameter changes explicitly and thus it is possible to perform dimension reduction in both state and parameter spaces. The high-dimensional state space is reduced by the proper orthogonal decomposition, which can capture key features of states for complex systems, while the high-dimensional parameter space is reduced by the discrete cosine transform, which allows for efficient and robust parameterization of physical properties.

The efficiency and robustness of the reduced-order model are demonstrated by an uncertainty quantification example using the ensemble Kalman filter. It is shown that model predictions by the reduced-order are sufficiently accurate for updating uncertain model states and parameters. The channelized geological features presented in the example are well preserved and captured by the reduced representations of states and parameters. A further example, which combines reduced-order modeling with the ensemble closed-loop control, illustrates the possibility of performing robust control of large-scale problems under uncertainty with improved efficiency by reduced-order modeling.

Thesis Supervisor: Dennis McLaughlin
Title: H.M. King Bhumibol Professor of Civil and Environmental Engineering

Acknowledgements

Here I would like to express my sincere gratitude to the people who make this thesis possible.

I'm indebted to my supervisor, Professor Dennis McLaughlin, for his support, understanding, and patience in the past few years. Without his guidance this thesis would have been impossible. Working with him was truly an invaluable life experience. Also I would like to extend my sincere gratitude to my thesis committee members, Professor Ruben Juanes, Professor Youssef Marzouk, and Professor Karen Willcox, for their valuable guidance and criticism throughout my academic lift at MIT.

I would like to thank funding for this research, provided by Shell International Exploration and Production B.V. under the Investigation of Robust Estimation for Smartfields Applications project, and the Eni Multiscale Reservoir Science Project within the Eni-MIT Energy Initiative Founding Member Program.

I appreciate the assistance from the staff at Parsons Lab and CEE department including Sheila Frankel, Kris Kipp, James Long, and Darlene Strother. In particular, I would like to thank Patricia Dixon, who gave me invaluable help and suggestions during my hard times.

I have benefited from and greatly enjoyed communications with the data assimilation research group members. A special thanks goes to Behnam Jafarpour, who gave my enormous help at the starting point of my research. Thanks to Marco Iglesias-Hernandez for providing valuable advice on my research. I'm also very grateful to Rafal Wojcik, who always answered my questions promptly and precisely.

I have been privileged to have great friends in Boston who make the past few years a memorable and cheerful experience. I would like to thank Fuxian Song and Yang Chen, who have become my friends soon after my arrival in Boston and stayed supportive ever since. In particular, I would like to thank Haijie Chen, Shangchao Lin, Wener Lv, Shaobai Wang, and Xiaoting Jia, who enlighten my life in Boston and relieve the tension of my concentrated study. Thanks very much to Junlun Li, Marcos, Zengchao Hao, Rui Wei, Di Long, Rongzhu Ke, Xiang Li, Kai Liao, Ye Lu, Junkai Zhang, Ping Wang, etc.

I dedicate this thesis to my family, to whom I owe everything, for their long-time support and dedication.

Contents

List of Figures

Chapter 1

Introduction

1.1 Motivation

1.1.1 Heterogeneity and Uncertainty in Subsurface Transport Problems

In many fields of science and engineering, mathematical models play an important role in representing complex physical processes. Results from model simulations are used for system management and risk analysis. Once mathematical models have been established, how state variables evolve is determined by model parameters (such as physical properties) and exogenous forcing. Identifying model parameters then becomes crucial for accurate description of system dynamics. However, limited observations and spatial/temporal variations of parameters often make a precise representation of model parameters infeasible.

The flow through subsurface materials is influenced not only by the distribution of external forcing in time and space, but also by the nature of the materials. Characterization of hydraulic properties is of crucial importance for the exploitation of subsurface resources (e.g., water, oil and gas). Variations in geologic processes create earth materials that have highly variable hydraulic properties [1]. Field measurements reported in the literature show as a rule that hydraulic properties are spatially variable, i.e. aquifers are heterogeneous [2-5].

Since hydraulic properties of natural subsurface flow systems are extremely variable, it is then important to choose an appropriate description of natural variability and combine it with the well-established mathematical models in permeable materials to describe the dynamics of subsurface flow systems. A straightforward way is to measure the hydraulic properties in detail for the field site and implement the actual three-dimensional representation in mathematical models to capture all the effects of variability. However, this method is not only computational expensive, but also not practical to require detailed measurements of hydraulic properties. One obstacle to acquire a detailed description is that the measurement process in filed will alter actual properties in aquifers.

A second approach is to ignore small-scale variability of hydraulic properties, and divide the porous media into homogenous zones, which are presumed to be adequate to describe the situation. Then mathematical models with zonal homogeneous parameters can simulate the dynamics of large-scale subsurface flow in an average sense. The reliability of predictions from the model, however, is highly questionable.

To account for the small-scale variability a simple approach is the one in which hydraulic properties are treated as being random [6]. This is the method of geostatistics. Geostatistics in a probabilistic form assumes that hydraulic properties distributed in space can be considered as a realization of a random field, defined by its jointly probability distribution for all points of the medium. Freeze [2] described the distribution of a one-dimensional hydraulic conductivity field with a lognormal distribution, but ignored the spatial correlation structure of the random field. The statistical analysis of measurements at the Borden site in Canada [7] indicated that hydraulic conductivity fits quite accurately a lognormal distribution. An analysis of the spatial correlation structure revealed that the random field could be regarded as stationary, and the covariance of hydraulic conductivity could be described in an exponential form, which decreases with distance. Thus, the natural formation could be categorized as statistically homogeneous (stationary) and anisotropic.

Traditional geostatistics is based on random function models such as the lognormal random function, the truncated Gaussian random function, and the Boolean random set [8]. Although this approach has been successfully applied to many cases in subsurface modeling, it is always impossible to establish a random function model that can represent more realistic geological features, such as channelized structures. An alternative to the traditional geostatistics is the multi-point geostatistics, in which empirical multivariate distributions are inferred from training images, and thus explicit definitions of random functions are not required. This approach is much more flexible and can represent complex geological structures.

Due to complexity of heterogeneity of subsurface hydraulic properties, acquisition of in-situ measurements for characterization of geostatistical structures needs to be comprehensive. However, exploratory drilling is expensive and hard to maintain consistency of in-situ properties with current measurement techniques. Hence, heterogeneity and lack of data have lead to uncertainty in representation of subsurface geological properties. The uncertainty in the spatial distribution of subsurface hydraulic properties can lead to unreliable predictions of flow displacement behavior of subsurface systems. Identification of appropriate probabilistic models and estimation of parameters for the models with limited data are thus essential for applications of mathematical modeling to subsurface problems.

1.1.2 Inverse Problems in Subsurface Modeling

While the mathematical model is a powerful tool to assess subsurface dynamics, its performance highly depends on the accuracy of representation of hydraulic properties. Inverse methods are used to estimate uncertain properties from relevant observations. An inverse method can be characterized by [9]: (1) parameterization of uncertain properties; (2) the forward equation used to relate parameters and measurements; (3) the performance criterion used to evaluate parameters; (4) and solution methods used to find parameters estimates. This work focuses on parameterization and estimation of uncertain parameters.

One approach for describing spatial heterogeneity is to identify a distinct property value in every cell of the numerical grid used to solve the forward model equations. The resulting vector of uncertain model parameters is high dimensional, leading to a difficult and ill-posed inverse problem. An ill-posed problem is one where either a solution does not exist, the solution is not unique, and/or the solution does not depend continuously on the data [10]. For subsurface problems, large parameter vectors and limited data typically combine to give non-unique solutions since many different parameter combinations give comparable fits to available observations. One approach to resolve this issue is to parameterize high dimensional unknown parameters, that is, describe spatial variability of parameters in a more concise way than the numerical grid cell-based option described above. A cell-based description of spatial variability doesn't take advantage of knowledge about subsurface geological features, such as large-scale faults, finer-scale bedding planes, fractures, and channelized structures. There is much redundancy in the cell-based description since properties tend to be highly correlated across cells so. Parameterization aims at reducing the redundancy in description of spatial variability before solving inverse problems.

A geostatistical description, in which hydraulic properties are treated as random fields [11], often represents geological features better than a cell-based description. If $\alpha(\boldsymbol{\omega})$ is defined as a random function in space $\boldsymbol{\omega}$ for a hydraulic property (or a function of a hydraulic property) α, then under some regularity conditions, α can be decomposed as an expansion [9]

$$\alpha(\boldsymbol{\omega}) = \boldsymbol{\Psi}^T \mathbf{a} \tag{1.1}$$

where $\boldsymbol{\Psi}$ is a matrix with linearly independent basis functions $\psi_i(\boldsymbol{\omega})$, $i = 1,\ldots,N_\alpha$, in each column, and $\mathbf{a}$ is a random vector containing coefficients for each basis function. N_α is often small compared to the number of cells in the numerical grid. The inverse problem can then be posed as estimation of the elements of $\mathbf{a}$ rather than the unknown function $\alpha(\boldsymbol{\omega})$.

Different types of basis functions can be chosen based on characteristics of random fields and geological features that need to be characterized. If we choose basis functions as step functions with 1's in some regions and 0's in other places in the domain of interest, then equation (1.1) is reduced to a regionalized representation [12, 13] of the random field with each region having uniform hydraulic properties in some average sense. Another classical approach is using a truncated Karhunen-Loève decomposition [14, 15] of the random field. In this case, $\psi_i(\omega)$ are eigenfunctions of the covariance of $\alpha(\omega)$, and $\mathbf{a}$ is a vector of uncorrelated random variables. When there is significant spatial structure, the leading eigenfunctions carry most of the important information and thus truncation can be used to discard less important coefficients and reduce the number of unknowns. A relatively recent alternative is developed by Jafarpour and McLaughlin [16] in which the random field is treated as an image and decomposed into pre-specified orthogonal basis functions having regular spatial structure. Most of the information in the image is concentrated in a few low-frequency components and thus the high-frequency ones can be discarded. This method has proven to be effective for channelized geological structures [16-20] and will be discussed more in the following chapters.

The task of parameter estimation is then to find coefficients $\mathbf{a}$ in equation (1.1) such that predictions from forward modeling fits measurements best. The criterion to measure this agreement can be set up under the Bayesian framework. Based on the Bayesian interpretation of parameter uncertainty and Gaussian statistical assumptions, the maximum a posterior estimate of $\mathbf{a}$ (mode of the a posteriori probability density) can be found by minimizing the following deterministic objective function [9, 18, 21]

$$\begin{aligned} J(\mathbf{a}) = &\left[\mathbf{z} - \mathbf{g}\left(\boldsymbol{\Psi}^T\mathbf{a}\right)\right]^T \mathbf{C}_v^{-1}\left[\mathbf{z} - \mathbf{g}\left(\boldsymbol{\Psi}^T\mathbf{a}\right)\right] \\ &+\left[\mathbf{a} - \mathbf{a}_0\right]^T \mathbf{C}_a^{-1}\left[\mathbf{a} - \mathbf{a}_0\right] \end{aligned} \tag{1.2}$$

where $\mathbf{z}$ is a measurement vector, $\mathbf{g}$ is a vector function that maps $\alpha(\omega)$ to the measurement, and $\mathbf{a}_0$ is the prior coefficient vector. $\mathbf{C}_v$ and $\mathbf{C}_a$ are weighting matrices that compromise the solution between the best-fit estimate and the prior information.

This approach is equivalent to a regularized weighted nonlinear least-squares estimation procedure.

The maximum a posteriori optimization can be solved using gradient-based search algorithms such as steepest descent, conjugate gradient, Gauss-Newton, Newton, and quasi-Newton methods. A brief review and comparison of these methods applied to estimation of uncertain parameters in oil recovery can be found in [22]. All of these methods require gradients of a specific objective function as in equation (1.2) with respect to uncertain parameters. The adjoint method [23-26] is an efficient approach to calculate the gradients for high-dimensional nonlinear forward models, which has been successfully applied in meteorology and oil reservoir engineering. Non-gradient search methods such as simulated annealing and genetic algorithms [27] have also been implemented to solve the optimization problem. Typically, computational cost of these methods increases exponentially with the number of uncertain parameters.

Due to nonlinearity and complexity of subsurface systems, the maximum a posteriori optimization problem is often ill-posed and can yield multiple solutions that match the data even after parameterization. Stochastic inversion methods include uncertainty assessment and quantification as part of parameter estimation to characterize heterogeneous hydraulic properties. These provide a useful alternative to maximum a posteriori inverse methods that rely exclusively on deterministic optimization. Recursive Monte Carlo versions of the stochastic inversion approach update individual replicates of hydraulic properties drawn at random from a prior distribution with newly acquired measurements. This updating process generates replicates from the a posteriori distribution of properties conditioned on the new measurements [28-33]. The ensemble Kalman filter (EnKF) is a classic example that has been successfully applied to large-scale complex systems in many geoscience fields.

Both the maximum a posteriori and recursive Monte Carlo inversion methods summarized above are computationally expensive due to the fact that many forward simulations required. A detailed three-dimensional subsurface model can be very complex, as it may contain tens of thousands of grid cells with multiple unknowns

(e.g., head/pressure, velocity and concentration/saturation) in each cell. For realistic applications even a single forward simulation can take hours to days to run. During the maximum a posteriori optimization search hundreds of forward simulations will be needed, and recursive Monte Carlo methods such as the EnKF typically require hundreds of replicates to properly represent the complex spatial variability of hydraulic properties. Hence, it is then very useful to reduce the computational burden to enable practical applications of parameter estimation and uncertainty quantification.

1.1.3 Implications of Uncertainty for Subsurface Flow Control

This thesis considers the control of complex subsurface systems characterized by significant geological uncertainty. A typical subsurface flow control problem is plume management, which refers to indirect control of subsurface pollutants through direct control of the movement of the water phase [34]. Well systems used for control of water movement manipulate the subsurface hydraulic gradient through injection or pumping of water and treat the pumped contaminants ex situ (after removal from the subsurface). The ex situ pump and treat approach is presently the most common method of subsurface pollution control. One of the reasons is that hydrogeologists have a firmer understanding of the mechanics of well hydraulics than they do of in-situ aquifer restoration strategies. The cost of pump and treat remediation includes installation of well systems and ex situ treatment operation and maintenance costs. These costs could be substantial in practice, and thus an efficient plume management approach needs to simultaneously minimize the pumping and treatment costs as well as the hazardous effects of pollution. In a complex site, there are a large number of factors that will affect the efficiency of the management system, such as the number and locations of the injection and pumping wells, the heterogeneous distribution of contaminants, the heterogeneous distribution of hydraulic properties, and the ex situ treatment option selected [35]. This is why an optimal solution is hard to identify without a rigorous optimization scheme. Such a scheme must rely on numerical simulation of subsurface flow and contaminant transport to forecast the spatial distribution of contami-

nants at different time instances. However, the uncertainty in hydraulic properties will affect these forecasts, making them uncertain as well. The optimization scheme can then produce unreliable pump and treat solutions, which turn out to be inefficient and/or ineffective in practice. To improve performance it is crucial to develop a scheme that incorporates parameter identification, which will reduce uncertainty sequentially, as well as robust optimization, which will produce reliable solutions under a range of different geological conditions.

Another subsurface flow control problem that has received increasing attention in recent years is reservoir management for better oil recovery. During the development phase of an oil field, it is critical to determine recovery design factors, such as the positions of wells and well injection and pumping schedules, to improve the recovery factor, namely the fraction of the total amount of oil in place that is recovered. To improve recovery over the production life of the reservoir, reservoir simulation is traditionally utilized during the development phase as well as operation phase. One of the major challenges of model-based reservoir management is the presence of very large uncertainties in the geological structures and hydraulic properties that influence the subsurface flow. Seismic information, which is a major source during the development phase on subsurface structures, is generally too coarse to guide numerical simulations for enhanced recovery [36].

Recent technological advancements in reservoir management, namely the use of smart wells, have made significant impact on the improvement of oil recovery [37]. Extraction of subsurface resources (e.g., oil and gas) can be controlled using smart wells on-line by manipulating flow rates and pressure, and at the same time real-time data, such as pressure and flow rates in the wells, can be provided for on-line monitoring. The flexibility provided by the smart well approach makes it possible to apply a closed-loop reservoir management framework that can optimize well settings and improve reservoir characterization in real time, incorporating new measurements as they become available [36, 38-40]. As depicted in Figure 1-1, closed-loop reservoir management is typically performed in two linked steps: 1) a parameter identification

and updating step, and 2) an optimization step. In this approach sensor measurements and predictions from numerical models can be used together to determine the best management strategy for a given reservoir. In particular, model parameters and control strategies can be continually adjusted to give better predictions of future system response and to improve economic performance over the long term.

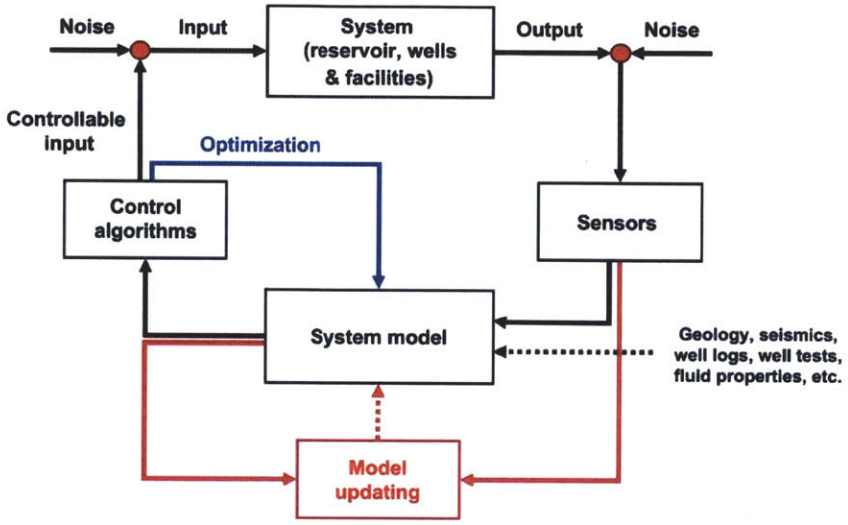

Figure 1-1: Schematic illustration of the closed-loop reservoir management [41].

1.1.4 Necessity for Robust Reduced-Order Modeling

As mentioned above, numerical simulation is an indispensable tool for subsurface flow control. It can be used to guide contaminant remediation and oil recovery and to assess sensitivity to uncertain parameters and quantify risk. However, the complexity of subsurface numerical modeling makes it difficult to use traditional optimization and uncertainty analysis methods, frustrating the real world application of advanced control and decision-making technologies. For example, a typical number of state variables in an oil reservoir model is in the order of 10^4 to 10^6, with similar numbers for the model parameters [42]. Numerical simulation of a few decades of oil production typically involves hours to tens of hours computing time. Maximum a posteriori optimization and

Monte Carlo methods for estimating model parameters both require hundreds of forward simulations for a complex reservoir. Determining the number and position of wells, or the optimal water injection and oil production flow rates over the life of the reservoir requires hundreds or even thousands of additional forward simulations. Thus, the curse of dimensionality of subsurface systems becomes a primary factor that needs to be addressed in order to optimize control strategies efficiently in the presence of uncertainty.

Reduced-order modeling is the transformation of high-dimensional numerical models into more concise low-dimensional representations. While the reduced-order model is a simplified and efficient representation of the dynamics of large-scale systems, it should still preserve critical aspects of the original model, such as the model's overall input-output behavior. Applying reduced-order models to large systems of equations that result from spatial and temporal discretization of mathematical descriptions of dynamics has proven to be a viable way to cope with the computational challenge posed by applications of parameter estimation and real-time control optimization methods.

Many model order reduction techniques has been proposed for linear time-dependent systems, such as proper orthogonal decomposition (POD) [43], balanced truncation [44], and various related hybrids [45]. All of these approaches are projection methods, which project the high-dimensional state space of original models into a low-dimensional space, using basis functions such as those described in (1.1). By applying these methods, significant computational reduction can be expected for linear large-scale systems. However, there are several vital limitations that need to be resolved before applying model reduction techniques to subsurface flow problems. First, the governing equations of subsurface flow systems are usually nonlinear, which leads to time-variant system matrices in the discretized equations. These matrices need to be updated over time, making it difficult to apply model reduction techniques. Second, in the closed-loop control framework the uncertain model parameters must be updated when-

ever new measurements become available. However, the traditional reduced-order model cannot incorporate parameter variations, and thus the reduced-order model must be updated whenever parameters are modified. This will decease the efficiency of the reduced-order model dramatically. Third, in the closed-loop control framework the numerical model must be evaluated for different combinations of control strategies. The traditional POD reduced-order model cannot preserve the input-output behavior whenever the external forcing changes. Thus, usually intensive training or updating of the reduced-order model is needed during on-line simulations. To overcome these drawbacks and improve the efficiency of on-line simulations, a robust reduced-order model that can incorporate parameter variations and control changes will be attractive in the applications of reduced-order modeling to the closed-loop control of nonlinear subsurface systems.

1.2 Thesis Scope

The objective of this thesis is to derive a general framework for efficient real-time control of subsurface flow based on robust reduced-order models that avoid some of the computational and accuracy limitations encountered in traditional model order reduction methods. In particular, this thesis will:

① Set up a general ensemble real-time control framework for subsurface flow control, with specific focus on identification of uncertain geological structures and derivation of a robust nonlinear control strategy that explicitly accounts for uncertainty.

② Develop a systematic, automatic strategy to construct a robust reduced-order model that is valid over a range of parameter variations and input forcing.

③ Embed the reduced-order model into the ensemble real-time control framework.

④ Demonstrate the use of the reduced-order model for ensemble real-time control with an appropriate single-phase flow transport problem that relies on noisy measurements.

⑤ Compare the efficiency and performance of a real-time control approach based on a reduced-order model with one based on the corresponding full order model.

1.3 Thesis Outline

This thesis proceeds as follows. In Chapter 2, a robust reduced-order model is constructed for subsurface contaminant transport problems. A second order expansion is applied to the governing equations to incorporate variations of model parameters explicitly. A robust POD basis is constructed from snapshots of states as well as derivatives of the states with respect to parameters at different times and for different parameter realizations in a specified training set. The reduced-order model is then applied to selected realizations of uncertain parameters to test its performance under parameter variations.

In Chapter 3, the robust reduced-order model is incorporated into the EnKF that generates a posteriori (conditional) replicates of uncertain parameters and states (conditioned on well measurements). The reduced-order model is constructed off-line from a prior (unconditional) ensemble. The ensemble forecast step of the EnKF relies on the reduced-order model instead of the full order model to reduce computational time. The performance of the reduced-order model is tested by comparing the updated replicates to those obtained from the EnKF based on the original full-order model.

In Chapter 4, the reduced-order model is extended to not only incorporate parameter variations, but also control changes, such that the reduced-order model can be applied in a closed-loop control framework. The closed-loop control involves ensemble updating of replicates with the EnKF and robust optimization of control strategies using conditional replicates. Each of these operations requires a significant number of forward simulations. The reduced-order model is used for these forward simulations

and the results are compared with those of the full order model to assess the performance and robustness of the reduced-order model.

Finally, Chapter 5 summarizes all the work, identifies original contributions, and concludes with some suggestions for future work.

1.4 References

[1] L. W. Gelhar, *Stochastic Subsurface Hydrology*. New Jersey: Prentice-Hall, Inc, 1993.

[2] R. A. Freeze, "A stochastic-conceptual analysis of one-dimensional groundwater flow in nonuniform homogeneous media," *Water Resource Research,* vol. 11, pp. 725-741, 1975.

[3] J. P. Delhomme, "Spatial variability and uncertainty in groundwater flow parameters," *Water Resource Research,* vol. 15, pp. 269-280, 1979.

[4] A. W. Warrick and D. R. Nielsen, Eds., *Spatial variability of soil physical properties in the field* (Applications in Soil Physics. New York: Academic Press, 1980, p.^pp. Pages.

[5] L. W. Gelhar, "Stochastic subsurface hydrology from theory to applications," *Water Resources Research,* vol. 22, pp. 135-145, Aug 1986.

[6] G. Dagan, *Flow and Transport in Porous Formations*. Berlin Heidelberg: Springer-Verlag, 1989.

[7] E. A. Sudicky, "A natural gradient experiment on solute transport in a sand aquifer - spatial variability of hydraulic conductivity and Its role in the dispersion process," *Water Resources Research,* vol. 22, pp. 2069-2082, Dec 1986.

[8] L. Y. Hu and T. Chugunova, "Multiple-point geostatistics for modeling subsurface heterogeneity: A comprehensive review," *Water Resources Research,* vol. 44, pp. 1-14, Nov 12 2008.

[9] D. McLaughlin and L. R. Townley, "A reassessment of the groundwater inverse problem," *Water Resources Research,* vol. 32, pp. 1131-1161, May 1996.

[10] C. R. Dietrich, "Optimum Selection of Basis Functions for Ill-Posed Inverse Problems," *Modelcare 90 : Calibration and Reliability in Groundwater Modelling,* vol. 195, pp. 13-22, 1990.

[11] G. Dagan, "Stochastic modeling of groundwater-flow by unconditional and conditional probabilities - the inverse problem," *Water Resources Research,* vol. 21, pp. 65-72, 1985.

[12] P. Jacquard, "Permeability Distribution From Field Pressure Data," *SPE Journal,* vol. 5, pp. 281-294, 1965.

[13] S. I. Aanonsen, "Efficient history matching using a multiscale technique," *Spe Reservoir Evaluation & Engineering,* vol. 11, pp. 154-164, Feb 2008.

[14] M. Loève, *Probability Theory*, 4th ed. New York: Springer-Verlag, 1977.

[15] R. Ghanem and P. D. Spanos, *Stochastic Finite Elements : a Spectral Approach.* New York: Springer-Verlag, 1991.

[16] B. Jafarpour and D. B. McLaughlin, "History matching with an ensemble Kalman filter and discrete cosine parameterization," *Computational Geosciences,* vol. 12, pp. 227-244, Jun 2008.

[17] B. Jafarpour, "Estimation of channelized features in geological media using sparsity constraint," S m, Massachusetts Institute of Technology, 2008.

[18] B. Jafarpour, "Oil reservoir characterization using ensemble data assimilation," PhD, Massachusetts Institute of Technology, 2008.

[19] B. Jafarpour and D. B. McLaughlin, "Estimating Channelized-Reservoir Permeabilities With the Ensemble Kalman Filter: The Importance of Ensemble Design," *Spe Journal,* vol. 14, pp. 374-388, Jun 2009.

[20] B. Jafarpour and D. B. McLaughlin, "Reservoir Characterization With the Discrete Cosine Transform," *Spe Journal,* vol. 14, pp. 182-201, Mar 2009.

[21] G. de Marsily, J. P. Delhomme, A. Coudrain-Ribstein, and A. M. Lavenue, "Four decades of inverse problems in hydrogeology," *Theory, Modeling, and Field Investigation in Hydrogeology: A Special Volume in Honor of Shlomo P. Neuman's 60th Birthday,* pp. 1-17, 2000.

[22] F. Zhang and M. C. Reynolds, "Optimization algorithms for automatic history matching of production data," presented at the 8th European Conference on the Mathematics of Oil Recovery, Freiberg, Germany, 2002.

[23] Y. Chen, D. S. Oliver, and D. X. Zhang, "Efficient Ensemble-Based Closed-Loop Production Optimization," *Spe Journal,* vol. 14, pp. 634-645, Dec 2009.

[24] P. Sarma, K. Aziz, and L. J. Durlofsky, "Implementation of Adjoint Solution for Optimal Control of Smart Wells," in *SPE Reservoir Simulation Symposium*, the Woodlands, Texas, 2005.

[25] P. Sarma, W. H. Chen, L. J. Durlofsky, and K. Aziz, "Production optimization with adjoint models under nonlinear control-state path inequality constraints," *Spe Reservoir Evaluation & Engineering,* vol. 11, pp. 326-339, Apr 2008.

[26] P. Sarma, L. J. Durlofsky, K. Aziz, and W. H. Chen, "Efficient real-time reservoir management using adjoint-based optimal control and model updating," *Computational Geosciences,* vol. 10, pp. 3-36, Mar 2006.

[27] M. K. Sen, A. Dattagupta, P. L. Stoffa, L. W. Lake, and G. A. Pope, "Stochastic reservoir modeling using simulated annealing and genetic algorithms," *Spe Formation Evaluation,* vol. 10, pp. 49-55, Mar 1995.

[28] K. Brusdal, J. M. Brankart, G. Halberstadt, G. Evensen, P. Brasseur, P. J. van Leeuwen, E. Dombrowsky, and J. Verron, "A demonstration of ensemble-based assimilation methods with a layered OGCM from the perspective of operational ocean forecasting systems," *Journal of Marine Systems,* vol. 40, pp. 253-289, Apr 2003.

[29] G. Burgers, P. J. van Leeuwen, and G. Evensen, "Analysis scheme in the ensemble Kalman filter," *Monthly Weather Review,* vol. 126, pp. 1719-1724, Jun 1998.

[30] G. Evensen, "Sequential Data Assimilation with a Nonlinear Quasi-Geostrophic Model Using Monte-Carlo Methods to Forecast Error Statistics," *Journal of Geophysical Research-Oceans,* vol. 99, pp. 10143-10162, May 15 1994.

[31] G. Evensen, "The Ensemble Kalman Filter: theoretical formulation and practical implementation," *Ocean Dynamics,* vol. 53, pp. 343-367, 2003.

[32] G. Evensen, "Sampling strategies and square root analysis schemes for the EnKF," *Ocean Dynamics,* vol. 54, pp. 539-560, 2004.

[33] G. Evensen, "The Ensemble Kalman Filter for Combined State and Parameter Estimation MONTE CARLO TECHNIQUES FOR DATA ASSIMILATION IN LARGE SYSTEMS," *Ieee Control Systems Magazine,* vol. 29, pp. 83-104, Jun 2009.

[34] L. W. Canter and R. C. Knox, *Ground water pollution control.* Chelsea, Mich.: Lewis Publishers, 1986.

[35] G. Teutsch, H. Rügner, D. Zamfirescu, M. Finkel, and M. Bittens, "Source remediation vs. plume management: critical factors affecting cost-efficiency," *Land Contamination & Reclamation,* vol. 9, pp. 128-140, 2001.

[36] J. D. Jansen, O. H. Bosgra, and P. M. J. Van den Hof, "Model-based control of multiphase flow in subsurface oil reservoirs," *Journal of Process Control,* vol. 18, pp. 846-855, Oct 2008.

[37] D. R. Brouwer, J.-D. Jansen, S. van der Starre, C. P. J. W. van Kruijsdijk, and C. W. J. Berentsen, "Recovery increase through waterflooding using smart well technology," presented at the the SPE European Formation Damage Conference, the Hague, the Netherlands, 2001.

[38] J. D. Jansen, L. Durlofsky, K. Aziz, and C. van Kruijsdijk, "Closed-loop reservoir management - Preface," *Computational Geosciences,* vol. 10, pp. 1-2, Mar 2006.

[39] C. H. Wang, G. M. Li, and A. C. Reynolds, "Production optimization in closed-loop reservoir management," *Spe Journal,* vol. 14, pp. 506-523, Sep 2009.

[40] H. Zhao, Y. Li, J. Yao, and K. Zhang, "Theoretical research on reservoir closed-loop production management," *Science China-Technological Sciences,* vol. 54, pp. 2815-2824, Oct 2011.

[41] J. D. Jansen, S. D. Douma, D. R. Brouwer, P. M. J. v. d. Hof, O. H. Bosgra, and A. W. Heemink, "Closed-loop reservoir management," presented at the the 2009 SPE Reservoir Simulation Symposium, the Woodlands, Texas, 2009.

[42] J. D. Jansen, "Model-based control of subsurface flow," presented at the 8th International IFAC Symposium on Dynamics and Control of Process Systems, Cancún, Mexico, 2007.

[43] L. Sirovich and M. Kirby, "Low-Dimensional Procedure for the Characterization of Human Faces," *Journal of the Optical Society of America a-Optics Image Science and Vision,* vol. 4, pp. 519-524, Mar 1987.

[44] B. C. Moore, "Principal Component Analysis in Linear-Systems - Controllability, Observability, and Model-Reduction," *Ieee Transactions on Automatic Control,* vol. 26, pp. 17-32, 1981.

[45] C. W. Rowley, "Model reduction for fluids, using balanced proper orthogonal decomposition," *International Journal of Bifurcation and Chaos,* vol. 15, pp. 997-1013, Mar 2005.

Chapter 2

Generation of a Robust Reduced-Order Model for Ensemble Uncertainty Propagation

2.1 Introduction

Subsurface flow modeling is an indispensible tool for the management of subsurface resources including water, oil, and gas. It can be used for understanding flow and transport processes, for sensitivity and uncertainty analysis, and for assessment of performance under specific operating conditions. However, subsurface flow modeling today has been increasingly challenged by the ever-increasing size and complexity of subsurface geological systems. Moreover, optimization and uncertainty assessments of heterogeneous subsurface systems require a significant number of forward simulations. For example, the closed-loop control strategy described in [1] includes online model updating and optimization of operating control strategies, each requiring require hundreds of forward model simulations. Practical applications of subsurface modeling to optimization and uncertainty assessment are possible only if computational demands are reduced.

Reduced-order modeling aims at generation of an efficient representation of large-scale complex systems while preserving, as much as possible, input-output properties of these systems. It has been applied in diverse areas for simulation, classification,

visualization and compression of high-dimensional data. Many of reduced-order modeling algorithms were developed for linear dynamic systems or parameterized linear steady state problems [2, 3]. In the numerical examples of previous works the simulation models typically only consider responses to a limited number of parameters. In subsurface modeling, the number of uncertain parameters to be considered could be vast when a grid cell-based description of spatial variability is adopted [4]. A robust and efficient reduced-order model that can incorporate parameter uncertainty is then crucial. When such a reduced-order model is available, the high-dimensional model could be replaced with the reduced-order model during optimization and uncertainty assessment, and computational effort can be reduced substantially.

A general representation of the uncertainty in subsurface systems is provided by the probability distribution of hydraulic properties. An ensemble of realizations is usually used to represent the probability distribution when the explicit mathematic form is too complicated or hard to obtain. For complex systems, the ensemble size needs to be sufficiently large to represent the uncertainty. Forward modeling then propagates uncertainty in physical properties forward in time and results in uncertainty in model forecasts. For a recursive estimator, such as the ensemble Kalman filter [5], which is used for uncertainty characterization or reduction, the propagation in uncertainty is an essential part of the forecast step. For large-scale subsurface problems, assessments of uncertainty propagation can be computationally intractable for online simulations need to be performed for each replicate in the ensemble to assess the probability distribution of forecasts. Hence, an efficient approach to propagate uncertainty in the ensemble would be attractive for large-scale applications.

It is also common to use a concise representation of the spatial variability of the parameter uncertainty instead of a higher-dimensional grid-cell based description. This helps to insure that the parameter estimation problem is well-posed and computationally efficient. The simplest parameterization method is zonation of the reservoir into some homogeneous zones [6, 7]. A more effective procedure is to take advantage of the strong spatial correlation of geological properties such as permeability or po-

rosity. When properties are spatially correlated they may be projected to a subspace formed from a relatively small number of covariance matrix eigenvectors. The resulting method is called Karhunen-Loéve (K-L) expansion or linear principle component analysis (PCA). Jafarpour and McLaughlin [8] introduced the discrete cosine transform (DCT) to parameterize the reservoir fields. Compared to the K-L expansion, the DCT provides a robust parameterization alternative that doesn't require specific description of a priori covariance or other statistics. Since the DCT matrix is constant, there is no extra computational burden to determine the transform matrix. It has been shown that the DCT is a flexible and effective method for describing structural geological fields [8, 9].

To apply reduced-order modeling to online assessments of uncertainty propagation it is then crucial to make sure that: (1) the reduced-order model is robust such that the prediction of the reduced-order model is reasonably accurate for the uncertainty propagation process over the replicates in the ensemble; and (2) the reduced-order model can take advantage of the concise representation of uncertain parameters such that the uncertainty in the vast number of input parameters can be represented by a limited number of reduced coefficients. In a word, we seek for a reduced-order model for subsurface modeling that uses an efficient description of uncertain parameters and valid for a range of different parameter values encountered during uncertainty propagation (i.e. the reduced-order model is robust). We try to generate the reduced-order model off-line to avoid updating model structure (i.e. basis functions) during the real-time control process. This minimizes the computational burden of online simulations.

2.2 Literature Review on Reduced-Order Modeling

Most of the existing reduced-order modeling (ROM) algorithms for linear time-invariant systems are projection-based techniques. The key ingredient of these methods is to approximate the high-dimensional state space of the original system with a lower-dimensional state space. The projection can be achieved in many ways. Krylov

subspace methods are among the most popular methods to construct the projection bases. This group of methods aims at approximating the transfer function of the original system around a specified frequency, or a set of frequency points [10-12]. Most of the Krylov subspace methods are based on Lanczos method [11, 13, 14] or Arnodi algorithm [15-17]. This group of algorithms has proved to be efficient and thus is suitable for model reduction of large-scale linear models. The major drawbacks of these methods, in addition to their dependence on linear assumptions, include that there are no specific error bounds for model reduction, and no guarantees of preserving the stability and passivity of the original system.

The projection bases can also be derived from the Hankel norm approximants or balanced truncation method. The Hankel norm approximants try to approximate the linear system optimally by a lower-complexity system in the Hankel norm [18]. Balanced truncation methods are based on finding an appropriate coordinate system for the state-space in which the chosen Gramian matrices of the system are diagonal and equal [19-21]. Both Hankel norm approximants and balanced truncation methods belong to the family of absolute error methods, which try to minimize the error between the transfer function and the approximant in some system norm [22]. Hence, compared to Krylov subspace methods, these methods can provide provable error bounds, and the stability and passivity of the reduced-order models can be guaranteed. However, efficiency remains the bottleneck for this family of methods. For example, the solution of the Lyapunov equations in the balanced truncation methods is so expensive ($O(N^3)$) that it is inapplicable for large-scale problems under current computational conditions [23].

Another group of ROM methods belongs to the proper orthogonal decomposition (POD) family, which can be viewed as a data compression method to remove the redundant information in the state space [24-26]. Typically, snapshots of the solution of the system at different time instances are collected and compressed by the singular value decomposition (SVD) to generate projection bases. The Galerkin projection [27, 28], then, can be used to project the system equations onto a lower-dimensional space.

A more recent approach is to solve a minimization problem to derive the reduced-order model [28]. The POD method is efficient, easy to implement, and capable of capture complex system dynamics, which makes it popular for model order reduction of large-scale problems. However, the POD basis cannot contain more information than contained in the snapshots, and thus the ability of the POD method to approximate the original system totally depends on the collected snapshots. The connections between balanced truncation and the POD method have been illuminated in, for example, [29], [30], and [31].

Most of the aforementioned linear model order reduction techniques can be extended to the nonlinear case. A straightforward method is based on linearization, or polynomial expansion of the system nonlinearity [32, 33]. The linear projection-based methods can then be applied to the resulting systems. The nonlinear system can also be represented or accurately approximated by a Volterra series [34], and then a proper projection method follows. Empirical methods, which are based on experimental or simulation data for identifying the input-output behavior of nonlinear systems, have great popularity due to their capability of reducing complex nonlinear systems with a small number of inputs and outputs significantly [29, 35]. Most of these methods, however, are limited to weakly nonlinear cases and are not appropriate for real-time control applications.

For more general nonlinear systems, the trajectory piecewise linearization (TPWL) method [23] has gained greater popularity recently due to its effectiveness and robustness for model order reduction. The TPWL method provides a cost-efficient representation of system's nonlinearity, using state space projection methods based on the aforementioned linear model reduction methods [36, 37]. The TPWL method divides the state space of the nonlinear system into piecewise linear regions and then reduces the order of each region. Compared to the linearization or polynomial expansion methods, the TPWL method can capture the nonlinearity of the system in wider ranges, but might be unable to represent high order nonlinearity. Dong and Roychowdhury [38] extended this method and approximated each region with higher or-

der polynomials, aiming at capturing strong and weak nonlinearities simultaneously. This will likely sacrifice the computational efficiency carried by the TPWL method.

The POD method has been widely used for model order reduction of nonlinear systems [27, 39-41]. Also, the POD reduced models has been utilized to improve the efficiency for optimal control problems [26, 42-44]. A lot of computational effort is indeed saved if the optimization process is only based on low-order models. The generation of a good snapshot set is crucial for successful applications of the POD reduced models in an optimization setting, for the physics changes with the control variables. A simple approach is to sample the control variable space uniformly and use the sample points to generate the snapshots. This will, however, require a lot of evaluations of the full order model. Centroidal Voronoi Tessellations [45] could be an intelligent alternative to sample the control variable space. Another approach for effective optimal control based on reduced models uses an adaptive procedure that improves the reduced-order model by successively updating the snapshots when the existing POD reduced model is considered to be insufficient [46]. Bergmann et al. [47] proposed a trust-region proper orthogonal decomposition (TRPOD) approach to update the reduced-order model successively. This approach will guarantee the convergence of the optimization based on the reduced-order model to the solution of the original optimization problem defined by the full order model. The main drawback of these adaptive approaches is that the full order model needs to be run in real time, which defeats much of the point of using a reduced-order model.

The ROM can also be applied to efficient real-time estimation of ensembles that are conditioned on measurements. Similar to the optimal control problems, the quality of the POD reduced-order model used for conditioning is very dependent on the choice of parameters over which the snapshots are generated. The aforementioned techniques for optimal control based on reduced-order models are also applicable for ensemble conditioning. Many authors are still contributing to parameterized model order reduction. Bui-Thanh et al. [48] proposed a model-constrained adaptive sampling method to sample the high-dimensional parameter space based on minimization

of output errors between the full order model and reduced-order model, aiming at capturing variations over the parameter space. Bond and Daniel [49] combined parameterized reduction of linear systems with the TPWL method to approximate large nonlinear systems over a practical range of geometric parameter variations. Amsallem and Farhat [50] used an interpolation method based on the Grassmann manifold and its tangent space to construct a new reduced basis associated with new sets of parameters. Currently, this method is only suitable for problems with a limited number of parameters. Moreover, the robustness of this method is closely related to the dependency of the system on the parameters.

In the field of subsurface modeling, an early attempt at applying ROM to real-time control of water flooding was contributed by Markovinovic et al. [51]. They employed a black-box method, identifying low-order models of heterogeneous reservoirs based on flowrate-pressure input-output behavior. The method was tested on a single-phase flow in a 2D reservoir, and proved to be successful for identifying low-order models for the synthetic reservoir.

Heijn et al. [52] presented five methods (i.e. modal decomposition, balanced realization, a combination of modal decomposition and balanced realization, subspace identification, and POD) to derive low-order models of two-phase (oil-water) reservoir flow which were applied to synthetic examples. Based on the linearized reservoir model, the first three methods resulted in low-order linear models, which were only valid for a short timespan. The identification and POD methods, which remained valid for longer periods, were more promising than the first three methods. However, in their applications, the resulting nonlinear POD reduced-order model required computation with the full order state vector. This adversely affected the efficiency of the reduced model.

Van Doren et al. [53] developed a nested approach in which the POD method was used to reduce the state space dimensions of both the reservoir model and the adjoint model. This approach was applied to a synthetic 2D reservoir to optimize the water flooding strategies. The optimization was first based on the POD reduced model to

obtain the optimal strategies, and then a verification procedure based on the full order model was carried out to ensure that the reduced-order model generated valid optimal control strategies. If this was not the case, a new POD reduced model was generated based on new sets of snapshots and an optimization procedure followed until convergence criteria satisfied. In their approach, however, computation with the full order state vector was still unavoidable.

To avoid evaluations of nonlinear terms with full order state vectors, Cardoso and Durlofsky [54] used the TPWL method to approximate the nonlinear two-phase reservoir model and utilized the POD method to construct the reduced-order model for production optimization. The snapshots used to generate the POD basis were chosen under selected control settings. The resulting reduced-order model was applied to a heterogeneous 3D reservoir with six wells over six control steps. The results obtained from the reduced-order model showed consistent agreement with the results obtained from the full order model. As pointed out in their later paper [55], it was necessary to evaluate the mass balance errors during the simulation of the reduced-order model. If the balance was violated, the full order model was then used to perform the simulation for the current time step. This can significantly reduce the efficiency of the reduced-order model.

2.3 Methodology

Here we investigate 2D solute transport in a thin layer of isotropic saturated aquifer. We assume a constant layer height. Pressure head and solute concentration are approximately vertically constant. Then the vertical flux and gravity can be neglected.

Based on the conservation of mass and momentum, the forward model for 2D non-gravitational solute transport in porous media can be written as:

$$
\begin{aligned}
s\frac{\partial h}{\partial t} &= -\nabla\cdot\mathbf{q}+u \\
\mathbf{q} &= -k\cdot\nabla h \\
\theta\frac{\partial c}{\partial t} &= -\nabla\cdot\left(\mathbf{q}c\right)+\theta D\cdot\nabla^2 c+u\cdot c_s
\end{aligned}
\tag{2.1}
$$

Here h is the piezometric head, $\mathbf{q}$ is the Darcy velocity vector, s is the specific storage, and u is the volumetric flux per unit volume from the aquifer through the wells. Due to the isotropic property, the hydraulic conductivity k is a scalar. θ is the porosity, c is the solute concentration, and c_s is the concentration associated with the source/sink. To simplify the transport equation we assume the dispersion coefficient D is constant and isotropic in all directions.

2.3.1 Numerical Discretization and Second Order Expansion

Spatial discretization of the governing equations using traditional numerical schemes will result in nonlinear equations. For example, discretized flow equations in (2.1) with a traditional finite difference technique will include the harmonic mean of the hydraulic conductivity of adjacent grid cells. The resulting equations are nonlinear in both states and parameters. It is then difficult to apply linear model reduction techniques to flow equations. Here we seek a numerical scheme that can easily incorporate reduced representations of both states and parameters.

Possible numerical options include the mixed finite element approximation [56, 57] of two flow equations as well as the upwind finite different approximation [58] of the solute transport equation. With a uniform finite element partition of the computational domain and lowest-order Raviart-Thomas subspaces on rectangles [59], the flow equations in (2.1) can be discretized into the following form

$$
\begin{aligned}
s\frac{\partial \mathbf{h}}{\partial t}-\mathbf{B}\cdot\mathbf{q} &= \mathbf{R}_1 \\
\mathbf{B}^T\cdot\mathbf{h}+\mathbf{A}\left(\eta\right)\cdot\mathbf{q} &= \mathbf{R}_2
\end{aligned}
\tag{2.2}
$$

where $\mathbf{h}$ is the vector containing the pressure head at each grid cell, $\mathbf{q}$ is the vector containing the x and y components of the Darcy velocity at each cell, with all x components numbered first. The components of the matrix $\mathbf{B}$ are constant, while the components of matrix $\mathbf{A}$ depend linearly on the hydraulic resistivity $\boldsymbol{\eta}$, which is defined as $\eta_i = 1/k_i$ for i-th cell. The right-hand-side vectors $\mathbf{R}_1$ and $\mathbf{R}_2$ are dependent on the boundary conditions including the flow conditions at the source/sink.

The resulting equations in (2.2) are bilinear in $\mathbf{q}$ and $\boldsymbol{\eta}$. This feature makes it easy to substitute full order states with reduced representations. To see this, we first need to do a second order expansion of the discretized equations. Assume $\delta\mathbf{h} = \mathbf{h} - \mathbf{h}_0$, $\delta\mathbf{q} = \mathbf{q} - \mathbf{q}_0$, and $\delta\boldsymbol{\eta} = \boldsymbol{\eta} - \boldsymbol{\eta}_0$. $\mathbf{h}_0$ and $\mathbf{q}_0$ are solutions from the system equations for the nominal resistivity configuration $\boldsymbol{\eta}_0$, while $\mathbf{h}$ and $\mathbf{q}$ are solutions for the new configuration $\boldsymbol{\eta}$. The discretized equations can be expanded around the nominal states as follows:

$$\begin{aligned} s\frac{\partial(\delta\mathbf{h})}{\partial t} - \mathbf{B}\cdot\delta\mathbf{q} &= 0 \\ \mathbf{B}^T\cdot\delta\mathbf{h} + \mathbf{A}(\boldsymbol{\eta}_0)\cdot\delta\mathbf{q} + \mathbf{M}(\mathbf{q}_0)\cdot\delta\boldsymbol{\eta} + \mathbf{T}\cdot(\delta\boldsymbol{\eta}\otimes\delta\mathbf{q}) &= 0 \end{aligned} \tag{2.3}$$

where $\mathbf{M}(\mathbf{q}_0)$ is the gradient matrix of the term $\mathbf{A}(\boldsymbol{\eta})\cdot\mathbf{q}$ with respect to $\boldsymbol{\eta}$ evaluated at $\mathbf{q}_0$. Since $\mathbf{A}(\boldsymbol{\eta})\cdot\mathbf{q}$ is bilinear in $\mathbf{q}$ and $\boldsymbol{\eta}$, the Hessian matrix $\mathbf{T}$ is constant and sparse.

For an m by n matrix $\boldsymbol{\Gamma}$, and a p by q matrix $\boldsymbol{\Pi}$, the Kronecker product $\boldsymbol{\Gamma}\otimes\boldsymbol{\Pi}$ is defined as

$$\boldsymbol{\Gamma}\otimes\boldsymbol{\Pi} = \begin{bmatrix} \Gamma_{11}\boldsymbol{\Pi} & \cdots & \Gamma_{1n}\boldsymbol{\Pi} \\ \vdots & \ddots & \vdots \\ \Gamma_{m1}\boldsymbol{\Pi} & \cdots & \Gamma_{mn}\boldsymbol{\Pi} \end{bmatrix} \tag{2.4}$$

The resulting matrix is mp by nq. If the number of cells is N after the domain is discretized, then the dimension of the vector $\delta\boldsymbol{\eta}\otimes\delta\mathbf{q}$ is about $2N^2$.

With the same grid used in the mixed finite element spatial discretization of the flow equations, the transport equation can be discretized using the upwind finite difference method, and the resulting equation can be written as:

$$\theta\frac{\partial \mathbf{c}}{\partial t}+\mathbf{E}(\mathbf{q})\cdot\mathbf{c}+\mathbf{G}\cdot\mathbf{c}=\mathbf{R}_3 \tag{2.5}$$

where $\mathbf{c}$ is the vector containing the solute concentration at each grid cell. $\mathbf{E}(\mathbf{q})\cdot\mathbf{c}$ is the advection term and the matrix $\mathbf{E}$ nonlinearly depends on the Darcy velocity vector $\mathbf{q}$. In the dispersion term $\mathbf{G}\cdot\mathbf{c}$, $\mathbf{G}$ is constant if dispersion coefficients are constant. If the solute can only exit through the wells and the flow rates at the wells are prescribed, then the source/sink term $u\cdot c_s$ can be incorporated into the matrix $\mathbf{E}$. In this case, we have $\mathbf{R}_3=0$.

Note that if the specific storage s is very small then we can treat the flow equations as a steady state system when u doesn't change. In subsurface flow control the control variables at different wells are usually changed relatively infrequently so we need only solve a steady state problem for $\mathbf{h}$ and $\mathbf{q}$ over each interval. Then $\mathbf{q}$ is constant and the transport equation (2.5) is linear over each interval. We can then directly apply linear order reduction techniques to evaluate the transport equation efficiently at each control interval.

2.3.2 Proper Orthogonal Decomposition

Proper orthogonal decomposition (POD) has been widely used in control and estimation applications because of its ability to generate accurate reduced representations for very complex systems with a small number of elements. Here we use the POD method to develop reduced representations of the state vectors $\mathbf{h}$, $\mathbf{q}$, and $\mathbf{c}$ in equations (2.3) and (2.5).

POD [60] adopts the approximations:

$$\begin{aligned}\mathbf{h}&\approx\Phi_{\mathbf{h}}\mathbf{h}_r\\ \mathbf{q}&\approx\Phi_{\mathbf{q}}\mathbf{q}_r\\ \mathbf{c}&\approx\Phi_{\mathbf{c}}\mathbf{c}_r\end{aligned} \tag{2.6}$$

Here, $\mathbf{\Phi}_{\mathbf{h}}$, $\mathbf{\Phi}_{\mathbf{q}}$, and $\mathbf{\Phi}_{\mathbf{c}}$ are the matrices containing the POD basis for the head $\mathbf{h}$, Darcy velocity $\mathbf{q}$, and solute concentration $\mathbf{c}$. The reduced variables $\mathbf{h}_r$, $\mathbf{q}_r$, and $\mathbf{c}_r$ have the dimensions $N_{\mathbf{h}}$, $N_{\mathbf{q}}$, and $N_{\mathbf{c}}$, respectively, which are determined by the energy threshold and much smaller than the original dimensions.

The basis vectors are the leading singular vectors of matrices constructed from "snapshots" of the full-order model. Each column of a snapshot matrix consists of all states of the full-order model at a given time and for a given replicate of the uncertain resistivity or of derivatives of the states with respect to resistivity. The full-order model simulations used to obtain snapshots are commonly called "training runs". The leading singular vectors define the directions in the full-order state space that are most closely aligned with the snapshot vectors, as indicated by the magnitude of the corresponding singular values. These state-space directions are captured in the reduced-order model (i.e. the full-order model states are projected on the leading singular vectors). Careful adjustment is needed to select a representative but concise set of snapshots for the basis vector derivation.

A POD basis derived from a small number of snapshots normally works only well for the parameters lying near the parameters (e.g. resistivities) used in the corresponding training runs. In ensemble-based real-time control, a significant number of replicates corresponding to different parameter spatial distributions must be included in the ensemble to ensure that the training runs cover the range of states and parameters encountered during the estimation and control process. To insure this it is helpful to include in the snapshots the sensitivities of the states with respect to the parameters [61]. In principle, the sensitivities can improve the reduced-order model by approximating the differences between the new states and the states used to generate the POD basis. Numerical tests show that the POD basis of the states in the flow equations is more sensitive than the basis in the transport equation. Hence, only sensitivity analysis for the flow equations is performed here.

To simplify the procedure, assume that the flow equations are steady, i.e. $s=0$. Then after some derivation, we can obtain the equations of the form

$$
\begin{aligned}
-\mathbf{B}\frac{\partial \mathbf{q}}{\partial \eta_i} &= 0 \\
\mathbf{B}^T \frac{\partial \mathbf{h}}{\partial \eta_i} + \mathbf{A}(\boldsymbol{\eta})\frac{\partial \mathbf{q}}{\partial \eta_i} &= -\mathbf{m}_i
\end{aligned}
\tag{2.7}
$$

Here, $\mathbf{m}_i$ is i-th column of the derivation matrix $\mathbf{M}(\mathbf{q})$ as in equation (2.3), and η_i is the hydraulic resistivity for i-th cell. Equation (2.7) can be solved iteratively for the sensitivities $\partial \mathbf{h} / \partial \eta_i$ and $\partial \mathbf{q} / \partial \eta_i$, where $i = 1, \ldots, N$. Then these sensitivities $\partial \mathbf{h} / \partial \eta_i$ and $\partial \mathbf{q} / \partial \eta_i$ can be incorporated into the snapshot matrices.

Assume $\mathbf{X}_\mathbf{h}$, $\mathbf{X}_\mathbf{q}^x$, $\mathbf{X}_\mathbf{q}^y$, and $\mathbf{X}_\mathbf{c}$ are the snapshot matrices for $\mathbf{h}$, $\mathbf{q}^x$, $\mathbf{q}^y$, and $\mathbf{c}$. Here we reduce the x and y components, $\mathbf{q}^x$ and $\mathbf{q}^y$, of the velocity $\mathbf{q}$ separately. The columns of $\mathbf{X}_\mathbf{h}$ are composed of solutions for $\mathbf{h}$ as well as the derivatives $\partial \mathbf{h} / \partial \eta_i$. Similarly, $\mathbf{X}_\mathbf{q}^x$ and $\mathbf{X}_\mathbf{q}^y$ are composed of solutions for $\mathbf{q}^x$ and $\mathbf{q}^y$ as well as derivatives $\partial \mathbf{q} / \partial \eta_i$ in the columns. $\mathbf{X}_\mathbf{c}$ only includes solutions for $\mathbf{c}$. To obtain the POD basis matrix $\boldsymbol{\Phi}_\mathbf{h}$, we obtain singular vectors by solving the following eigenvalue problem

$$
\left(\mathbf{X}_\mathbf{h}^T \mathbf{X}_\mathbf{h}\right)\boldsymbol{\phi}_\mathbf{h}^j = \rho_\mathbf{h}^j \boldsymbol{\phi}_\mathbf{h}^j \tag{2.8}
$$

Here, $\rho_\mathbf{h}^j$ is the j-th largest eigenvalue. $\boldsymbol{\phi}_\mathbf{h}^j$ is the corresponding eigenvector and is the j-th column of the matrix $\boldsymbol{\Phi}_\mathbf{h}$. The dimension $N_\mathbf{h}$ of the reduced-order model head vector is determined by the energy threshold $\varepsilon_\mathbf{h}$

$$
\varepsilon_\mathbf{h} = \sum_{j=1}^{N_\mathbf{h}} \rho_\mathbf{h}^j \Big/ \sum_{j=1}^{N} \rho_\mathbf{h}^j \tag{2.9}
$$

We arrange the singular vectors in order of decreasing singular values and only keep the number of vectors $N_\mathbf{h}$ needed to insure that $\varepsilon_\mathbf{h} = 95 \sim 99\%$. The dimension of the head vector in the reduced-order model is $N_\mathbf{h}$.

By following the same procedure, we can obtain the matrices $\boldsymbol{\Phi}_\mathbf{q}^x$, $\boldsymbol{\Phi}_\mathbf{q}^y$, and $\boldsymbol{\Phi}_\mathbf{c}$. Note that

$$\Phi_q = \begin{bmatrix} \Phi_q^x & \\ & \Phi_q^y \end{bmatrix} \tag{2.10}$$

2.3.3 Discrete Cosine Transform

We can also derive a reduced representation for the parameter vector. The full order parameter vector η can be represented by the DCT basis in the matrix form [62]

$$\eta = \Theta\tilde{\eta} \tag{2.11}$$

where Θ is the constant DCT matrix, satisfying $\Theta^{-1} = \Theta^T$ and and $\tilde{\eta}$ is the DCT coefficient vector. Normally, there are only a few large coefficients and thus it's possible to use a truncated representation of the form

$$\eta \approx \Phi_\eta \eta_r \tag{2.12}$$

Here, Φ_η only contains columns of Θ that correspond to those largest DCT coefficients. The dimension of η_r, N_η, is usually significantly smaller than the original dimension.

Note that we cannot predetermine which are the significant columns for the true parameter configuration. One way to keep as few columns as possible and still obtain a good representation of the parameter configurations drawn from the same probability distribution is to apply the DCT to a representative ensemble. All the columns corresponding to the significant coefficients of each replicate are kept, and thus this representation will also be sufficient for the whole ensemble [8].

2.3.4 The Reduced-Order Model

Now that we have concise representations for both parameters and state variables we can substitute (2.6) and (2.12) into (2.3) and (2.5), and perform the Galerkin projection with Φ_h, Φ_q, and Φ_c. This gives the following set of second order reduced-order model equations:

$$
\begin{aligned}
s\frac{\partial(\delta\mathbf{h}_r)}{\partial t} - \mathbf{B}_r \cdot \delta\mathbf{q}_r &= 0 \\
\mathbf{B}_r^T \cdot \delta\mathbf{h}_r + \mathbf{A}_r \cdot \delta\mathbf{q}_r + \mathbf{M}_r \cdot \delta\boldsymbol{\eta}_r + \mathbf{T}_r \cdot (\delta\boldsymbol{\eta}_r \otimes \delta\mathbf{q}_r) &= 0 \\
\theta\frac{\partial \mathbf{c}_r}{\partial t} + \mathbf{E}_r(\mathbf{q}) \cdot \mathbf{c}_r + \mathbf{G}_r \cdot \mathbf{c}_r &= 0
\end{aligned}
\tag{2.13}
$$

Here, $\mathbf{B}_r = \boldsymbol{\Phi}_\mathbf{h}^T \mathbf{B} \boldsymbol{\Phi}_\mathbf{q}$, $\mathbf{A}_r = \boldsymbol{\Phi}_\mathbf{q}^T \mathbf{A}(\boldsymbol{\eta}_0) \boldsymbol{\Phi}_\mathbf{q}$, $\mathbf{M}_r = \boldsymbol{\Phi}_\mathbf{q}^T \mathbf{M}(\mathbf{q}_0) \boldsymbol{\Phi}_\boldsymbol{\eta}$, $\mathbf{G}_r = \boldsymbol{\Phi}_\mathbf{c}^T \mathbf{G} \boldsymbol{\Phi}_\mathbf{c}$, and $\mathbf{T}_r = \boldsymbol{\Phi}_\mathbf{q}^T \cdot \mathbf{T} \cdot (\boldsymbol{\Phi}_\boldsymbol{\eta} \otimes \boldsymbol{\Phi}_\mathbf{q})$, which can all be pre-computed. $\mathbf{E}_r(\mathbf{q}) = \boldsymbol{\Phi}_\mathbf{c}^T \mathbf{E}(\mathbf{q}) \boldsymbol{\Phi}_\mathbf{c}$, which must be recomputed each time the controls change. Note that the dimension of the Kronecker product $\boldsymbol{\Phi}_\boldsymbol{\eta} \otimes \boldsymbol{\Phi}_\mathbf{q}$ is about $2N^2 \times N_\eta N_\mathbf{q}$. The computation then requires a significant amount of memory.

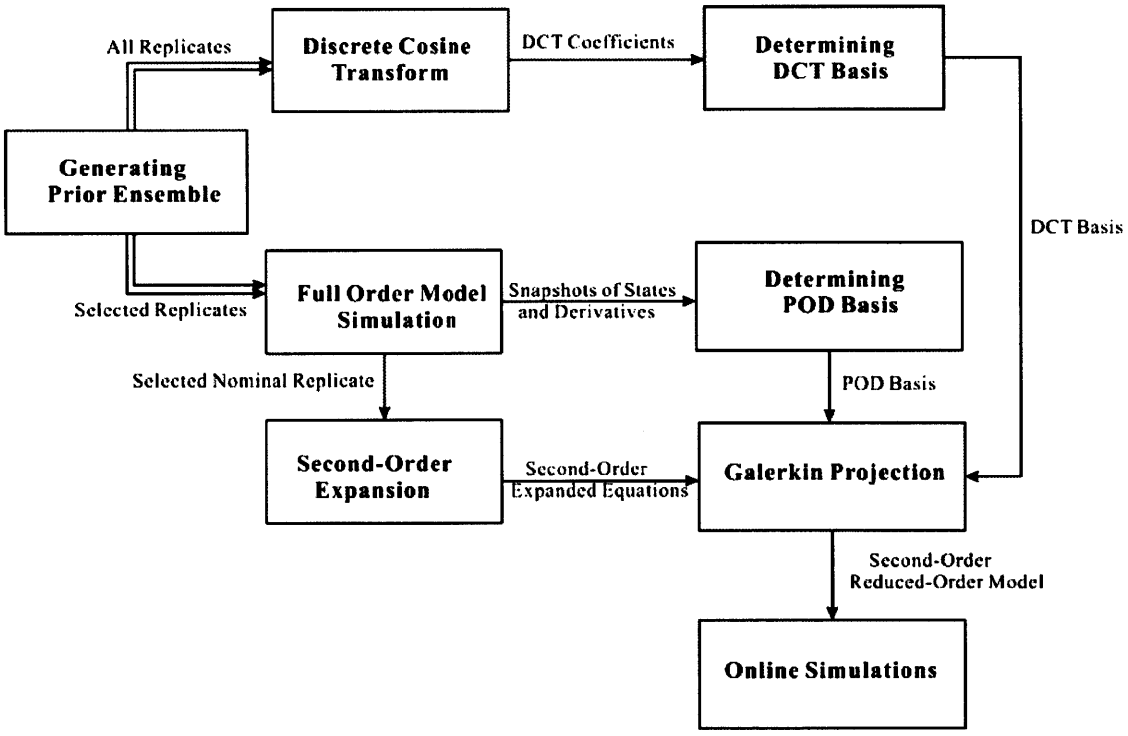

Figure 2-1: Flowchart showing ensemble-based generation of a reduced-order model. Double lines indicate multiple operations on replicates in the ensemble.

2.3.5 Implementation Issues

Figure 2-1 illustrates the process of generating a robust reduced-order model for an ensemble of uncertain parameter configurations. An ensemble is generated by using

the Gaussian indicator simulator in SGeMS, where the necessary conditional cumulative functions are inferred from the indicator kriging algorithm [63]. Two sets of projection basis vectors are needed to derive the reduced-order model. The first is the set of POD basis vectors used to project the state vectors into reduced spaces. The second is the set of DCT basis vectors used for parameterizing uncertain parameter fields. Although the DCT basis vectors are constant, we need to determine which basis vectors to retain. In both cases we need to make sure those basis vectors span the spaces of the entire ensemble as sufficiently as possible. This can be done by comparing the results of reduced-model simulations with corresponding full-order model results, as described in the next section.

A nominal parameter configuration as well as its corresponding full order solutions is selected to perform the second-order expansion of the discretized governing equations around the nominal parameters and solutions. The POD and DCT basis vectors are then substituted into the second-order expanded equations and Galerkin projection is performed to reduce the number of equations. These operations are all performed off-line. The resulting second order reduced-order model can then be applied to online simulations of the entire ensemble. The robustness and accuracy of the reduced-order model can be validated by the following numerical examples.

2.4 Numerical Experiments

2.4.1 Experimental Setup

Here we consider a model of 2D non-gravitational solute transport in a porous medium. In this synthetic example, a 640 m×640 m×1 m porous domain is discretized into a 2D 64×64×1 uniform grid cell system. The size of each cell is 10 m×10 m×1 m. The whole domain has the constant porosity of 0.2. Figure 2-2(a) shows the simulation domain and the locations of 4 pumping wells. The length of the simulation horizon is 800 days, and the pumping rates given by the control schedule for the 4 pumping wells are illustrated in Figure 2-2(b). The simulation horizon is divided into 4

constant intervals. Each of the intervals represents a control step. The solute is injected into the domain at the mid-lower cells with a constant rate of 5 m^3/day and constant concentration of 50 mg/L for the first 400 days. Here specific storage $s = 0$ is used to represent steady-state flow conditions, and the head is constant over each control step. The flow equation has no water flux boundaries on the east and west sides and constant head boundaries of 30 m and 0 m on the south and north sides. The transport equation also has no solute flux boundaries on the east and west sides, but has prescribed zero solute concentration boundaries condition on the south and north sides. The dispersion coefficient is assumed to be constant over the whole domain in all direction, and thus the transport equation is linear for each control step.

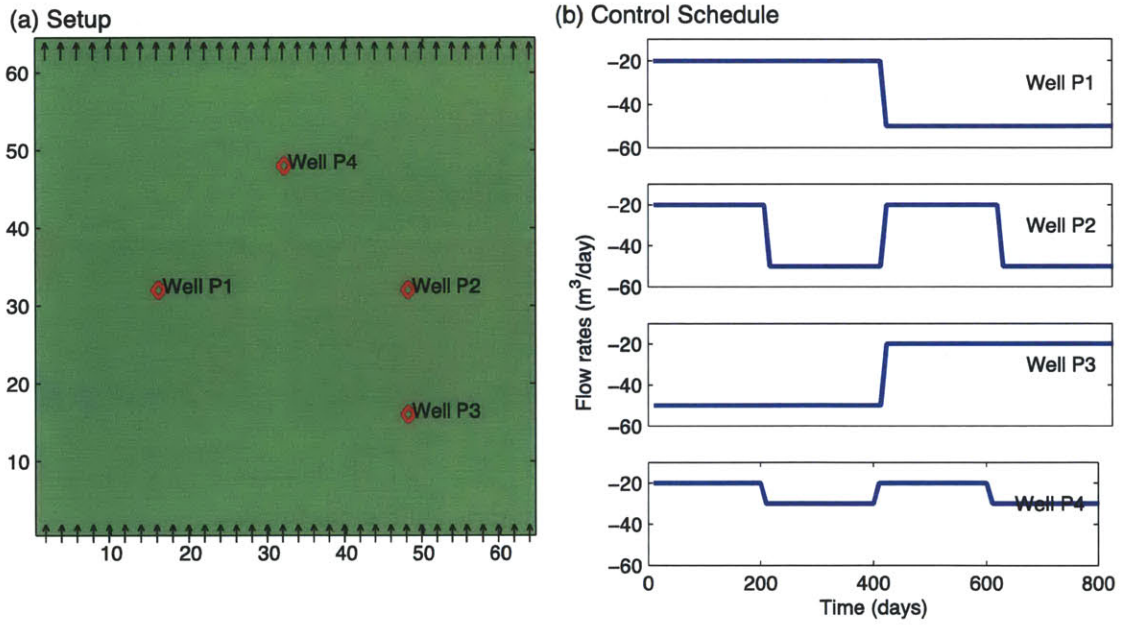

Figure 2-2: Experimental setup. (a) Simulation domain with locations of four pumping wells. (b) Pre-determined pumping rates for the four wells.

The unknown parameters are the hydraulic resistivity in each cell of the discretized computational grid. We want to generate a reduced-order model that can incorporate the uncertainty in hydraulic resistivity and then test its robustness and effectiveness for various realizations of hydraulic resistivity. To this end, an ensemble of 50 realizations of conductivity fields is generated using Gaussian indicator simulator

in the Stanford SGeMS. The simulated ensemble is then parameterized by the DCT so that each high-dimensional hydraulic conductivity replicate can be represented by a corresponding set of truncated reduced-dimensional DCT coefficients. To obtain accurate and effective representations of the conductivity fields, the DCT is performed for all replicates in the original ensemble. The DCT basis vectors corresponding to the first few largest DCT coefficients for each replicate are retained while the others are discarded. The distinctive retained DCT vectors are combined to construct the DCT projection matrix. For this ensemble, 110 out of 4096 DCT basis vectors are kept. Five of reconstructed conductivity replicates obtained by multiplying the projection matrix and the reduced-order DCT coefficients are shown in Figure 2-3. We can clearly see that the conductivity fields have high permeable and low permeable zones, which create pathways for solute transport. The resulting reconstructed ensemble is used in the experiments instead of the original ensemble.

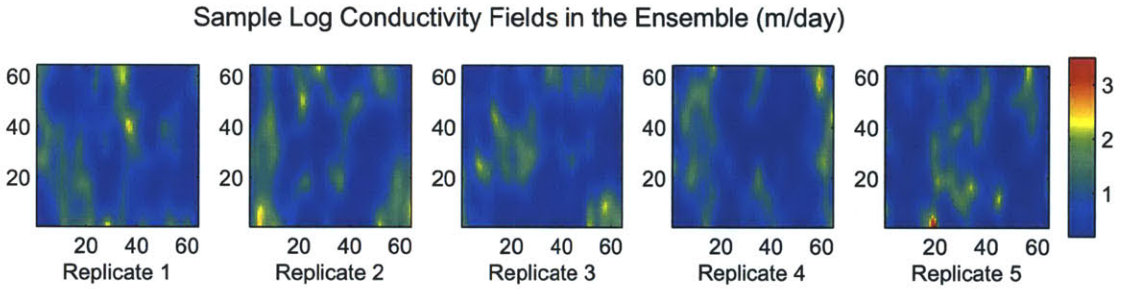

Figure 2-3: Five replicates of hydraulic conductivity in the ensemble.

2.4.2 Generation of the Reduced-Order Model

As shown in Figure 2-1, two sets of basis vectors need to be constructed to generate the reduced-order model. Construction of the first one includes the aforementioned DCT parameterization. Each replicate of the ensemble can then be represented by reduced-order DCT coefficients, which are now used as inputs to the reduced-order model instead of the original high-dimensional conductivity fields.

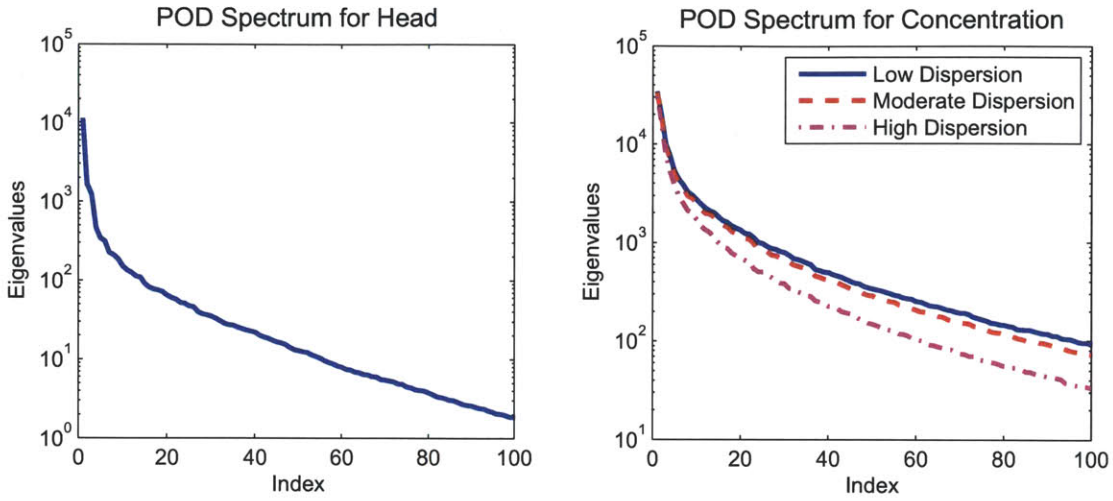

Figure 2-4: POD spectra for head and concentration. Note that in the figure on the right there are three different lines with each corresponding to various dispersion coefficients.

To construct the projection matrices for the state vectors the full order model needs to be run to collect snapshots of state vectors and derivatives of states with respect to hydraulic resistivity. Note that only 10 of the replicates in the ensemble are used to generate state vectors and 3 of the 10 replicates are used to calculate the necessary derivatives. To obtain a compact representation of the states, the POD expansion is truncated at the number of basis function terms that account for 99%, 93%, 93%, and 99% of the energy in the head, x velocity, y velocity and concentration, respectively. This gives reduced dimensions of 69, 113, 84, and 184, for these four variables. The eigenvalues for corresponding eigenvectors are shown in Figure 2-4 for head and concentration. For the head, we can see that the eigenvalues decrease relatively fast and thus we need only keep a few of the total eigenvectors to achieve the 99% energy threshold. For concentration, however, how fast the eigenvalues decrease depends on the dispersion coefficients. The blue, red, and magenta lines in the right figure correspond to constant dispersion coefficients of 0.5, 1, and 4 m^2/day, respectively. Clearly, as dispersion increases, it becomes easier to perform order reduction for concentration. For the following simulations, we use the dispersion coefficient of 1 m^2/day.

Figure 2-5 shows the projection basis vectors corresponding to the largest or most important eigenvalues. We can identify interesting features of head and concentration evolutions in the figure. The first plot in Figure 2-5(a) shows gradients of head in the y direction. This corresponds to the head boundary conditions. The following plots show drawdowns of the head at the well locations, indicating the effects of well pumping on the head distributions. The first plot in Figure 2-5(b) shows an elongated solute transport path in the y direction, corresponding to constant injection of the solute and its propagation due to the head gradients in the y direction. The following plots show effects of well pumping on the solute propagations. From the figure we can see that the POD can identify the flow transport patterns and thus it is possible to represent the original high-dimensional head and concentration fields with low-dimensional subspaces spanned by those identified patterns.

2.4.3 **Prediction Using the Reduced-Order Model**

Here we use the reduced-order model to predict the evolutions of head and concentration for a specific conductivity field. The tested field is a replicate from the parameterized ensemble but is not used for the generation of the reduced-order model. Note that to generate the reduced-order model, first we need do a second-order expansion of the governing equations around the nominal conductivity and corresponding states. The nominal and tested conductivity fields are shown in Figure 2-6(a). Figure 2-6(b) and (c) show predicted head and concentration fields from the full order model and the reduced-order model. From the plots we can observe close agreement between simulations of the full order and reduced-order models, although some slight mismatches can be observed, especially for the concentration fields. The propagation of concentration fronts can be well captured by the reduced-order model. This can be further illustrated in Figure 2-7, in which the predictions of head and concentration at the well locations are shown. Although some disparities are present in the plots, the breakthrough of the solute is well captured by the reduced-order model, which is important for subsurface solute management.

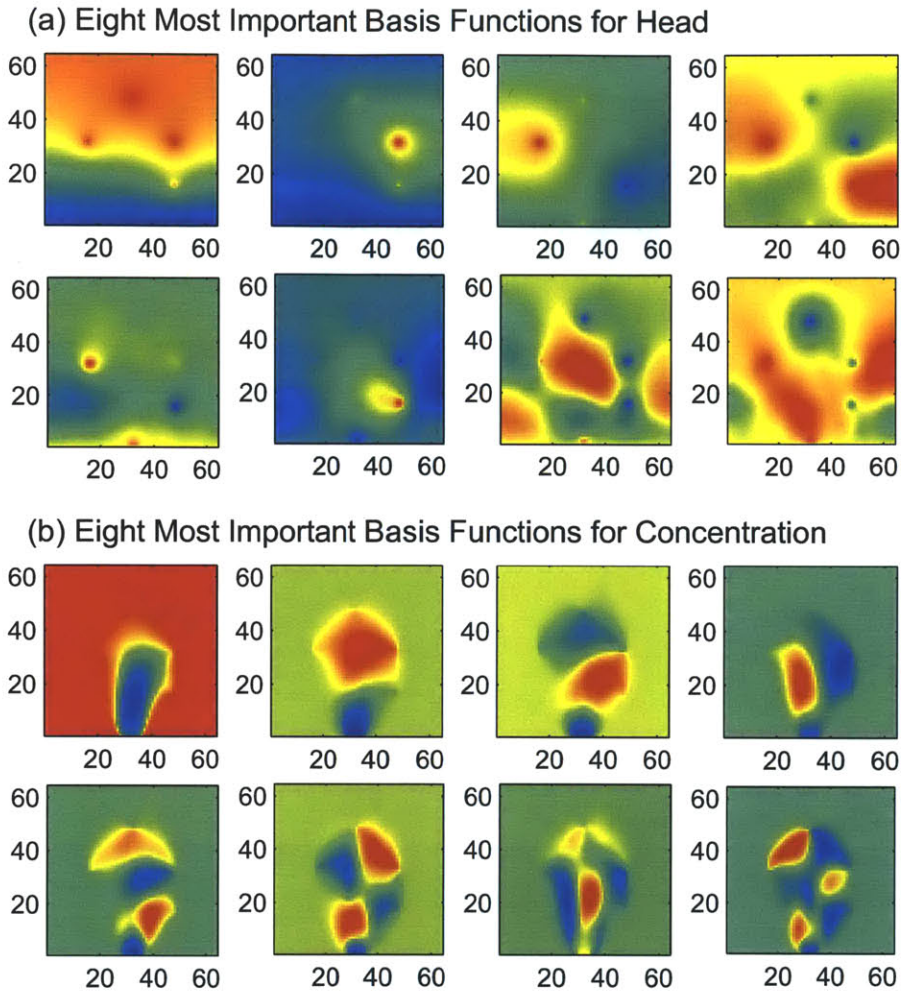

Figure 2-5: Most important projection basis vectors for head and concentration. (a) The first eight most important basis vectors for head. (b) The first eight most important basis vectors for concentration.

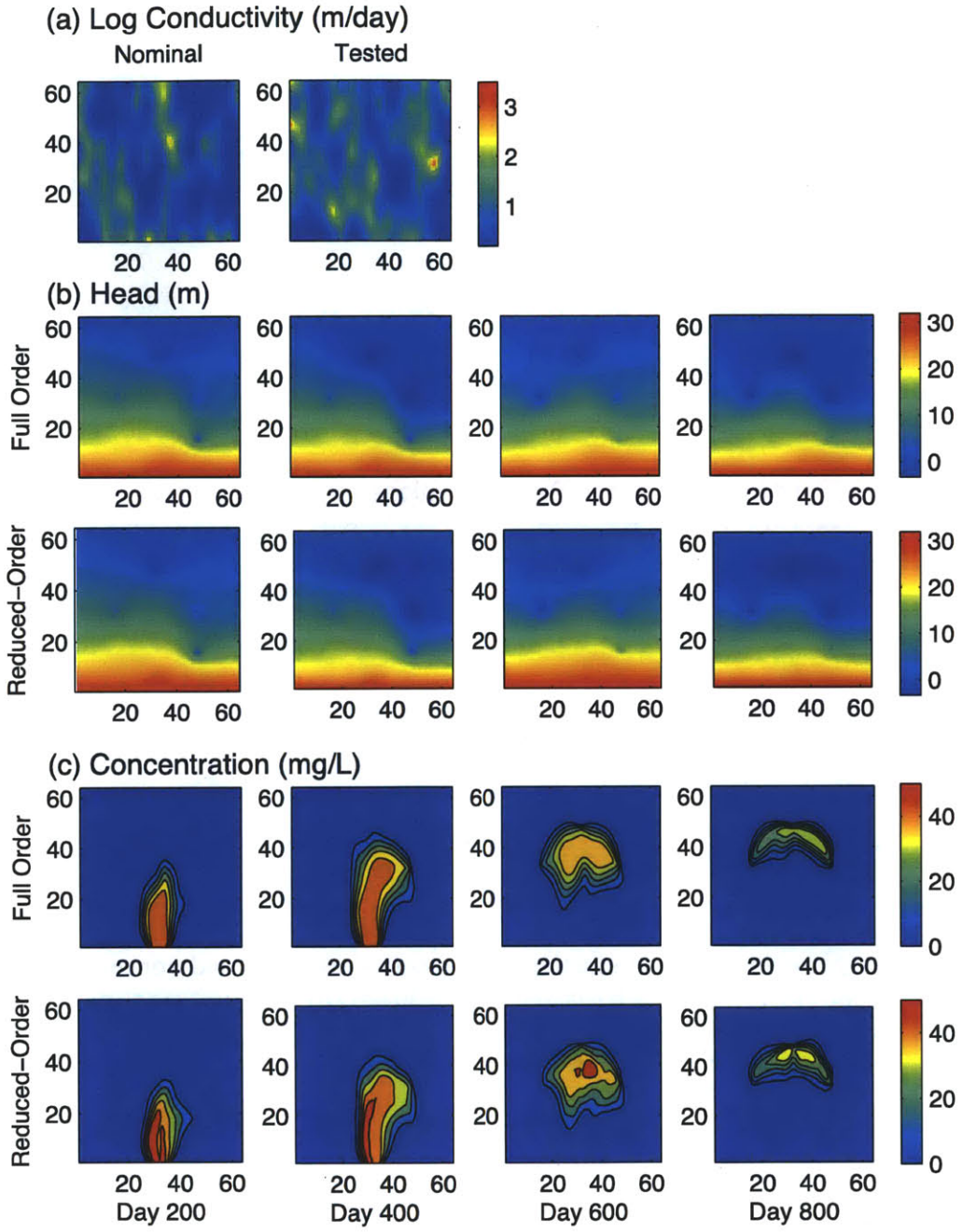

Figure 2-6: Log conductivity fields and snapshots of head and concentration simulated from the full order model and the reduced-order model for different time instances. (a) Nominal conductivity used for second-order expansion of the governing equations and the tested conductivity. (b) Snapshots of head fields simulated from the full order model and the reduced-order model for day 200, 400, 600, and 800, respectively. (c) Snapshots of concentration fields simulated from the full order model and the reduced-order model for day 200, 400, 600, and 800, respectively.

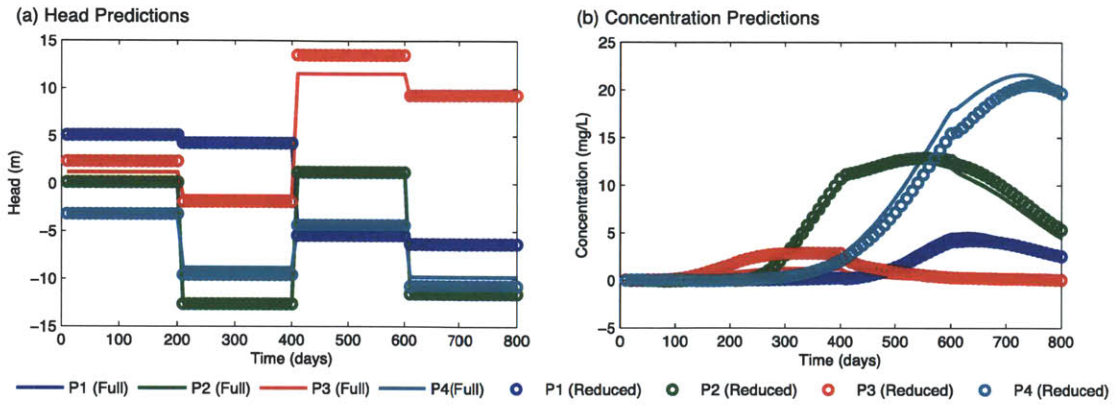

Figure 2-7: Predicted head and concentration at the four well locations for the tested replicate from the full order model and the reduced-order model. (a) Head predictions. (b) Concentration predictions.

The simulation for a single forward running of the full order model is about 19 seconds, while the simulation time using the reduced-order model is about 0.9 seconds. We can save about 95% of the time when using the reduced-order model, which is very attractive for simulations of large-scale problems.

2.4.4 **Uncertainty Propagation for the Ensemble**

The section assesses uncertainty propagation for the ensemble with full order and reduced-order modeling. Figure 2-8 illustrates the head and concentration predictions at the four well locations for the replicates in the ensemble. As shown in the figure, the spreads in the predictions are significant, indicating significant uncertainty in model parameters. Comparing the full order and reduced-order predictions, we can barely find significant differences. This indicates the reduced-order can produce comparable predictions for the ensemble.

To further illustrate the ability of the reduced-order model to assess uncertainty propagation for the ensemble, we generate the histograms of the head and concentrations predictions on day 600 at the four well locations for the ensemble as shown in Figure 2-9. Clearly the probability distribution of the reduced-order forecasts matches that of the full order forecasts quite well, indicating the effectiveness of the reduced-order model to propagate the uncertainty in the ensemble.

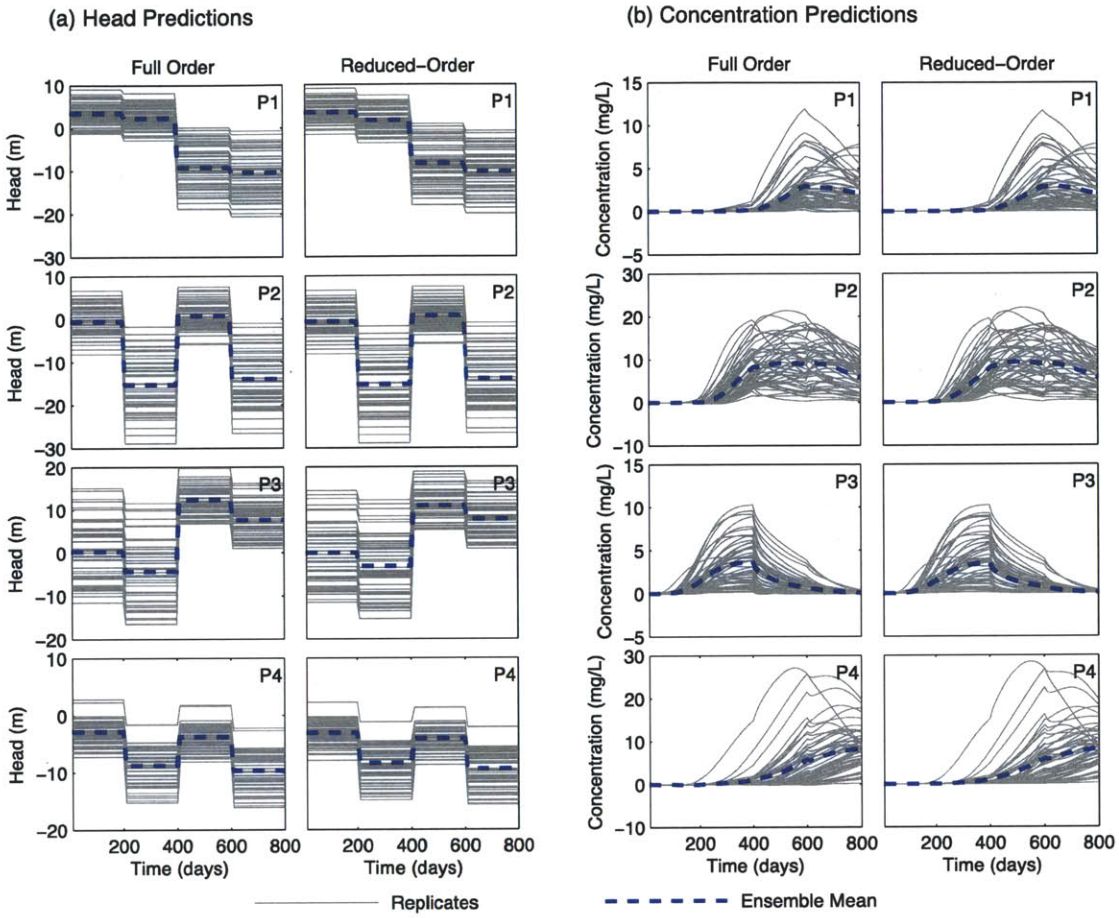

Figure 2-8: Predicted head and concentration at the four well locations for the ensemble from the full order model and the reduced-order model. (a) Head predictions for each replicate with blue lines indicating the mean over the ensemble. (b) Concentration predictions for each replicate.

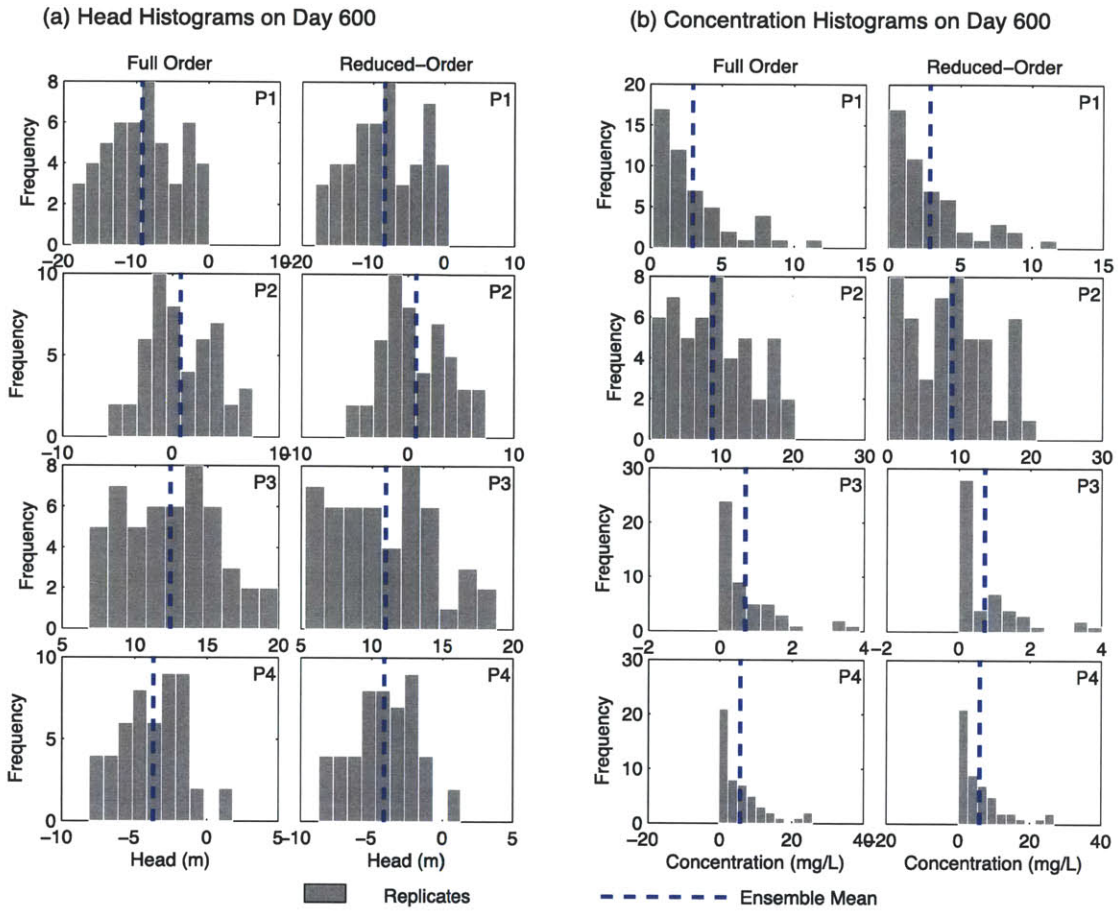

Figure 2-9: Histograms for head and concentration predictions on day 600 at the four well locations by the full order model and the reduced-order model. (a) Head histograms for the replicates in the ensemble with blue lines indicating the mean over the ensemble. (b) Concentration histograms for the replicates in the ensemble.

2.4.5 Error Quantification for the Ensemble

Since the second order expansion of the full order model is exact, errors arise in the reduced-order simulations for two main reasons: the reduction in the parameter space and the reduction in the state space. Note that here we separate these two sources of errors by using the reconstructed conductivity fields from DCT parameterization as inputs to the full order model. Errors from reduction in the parameter space can then be neglected. The accuracy of the reduced-order simulations depend merely on the

ability of the POD basis vectors of the states to span the state spaces of interest, that is the spaces corresponding to various parameter inputs.

Here we quantify the simulation errors by defining the following variables which represent the average errors in head and concentration at well locations over the whole simulation horizon [64]:

$$\varsigma_h = \frac{1}{N_w}\sum_{i=1}^{N_w}\left(\frac{\sum_{j=1}^{N_T}\left|h_{i,j}^r - h_{i,j}^f\right|}{\sum_{j=1}^{N_T}\left|h_{i,j}^f\right|}\right)$$
$$\varsigma_c = \frac{1}{N_w}\sum_{i=1}^{N_w}\left(\frac{\sum_{j=1}^{N_T}\left|c_{i,j}^r - c_{i,j}^f\right|}{\sum_{j=1}^{N_T}\left|c_{i,j}^f\right|}\right) \tag{2.14}$$

where ς_h and ς_c represent errors in head and concentration, respectively. N_w is the number of wells, which is four in our case, and N_T is the total number of simulation steps. $h_{i,j}^f$ and $c_{i,j}^f$ are predicted head and concentration from the full order model at well i for time step j, while $h_{i,j}^r$ and $c_{i,j}^r$ are predicted head and concentration from the reduced-order order model at well i for time step j. Those two variables are good indicators for the accuracy of the reduced-order model for two reasons. First, in the application of ensemble updating of the uncertain parameters, the head and concentration data at the well locations are the primary sources of data for the conditioning process. Second, in subsurface flow management, accurate predictions of solute or oil breakthrough are essential for accurate evaluations of the operation performance.

To demonstrate the ability of the reduced-order model to predict head and concentration evolutions on an ensemble base, we calculate the errors defined in (2.14) for each replicate in the ensemble as shown in Figure 2-3(b). The resulting errors are shown in the histograms of Figure 2-10(a). From the figure we can see that the majority of the replicates have less than 10% errors in head. The concentration predictions are less accurate than the head predictions. One reason is that we didn't include deriv-

atives of the concentration with respective to the conductivity in the snapshots matrices.

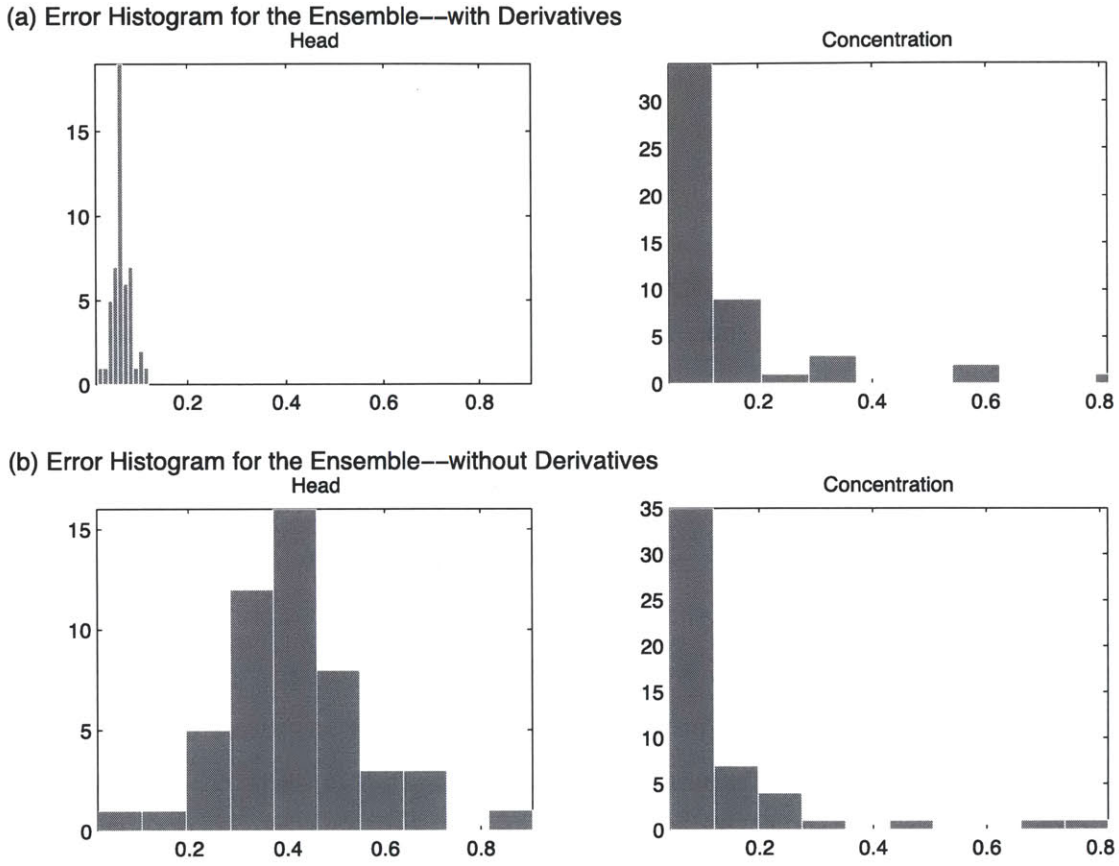

Figure 2-10: Error histograms for the ensemble. (a) Error histograms for the ensemble with derivatives in the snapshots. (b) Error histograms for the ensemble without derivatives in the snapshots.

To illustrate the importance of including the derivatives in the process of generating the reduced-order model, we construct a second reduced-order model in which the POD basis vectors are calculated purely based on snapshots of state solutions. The error histograms for this reduced-order model are shown in Figure 2-10(b). Clearly, the predictions of head evolutions from the reduced-order model are much poorer than those of the original one. For concentration predictions we don't observe much improvement by including derivatives of the head and velocity with respect to the conductivity. This indicates that errors in concentration predictions result mainly from the incapability of the POD basis of the concentration to span the space of interest tho-

roughly. It is evident the derivatives of the states with respect to parameters can improve the accuracy of the reduced-order model in a way that the resulting POD basis vectors can span more thoroughly the state spaces corresponding to various parameter changes.

2.5 Conclusion

In this chapter we constructed a reduced-order model that has reduced representations in both parameter and state spaces such that it can incorporate high-dimensional parameter changes as well as reduce the significant computational burden for large-scale problems. Reduced-order models for large-scale problems have been intensively investigated in the literature. However, it is still difficult to incorporate high-dimensional parameter changes into reduced-order models. Here, we addressed this problem by expanding the governing equations of subsurface solute transport around nominal parameters as well as nominal solutions. The resulting expanded equations can then incorporate reduced representations of parameters and states explicitly. Uncertain hydraulic conductivity is parameterized using the discrete cosine transform (DCT). This enables the parameter dimension to be dramatically reduced while still retaining important geological features. The state space reduction is done through the POD method.

Numerical examples in this chapter show that the DCT basis vectors can capture geological features of the uncertain conductivity fields, and the POD basis can capture temporal head and concentration patterns. The numerical examples also show the ability of the reduced-order model to predict head and concentration evolutions for a modified conductivity field that is significantly different from the nominal field. The efficiency of the reduced-order model can be illustrated by comparing the computation time of a single forward simulation with the full order model. It is shown that the reduced-order model can achieve 95% reduction in computation time. The histograms of the head and concentration predictions illustrate the ability of the reduced-order

model to propagate the uncertainty in the ensemble forward in time. To further validate the ability of the reduced-order model for head and concentration predictions for various conductivity configurations, an error analysis was performed for an ensemble generated using Gaussian indicator simulations. The results demonstrate the robustness of the reduced-order model for the ensembles with significant parameters changes and the importance of including derivatives of states with respect to parameters during the generation of the reduced-order model. The robustness and efficiency of the reduced-order model highlight the fact that it is a very promising alternative in the forward simulations of large-scale statistical inversion problems. This will be further illustrated in the next chapter.

2.6 References

[1] J. D. Jansen, S. D. Douma, D. R. Brouwer, P. M. J. v. d. Hof, O. H. Bosgra, and A. W. Heemink, "Closed-loop reservoir management," presented at the the 2009 SPE Reservoir Simulation Symposium, the Woodlands, Texas, 2009.

[2] A. C. Antoulas, "An overview of approximation methods for large-scale dynamical systems," *Annual Reviews in Control,* vol. 29, pp. 181-190, 2005.

[3] A. Antoulas, D. Sorensen, K. A. Gallivan, P. Van Dooren, A. Grama, C. Hoffmann, and A. Sameh, "Model reduction of large-scale dynamical systems," *Computational Science - Iccs 2004, Pt 3, Proceedings,* vol. 3038, pp. 740-747, 2004.

[4] R. L. Cooley, "Incorporation of Prior Information on Parameters into Non-Linear Regression Groundwater-Flow Models .2. Applications," *Water Resources Research,* vol. 19, pp. 662-676, 1983.

[5] G. Evensen, "Sequential Data Assimilation with a Nonlinear Quasi-Geostrophic Model Using Monte-Carlo Methods to Forecast Error Statistics," *Journal of Geophysical Research-Oceans,* vol. 99, pp. 10143-10162, May 15 1994.

[6] P. Jacquard, "Permeability Distribution From Field Pressure Data," *SPE Journal,* vol. 5, pp. 281-294, 1965.

[7] S. I. Aanonsen, "Efficient history matching using a multiscale technique," *Spe Reservoir Evaluation & Engineering,* vol. 11, pp. 154-164, Feb 2008.

[8] B. Jafarpour and D. B. McLaughlin, "Reservoir Characterization With the Discrete Cosine Transform," *Spe Journal,* vol. 14, pp. 182-201, Mar 2009.

[9] B. Jafarpour and D. B. McLaughlin, "History matching with an ensemble Kalman filter and discrete cosine parameterization," *Computational Geosciences,* vol. 12, pp. 227-244, Jun 2008.

[10] E. Grimme, "Krylov Projection Methods for Model Reduction," PhD, University of Illinois at Urbana-Champaign, 1997.

[11] Z. J. Bai, "Krylov subspace techniques for reduced-order modeling of large-scale dynamical systems," *Applied Numerical Mathematics,* vol. 43, pp. 9-44, Oct 2002.

[12] K. Gallivan, E. Grimme, and P. Vandooren, "Pade Approximation of Large-Scale Dynamic Systems with Lanczos Methods," *Proceedings of the 33rd Ieee Conference on Decision and Control, Vols 1-4,* pp. 443-448, 1994.

[13] P. Feldmann and R. W. Freund, "Efficient Linear Circuit Analysis by Pade-Approximation Via the Lanczos Process," *IEEE Transactions on Computer-Aided Design of Integrated Circuits and Systems,* vol. 14, pp. 639-649, May 1995.

[14] P. Feldmann and R. W. Freund, "Reduced-order modeling of large linear subcircuits via a block Lanczos algorithm," *32nd Design Automation Conference, Proceedings 1995,* pp. 474-479, 1995.

[15] L. M. Silveira, M. Kamon, I. Elfadel, and J. White, "A coordinate-transformed Arnoldi algorithm for generating guaranteed stable reduced-order models of RLC circuits," *1996 Ieee/Acm International Conference on Computer-Aided Design - Digest of Technical Papers,* pp. 288-294, 1996.

[16] I. M. Elfadel and D. D. Ling, "A block rational Arnoldi algorithm for multipoint passive model-order reduction of multiport RLC networks," *1997 Ieee/Acm International Conference on Computer-Aided Design - Digest of Technical Papers,* pp. 66-71, 1997.

[17] A. Odabasioglu, M. Celik, and L. T. Pileggi, "PRIMA: Passive reduced-order interconnect macromodeling algorithm," *1997 Ieee/Acm International Conference on Computer-Aided Design - Digest of Technical Papers,* pp. 58-65, 1997.

[18] K. Glover, "All Optimal Hankel-Norm Approximations of Linear-Multivariable Systems and Their L Infinity-Error Bounds," *International Journal of Control,* vol. 39, pp. 1115-1193, 1984.

[19] P. Benner, "A MATLAB repository for model reduction based on spectral projection," *2006 IEEE Conference on Computer-Aided Control System Design, Vols 1 and 2,* pp. 19-24, 2006.

[20] J.-R. Li, "Model reduction of large linear systems via low rank system gramians," Ph D, Massachusetts Institute of Technology, 2000.

[21] B. C. Moore, "Principal Component Analysis in Linear-Systems - Controllability, Observability, and Model-Reduction," *Ieee Transactions on Automatic Control,* vol. 26, pp. 17-32, 1981.

[22] P. Benner, E. S. Quintana-Orti, and G. Quintana-Orti, "Computing optimal Hankel norm approximations of large-scale systems," *2004 43rd Ieee Conference on Decision and Control (Cdc), Vols 1-5,* pp. 3078-3083, 2004.

[23] M. J. Rewienski, "A trajectory piecewise-linear approach to model order reduction of nonlinear dynamical systems," Ph D, Massachusetts Institute of Technology, 2003.

[24] L. Sirovich, "Turbulence and the Dynamics of Coherent Structures .1. Coherent Structures," *Quarterly of Applied Mathematics,* vol. 45, pp. 561-571, Oct 1987.

[25] X. Ma and G. E. Karniadakis, "A low-dimensional model for simulating three-dimensional cylinder flow," *Journal of Fluid Mechanics,* vol. 458, pp. 181-190, May 10 2002.

[26] M. Bergmann, L. Cordier, and J. P. Brancher, "Optimal rotary control of the cylinder wake using proper orthogonal decomposition reduced-order model," *Physics of Fluids,* vol. 17, Sep 2005.

[27] J. Weller, E. Lombardi, M. Bergmann, and A. Iollo, "Numerical methods for low-order modeling of fluid flows based on POD," *International Journal for Numerical Methods in Fluids,* vol. 63, pp. 249-268, May 20 2010.

[28] M. Couplet, C. Basdevant, and P. Sagaut, "Calibrated reduced-order POD-Galerkin system for fluid flow modelling," *Journal of Computational Physics,* vol. 207, pp. 192-220, Jul 20 2005.

[29] S. Lall, J. E. Marsden, and S. Glavaski, "A subspace approach to balanced truncation for model reduction of nonlinear control systems," *International Journal of Robust and Nonlinear Control,* vol. 12, pp. 519-535, May 2002.

[30] K. Willcox and J. Peraire, "Balanced model reduction via the proper orthogonal decomposition," *Aiaa Journal,* vol. 40, pp. 2323-2330, Nov 2002.

[31] C. W. Rowley, "Model reduction for fluids, using balanced proper orthogonal decomposition," *International Journal of Bifurcation and Chaos,* vol. 15, pp. 997-1013, Mar 2005.

[32] J. H. Chen and S. M. Kang, "An algorithm for automatic model-order reduction of nonlinear MEMS devices," *Iscas 2000: Ieee International Symposium on Circuits and Systems - Proceedings, Vol Ii,* pp. 445-448, 2000.

[33] Y. Chen and J. White, "A quadratic method for nonlinear model order reduction," *2000 International Conference on Modeling and Simulation of Microsystems, Technical Proceedings,* pp. 477-480, 2000.

[34] M. J. Korenberg and I. W. Hunter, "The identification of nonlinear biological systems: Volterra kernel approaches," *Annals of Biomedical Engineering,* vol. 24, pp. 250-268, Jul-Aug 1996.

[35] C. Brennan, M. Condon, and R. Ivanov, "Model order reduction of nonlinear dynamical systems," *Progress in Industrial Mathematics at ECMI 2004,* vol. 8, pp. 114-118, 2006.

[36] D. Vasilyev, M. Rewienski, and J. White, "A TBR-based trajectory piecewise-linear algorithm for generating accurate low-order models for nonlinear analog circuits and MEMS," *40th Design Automation Conference, Proceedings 2003,* pp. 490-495, 2003.

[37] D. Gratton, "Reduced-order, trajectory piecewise-linear models for nonlinear computational fluid dynamics," S m, Massachusetts Institute of Technology, 2004.

[38] N. Dong and J. Roychowdhury, "General-purpose nonlinear model-order reduction using piecewise-polynomial representations," *IEEE Transactions on*

Computer-Aided Design of Integrated Circuits and Systems, vol. 27, pp. 249-264, Feb 2008.

[39] H. Aling, R. L. Kosut, A. EmamiNaeini, and J. L. Ebert, "Nonlinear model reduction with application to rapid thermal processing," *Proceedings of the 35th Ieee Conference on Decision and Control, Vols 1-4,* pp. 4305-4310, 1996.

[40] E. S. Hung and S. D. Senturia, "Generating efficient dynamical models for microelectromechanical systems from a few finite-element simulation runs," *Journal of Microelectromechanical Systems,* vol. 8, pp. 280-289, Sep 1999.

[41] Y. C. Zhang, M. A. Henson, and Y. G. Kevrekidis, "Nonlinear model reduction for dynamic analysis of cell population models," *Chemical Engineering Science,* vol. 58, pp. 429-445, Jan 2003.

[42] K. Kunisch and S. Volkwein, "Control of the Burgers equation by a reduced-order approach using proper orthogonal decomposition," *Journal of Optimization Theory and Applications,* vol. 102, pp. 345-371, Aug 1999.

[43] A. Theodoropoulou, R. A. Adomaitis, and E. Zafiriou, "Model reduction for optimization of rapid thermal chemical vapor deposition systems," *Ieee Transactions on Semiconductor Manufacturing,* vol. 11, pp. 85-98, Feb 1998.

[44] J. A. Atwell and B. B. King, "Proper orthogonal decomposition for reduced basis feedback controllers for parabolic equations," *Mathematical and Computer Modelling,* vol. 33, pp. 1-19, Jan-Feb 2001.

[45] Q. Du, V. Faber, and M. Gunzburger, "Centroidal Voronoi tessellations: Applications and algorithms," *Siam Review,* vol. 41, pp. 637-676, Dec 1999.

[46] S. S. Ravindran, "Reduced-Order Adaptive Controllers for Fluid Flows Using POD," *Journal of Scientific Computing,* vol. 15, pp. 457-478, 2000.

[47] M. Bergmann, L. Cordier, and J. P. Braucher, "Drag minimization of the cylinder wake by trust-region proper orthogonal decomposition," *Active Flow Control,* vol. 95, pp. 309-324, 2007.

[48] T. Bui-Thanh, K. Willcox, and O. Ghattas, "Model Reduction for Large-Scale Systems with High-Dimensional Parametric Input Space," *SIAM Journal on Scientific Computing,* vol. 30, pp. 3270-3288, 2007.

[49] B. Bond and L. Daniel, "Parameterized model order reduction of nonlinear dynamical systems," *Iccad-2005: International Conference on Computer Aided Design, Digest of Technical Papers,* pp. 487-494, 2005.

[50] D. Amsallem and C. Farhat, "Interpolation method for adapting reduced-order models and application to aeroelasticity," *Aiaa Journal,* vol. 46, pp. 1803-1813, Jul 2008.

[51] R. Markovinovic, E. L. Geurtsen, and J. D. Jansen, "Subspace identification of low-order reservoir models," *Computational Methods in Water Resources, Vols 1 and 2, Proceedings,* vol. 47, pp. 281-288, 2002.

[52] T. Heijn, R. Markovinovic, and J. D. Jansen, "Generation of low-order reservoir models using system-theoretical concepts," *Spe Journal,* vol. 9, pp. 202-+, Jun 2004.

[53] J. F. M. van Doren, R. Markovinovic, and J. D. Jansen, "Reduced-order optimal control of water flooding using proper orthogonal decomposition," *Computational Geosciences,* vol. 10, pp. 137-158, Mar 2006.

[54] M. A. Cardoso and L. J. Durlofsky, "Use of Reduced-Order Modeling Procedures for Production Optimization," *Spe Journal,* vol. 15, pp. 426-435, Jun 2010.

[55] M. A. Cardoso and L. J. Durlofsky, "Linearized reduced-order models for subsurface flow simulation," *Journal of Computational Physics,* vol. 229, pp. 681-700, Feb 1 2010.

[56] R. E. Ewing, "Finite element methods for nonlinear flows in porous media," *Computer Methods in Applied Mechanics and Engineering,* vol. 51, pp. 421-439, 1985.

[57] R. E. Ewing and R. F. Heinemann, "Mixed finite element approximation of phase velocities in compositional reservoir simulation," *Computer Methods in Applied Mechanics and Engineering,* vol. 47, pp. 161-175, 1984.

[58] C. Zheng and G. D. Bennett, *Applied contaminant transport modeling*, 2nd ed. New York: Wiley-Interscience, 2002.

[59] I. Galligani, E. Magenes, Istituto per le applicazioni del calcolo., and Laboratorio di analisi numerica., Eds., *Mathematical aspects of finite element methods: proceedings of the conference held in Rome, 10-12 December 1975* (Lecture notes in mathematics 606. New York: Springer-Verlag, 1977, p.^pp. Pages.

[60] L. Sirovich, "Turbulence and the dynamics of coherent structures. I: Coherent structures. II: Symmetries and transformations. III: Dynamics and scaling," *Quarterly of Applied Mathematics,* vol. 45, pp. 561-590, 1987.

[61] K. Carlberg and C. Farhat, "A low-cost, goal-oriented 'compact proper orthogonal decomposition' basis for model reduction of static systems," *International Journal for Numerical Methods in Engineering,* p. in press, 2010.

[62] B. Jafarpour, "Oil reservoir characterization using ensemble data assimilation," PhD, Massachusetts Institute of Technology, 2008.

[63] P. Goovaerts, *Geostatistics for natural resources evaluation*. New York: Oxford University Press, 1997.

[64] M. A. Cardoso, L. J. Durlofsky, and P. Sarma, "Development and application of reduced-order modeling procedures for subsurface flow simulation," *International Journal for Numerical Methods in Engineering,* vol. 77, pp. 1322-1350, 2009.

Chapter 3

Application of Reduced-Order Modeling for Ensemble Conditioning

3.1 Introduction

Subsurface flow modeling has been widely used for the management of subsurface hydrological and energy resources. Subsurface flow and solute transport are often simulated using discretized mathematical models with model parameters and external forcing that govern the transport process. Relevant parameters include hydraulic properties such as hydraulic conductivity and porosity and relevant forcing variables include well pumping. The complexity associated with the spatial heterogeneity of subsurface hydraulic properties, together with the high cost of data acquisition and inconvenient access to in-situ measurements, leads to large uncertainty and inevitable causes errors in the predictions of system models for investigating subsurface problems [1, 2]. In order to address this problem uncertain parameters are inferred, as much as possible, from measurements of related states, such as pressure and solute concentration. This inference or estimation process is typically posed as an inverse problem.

Stochastic inversion methods have become increasingly popular for solving subsurface inverse problems in subsurface modeling due to their capabilities for dealing

with ill-posedness and nonuniqueness problems. These methods explicitly account for uncertainty in parameters and predictions and are useful for assessing how measurements can improve forecasts through better estimation of poorly known parameters. The objective of most stochastic inverse methods is to derive a posteriori (or conditional) probability distributions for uncertain parameters. These distributions, which summarize all available knowledge about the parameters of interest, are obtained by conditioning prior (or unconditional) probability distributions on relevant measurements. In complex problems involving spatial heterogeneity it is useful to describe probabilities in terms of ensembles of random replicates of the uncertain variables rather than in terms of closed-form probability functions. An example is the ensemble Kalman filter (EnKF) [3], which can be viewed as a Monte Carlo version of the classical Kalman filter. The EnKF uses prior and a posteriori ensembles to represent statistics, such as the means and covariances of uncertain parameters and states. The EnKF is a recursive estimation method that has been effectively applied to large-scale nonlinear inverse problems.

There are several variants of the EnKF, of which the square root filter [3, 4] is probably the most widely used one with successful applications in the areas of weather forecasting, oceanography, and petroleum [5-11]. In subsurface modeling the EnKF is usually used for identification of uncertain hydraulic properties, such as conductivity and porosity. The success of parameter estimation by the EnKF in subsurface modeling is largely attributed to the strong spatial correlations in hydraulic properties as well as strong correlations between the parameters and system states such as fluid pressure and velocity [12]. The EnKF can be divided into two separate steps: 1) the forecast step, in which the model equations are used to propagate replicates of system states forward in time, and 2) the update step, in which the forecast replicates are updated with measurements. The update step is based on the first and second order moments of the probability distribution represented by the ensemble. This reliance on first and second moment implicitly assumes that the relevant prior and a posteriori probability distributions are Gaussian [5].

In the subsurface inverse problems of interest here the forecast step of the EnKF, requires many evaluations of large systems of partial differential equations. This poses significant computational challenges and is a serious limitation for practical applications of the EnKF. Most practical subsurface applications use a relatively small ensemble, in which the number of replicates is far less than the dimension of states, to calculate the covariance matrices that are essential for the EnKF update. A small sample size could also seriously deteriorate the performance of the EnKF update due to the influence of sample variability [13, 14]. The update is restricted to the space spanned by the members of forecast ensemble. Sampling errors due to small ensemble size can give spurious correlations between observations and model states. In such cases the EnKF can incorrectly update the state variables in regions of no real influence by the observations. This causes the ensemble to diverge from the true parameters and states. Localization [15, 16] is an empirical process that addresses divergence by imposing constraints on the covariance estimate. Localization can increase the rank of the update equation [17, 18]. However, it can also distort the physical relationships between different physical variables that are implicit in properly estimated unlocalized covariances [18]. Covariance inflation [13] is another empirical strategy for addressing problems created by small sample size. Inflation artificially increases the variance of the ensemble by moving the ensemble members far from the ensemble mean [19]. This method can avoid filter divergence caused by insufficient covariance but suffers the same problem as the localization method since it can violate physical balances that should be conveyed through the parameter and state covariances.

The best option for addressing problems created by small ensembles is to reduce the significant computational burden posed by the EnKF by using model order reduction techniques that replace the original high dimensional forecast model with much lower dimensional approximate model that preserves the key input-output properties of the system. Most practical model order reduction techniques are projection-based methods, which derive the reduced-order model by projecting the high-dimensional governing equations onto the subspace spanned by basis vectors [20]. The basis can

be generated by several techniques, including Krylov subspace methods [21-23], balanced truncation and its variants [24, 25], and proper orthogonal decomposition (POD) [26-28].

Several methods have been proposed to generate basis vectors that insure the reduced-order model is effective and accurate over the entire parameter space of interest. These methods include POD and Krylov-based sampling methods [29, 30], greedy sampling approaches [31, 32], and interpolation methods [33, 34]. In most studies, the model reduction process focuses only on the system states. However, reduction of the number of parameters is also important, especially in subsurface applications, where uncertain parameters vary dramatically over space.

A recent paper by Lieberman et al. [35] addressed the high cost of repeated evaluations of large-scale models, as well as the difficulty of effectively exploring the uncertain space due to high-dimensional input parameter spaces, by constructing a reduced-order model that can accept low-dimensional parameter inputs. The parameter reduction was carried out separately from the state space reduction. In their study, a Markov Chain Monte Carlo (MCMC) procedure was used for uncertainty quantification. The reduced parameter basis was derived from sampled parameters incorporating prior information by solving an optimization problem that minimized output errors between full order and reduced-order models and penalized parameters of low probability. The reduced-order model was applied to 1D and 2D steady flow problems in porous media with uncertain hydraulic conductivity. The results from their experiments are promising for relatively smooth conductivity fields. However, uncertainty propagation for transport of solute or other components and preservation of geological features were not addressed in their study.

In this chapter, we consider uncertainty quantification for subsurface modeling with channelized geological features. We apply a reduced-order model derived using the concepts outlined in Chapter 2 to the forecast step of the EnKF. In Section 3.2, we provide a brief overview of the EnKF as well as the method used to generate the robust reduced-order model. The procedure to embed the reduced-order model into the

EnKF is also introduced. In Section 3.3, we evaluate the performance of the EnKF combined with the reduced-order model by considering several unsteady solute transport problems. In Section 3.4, we conclude this chapter.

3.2 Methodology

3.2.1 The Ensemble Kalman Filter

Bayes rule relates the a posteriori probability distribution of uncertain states and parameters conditioned on measurements to the prior probability distribution and the likelihood function, which describes measurement uncertainty. Sequential application of Bayes rule is often used in real-time estimation of states and parameters of a dynamic system. For linear Gaussian systems, the Kalman filter [36] derives updating equations for the mean and error covariance of the a posteriori distribution. For nonlinear systems, which generally have non-Gaussian distributions, the EnKF [3, 37] uses Monte Carlo methods to approximate these moments..

Assume there are M replicates in the ensemble. The EnKF can be divided into two stages at each time step: 1) a forecast of the new state variable $\mathbf{x}_{t|t-1}^{j}$ for replicate j at current time t based on the states and parameters at time $t-1$ using the system model; and 2) an update of the state variable to obtain analysis replicate $\mathbf{x}_{t|t}^{j}$ based on the Kalman gain and the perturbed observation ensemble $\left\{\mathbf{z}_{t|t-1}^{j}\right\}_{j=1}^{M}$ at time t. Assuming there is no model error, the forecast step proceeds by applying the system equations to each of the replicates [12]

$$\begin{aligned} 0 &= \mathbf{F}_{t-1}^{j}\left(\mathbf{x}_{t|t-1}^{j}, \mathbf{x}_{t-1|t-1}^{j}, \mathbf{u}_{t-1}, \boldsymbol{\alpha}_{t-1|t-1}^{j}\right) \\ \mathbf{z}_{t|t-1}^{j} &= \mathbf{g}\left(\mathbf{x}_{t|t-1}^{j}\right) + \mathbf{v}_{t}^{j} \end{aligned} \tag{3.1}$$

where $j = 1, \ldots, M$ denotes the j-th replicate in the ensemble, $\mathbf{u}_{t-1}$ is a nonrandom input or control vector, $\boldsymbol{\alpha}_{t-1|t-1}^{j}$ is the updated parameter replicate at time $t-1$, $\mathbf{v}_{t}^{j}$ is the j-th realization of measurement errors, and $\mathbf{F}_{t-1}^{j}$ and $\mathbf{g}(\cdot)$ are the nonlinear state transition function and measurement operator that relates the states and measure-

ments. Note that we write the state equation using an implicit rather than an explicit time discretization.

In the applications of interest here the function $\mathbf{g}(\cdot)$ is reduced to a linear operator that multiplies the state vector by a selection matrix that specifies where measurements are located. Also, we need to generate conditional ensembles for both the uncertain states and parameters. This can be easily accomplished by augmenting the state vector with uncertain parameters, that is

$$\left(\mathbf{x}_t^j\right)^{\text{aug}} = \begin{bmatrix} \mathbf{x}_t^j \\ \boldsymbol{\alpha}_t^j \end{bmatrix} \tag{3.2}$$

where $\boldsymbol{\alpha}_t^j$ is the parameter vector at time t. In this case the system of state equations is also be augmented by linear parameter transition equations of the form:

(3.3)

Once the ensemble forecast $\left\{\mathbf{x}_{t|t-1}^j\right\}_{j=1}^M$ as well as the perturbed observations $\left\{\mathbf{z}_{t|t-1}^j\right\}_{j=1}^M$ is obtained we can write the update equation for each replicate as [38]:

$$\left(\mathbf{x}_{t|t}^j\right)^{\text{aug}} = \left(\mathbf{x}_{t|t-1}^j\right)^{\text{aug}} + \text{Cov}\left(\left(\mathbf{x}_{t|t-1}^j\right)^{\text{aug}}, \mathbf{z}_{t|t-1}^j\right) \cdot \text{Cov}^{-1}\left(\mathbf{z}_{t|t-1}^j, \mathbf{z}_{t|t-1}^j\right) \cdot \left(\mathbf{d}_t - \mathbf{z}_{t|t-1}^j\right) \tag{3.4}$$

where $\text{Cov}(\cdot,\cdot)$ denotes the covariance between two arguments, and $\mathbf{d}_t$ is the actual observation vector. Note that, for the original model, the augmented state vector contains the system states (such as pressure, velocity, and concentration), and the parameters (such as hydraulic conductivity.

Equations (3.1) through (3.4) together with initial conditions define a complete ensemble recursion. Note that instead of updating the mean and error covariance of the state vector, the EnKF updates individual replicates. The desired statistics can then be derived from the updated ensemble. In practice it is desirable to update the ensemble mean and the ensemble perturbations separately [4]. This approach is commonly described as the ensemble square root filter (EnSRF). A number of variants of this approach have been introduced, including the ensemble Kalman transform filter

[39], the ensemble adjustment filter [40], and the local ensemble filter [17]. Not all of the square root filters bear the desired relationship that the mean of the updated ensemble mean (computed by averaging all the replicates) is equal to the actual a posteriori mean (i.e. the ensemble mean should be unbiased). Livings et al. [41] proposed an unbiased square root filter by restricting the updating equation of the covariance matrix. An alternative approach for obtaining an unbiased estimate is to use the formulation proposed by Sakov and Oke [42]. In this work, we will choose an unbiased filter between these two versions based on their performance.

3.2.2 Parameterization and Reduced-Order Modeling

The forecast stage involves M evaluations of the system model, one for each replicate, which is usually computationally expensive. This computational burden is the bottleneck for successful applications of the EnKF to large-scale nonlinear problems. One way to overcome this problem is to include only a limited number of replicates but use some techniques such as covariance inflation [19] to prevent ensemble divergence and model errors. However, this method involves artificial manipulations and there is no guarantee of good performance of the EnKF if the prior ensemble has a large bias. In this work we try to overcome this problem by using the reduced-order model to obtain the state forecast. Since the evaluation of the reduced-order model is efficient, it's possible to generate a larger prior ensemble to achieve good performance of the EnKF.

The first step to derive the reduced-order that can be applied in the EnKF is to generate reduced representations of the states, which can be written as

$$\mathbf{x} \approx \mathbf{\Phi}_{\mathbf{x}}^{T} \hat{\mathbf{x}} \tag{3.5}$$

where $\hat{\mathbf{x}}$ is a reduced representation of the state vector $\mathbf{x}$ and has a much small dimension than $\mathbf{x}$, $\mathbf{\Phi}_{\mathbf{x}}$ is a transform matrix containing basis vectors. The basis vectors can be derived using the proper orthogonal decomposition (POD) [43].

For nonlinear systems the distribution of the states is usually non-Gaussian. The update from the traditional EnKF can be poor for non-Gaussian cases [44]. Also, for uncertainty quantification of complex geological structures inversion problems are often underdetermined. Parameterization provides a remedy for these problems by transforming non-Gaussian variables to a more nearly Gaussian variables [45] or by reducing the dimension of uncertain variables [46]. The reduced-order model used here is parameterized using the discrete cosine transform (DCT) [46], in which the uncertain parameter vector is represented by

$$\boldsymbol{\alpha} \approx \boldsymbol{\Phi}_{\alpha}^{T} \hat{\boldsymbol{\alpha}} \tag{3.6}$$

where $\hat{\boldsymbol{\alpha}}$ is a reduced representation of the parameter vector $\boldsymbol{\alpha}$ and has a much small dimension than $\boldsymbol{\alpha}$. Compared to the POD transform matrix, $\boldsymbol{\Phi}_{\alpha}$ is the DCT matrix containing constant vectors. The DCT method are more efficient, effective, and flexible compared to the other methods such as the Karhunen-Loéve transform, which needs to perform expensive singular value decomposition and is unsuitable for compression of arbitrary fields that are not well characterized by the prior ensemble [46].

By substituting equations (3.5) and (3.6) into the system model and then applying Galerkin projection, the forecast equations in (3.1) can be reduced to

$$\begin{aligned} 0 &= \hat{\mathbf{F}}_{t-1}^{j}\left(\hat{\mathbf{x}}_{t|t-1}^{j}, \hat{\mathbf{x}}_{t-1|t-1}^{j}, \mathbf{u}_{t-1}, \hat{\boldsymbol{\alpha}}_{t-1|t-1}^{j}\right) \\ \mathbf{z}_{t|t-1}^{j} &= \hat{\mathbf{g}}\left(\hat{\mathbf{x}}_{t|t-1}^{j}\right) + \mathbf{v}_{t}^{j} \end{aligned} \tag{3.7}$$

where $\hat{\mathbf{F}}_{t-1}^{j}(\cdot)$ and $\hat{\mathbf{g}}(\cdot)$ operate on the reduced state vector $\hat{\mathbf{x}}$ and parameter vector $\hat{\boldsymbol{\alpha}}$. The EnKF simultaneously updates the reduced states and reduced parameters. This is done by working with an augmented state vector, which can be written as

$$\left(\hat{\mathbf{x}}_{t}^{j}\right)^{\text{aug}} = \begin{bmatrix} \hat{\mathbf{x}}_{t}^{j} \\ \hat{\boldsymbol{\alpha}}_{t}^{j} \end{bmatrix} \tag{3.8}$$

and the updating equation is in the form of

$$\left(\hat{\mathbf{x}}_{t|t}^{j}\right)^{\text{aug}} = \left(\hat{\mathbf{x}}_{t|t-1}^{j}\right)^{\text{aug}} + \text{Cov}\left(\left(\hat{\mathbf{x}}_{t|t-1}^{j}\right)^{\text{aug}}, \mathbf{z}_{t|t-1}^{j}\right) \cdot \text{Cov}^{-1}\left(\mathbf{z}_{t|t-1}^{j}, \mathbf{z}_{t|t-1}^{j}\right) \cdot \left(\mathbf{d}_{t} - \mathbf{z}_{t|t-1}^{j}\right) \tag{3.9}$$

Detailed derivation of the reduced-order model for subsurface solute transport can be found in Chapter 2. Here we emphasize the fact that to preserve the efficiency gained from reduced-order modeling, we should avoid updating of the reduced-order model during online sequential data assimilation. Since the updated ensemble can be characterized as a weakly nonlinear combination of the forecast ensemble [5], it is expected that if the reduced-order model is valid in the space spanned by the initial ensemble, it will still be valid during the updating steps. To ensure that the reduced-order model is valid in the space spanned by the initial ensemble, both the basis vectors of the states and the parameters should spanned the spaces characterized by the initial ensemble. A good set of basis vectors for the state variables can be obtained by choosing several replicates from the initial parameter ensemble to generate snapshots of corresponding state vectors as well as derivatives of states with respect to parameters, as described in Chapter 2. This training process transmits information about the full order model through the snapshots to the reduced-order model basis so that the reduced-order model is able to capture the dominant features of the full order model. To choose DCT basis vectors properly for parameters, we should apply DCT to the whole initial ensemble and then retain only the DCT basis vectors corresponding to the largest DCT coefficients.

The resulting system equations (3.7) and (3.9) have much fewer dimensions than the full order ones and yield a better-posed inverse problem. It is anticipated that if the uncertain parameters fields are parameterized so that they preserve geological structure, we should obtain a better conditional ensemble. This will be shown in the numerical examples.

3.2.3 Implementation Issues

The whole procedure of the application of the EnKF with the reduced-order model can be divided into offline and online stages. Figure 3-1 shows that at the offline training stage, an initial ensemble of uncertain parameters is generated based on prior information. A few of the prior ensemble members are selected to generate the snap-

shots of the states and derivatives using the full order model, and then the POD basis vectors are obtained based on those snapshots. Here, the selection of training replicates is purely arbitrary. As discussed in Chapter 2, including the derivatives can improve the POD basis so that it is better able to capture the response of the states to variations in the parameters. After taking the DCT of the prior ensemble, we can select the DCT basis vectors that contribute most to spatial variability. This is done by ordering the DCT coefficients for each replicate in the ensemble, and keeping the DCT basis vectors corresponding to the first few largest coefficients for each replicate. The original discretized full order model can be expanded into second-order equations around nominal parameters and states, as described n Chapter 2. The reduced representations of states and parameters can be substituted into the second-order equations. The resulting Galerkin projection gives the reduced-order model needed for efficient online simulations.

In the EnKF experiments described in this Chapter a pre-determined control schedule gives trajectories of control variables (e.g., well pumping rates) for each control step. New measurements come in as field data in realistic applications. In the virtual experiment considered here the pre-determined control schedule and the "true" parameter values are fed into the full-order model to generate synthetic measurements that can be used for updating reduced-order parameters and states in the EnKF. The EnKF predicts the measurements that would be obtained with each of the parameter replicates and uses the errors between synthetic and predicted measurements (the "innovations") to compute the update for each replicate.

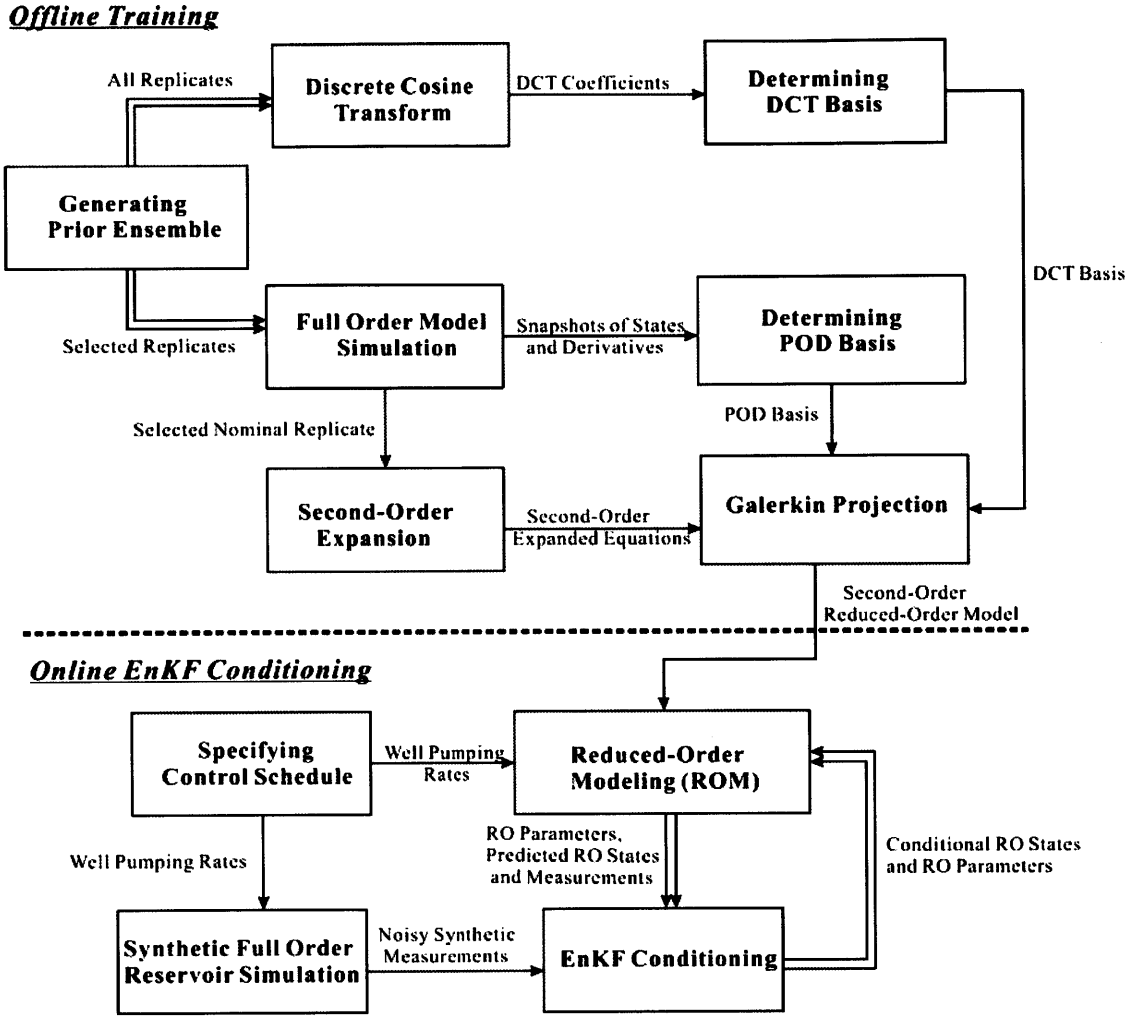

Figure 3-1: Flowchart showing offline ensemble-based generation of a robust reduced-order model with order reduction in both parameter and state spaces, and online ensemble updating of uncertain reduced-order (RO) states and reduced-order (RO) parameters. Double lines indicate multiple operations on replicates in the ensemble.

The performance of the EnKF incorporating reduced-order forward simulations can be evaluated by comparing the reduced-order and full-order updated ensembles. As shown in Figure 3-2, at the online assimilation stage, the forward simulations are based on the full-order model instead of the reduced-order model as shown in Figure 3-1.

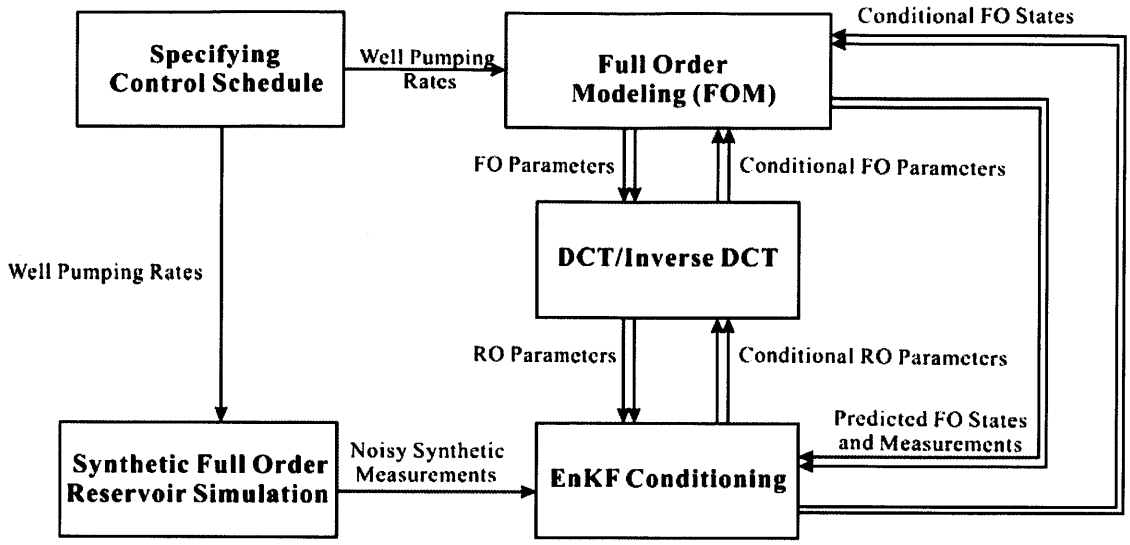

Figure 3-2: Flowchart showing online ensemble updating of uncertain full order (FO) states and full order (FO) parameters. Forward simulations are based on the full order model, and uncertain parameters are parameterized using DCT. Double lines indicate multiple operations on replicates in the ensemble.

3.3 Numerical Experiments

3.3.1 Experimental Setup

Here we consider a model of 2D non-gravitational solute transport in a porous medium. The governing equations can be written as

$$\begin{aligned} s\frac{\partial h}{\partial t} &= -\nabla\cdot\mathbf{q}+u \\ \mathbf{q} &= -k\cdot\nabla h \\ \theta\frac{\partial c}{\partial t} &= -\nabla\cdot\left(\mathbf{q}\cdot c\right)+\theta D\cdot\nabla^2 c+u\cdot c_s \end{aligned} \tag{3.10}$$

where h, $\mathbf{q}$, and c are the pressure head, velocity, and solute concentration, respectively. s, θ, and D are the specific storage, porosity, and dispersion coefficient for the aquifer, which are assumed to be constant over the whole domain. The vector u contains the pre-determined control variables, i.e. the water pump rates at each well. These are constant within each control step. The vector c_s contains the solute concentration at each pumping well.

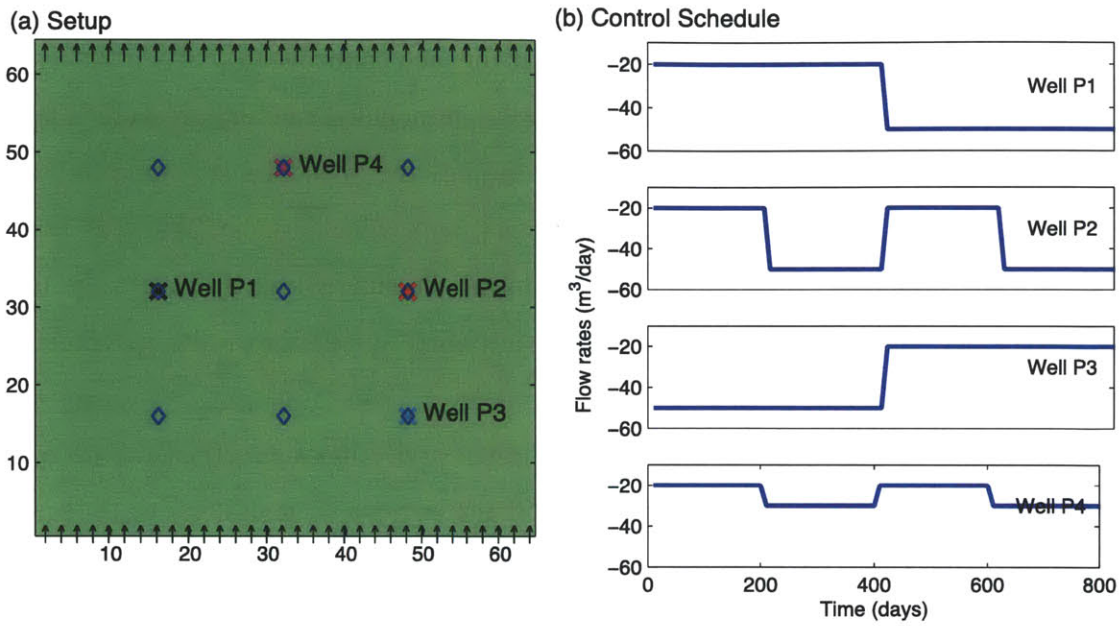

Figure 3-3: Experimental setup. (a) Simulation domain with 9 measurement locations (blue diamonds) and 4 pumping well locations: Well P1 (black cross), Well P2 (red cross), Well P3 (cyan cross), and Well P4 (magenta cross). (b) Pre-determined pumping rates for the four wells.

In this synthetic example, a 640 m×640 m×1 m porous domain is discretized into a 2D 64×64×1 uniform grid cell system. The size of each cell is 10 m×10 m×1 m. The whole domain has the constant porosity of 0.2. Figure 3-3(a) shows the simulation domain and the locations of 4 pumping wells. The length of the simulation horizon is 800 days, and the pumping rates given by the control schedule for the 4 pumping wells are illustrated in Figure 3-3(b). The simulation horizon is divided into 4 constant intervals. Each of the intervals represents a control step. The solute is injected into the domain at the mid-lower cells with a constant rate of 5 m^3/day and constant concentration of 50 mg/L for the first 400 days. Here specific storage $s = 0$ is used to represent steady-state flow conditions so the head is constant over each control step. The flow equation has no water flux boundaries on the east and west sides and constant head boundaries of 30 m and 0 m on the south and north sides. The transport equation also has no solute flux boundaries on the east and west sides, but has pre-

scribed zero solute concentration boundary conditions on the south and north sides. The dispersion coefficient is assumed to be constant over the whole domain in all direction, and thus the transport equation is linear for each control step.

The measurements at the data assimilations step include head and pressure information at 9 measurement locations indicated by the blue diamonds in Figure 3-3(a). The measurements are taken at the end of control steps, which are day 200, 400, 600, and 800, and thus there are 4 EnKF updates during the simulations. In this study, the measurements are drawn from predictions of full order simulations using a synthetic true conductivity field as described above.

The unknown parameters are the hydraulic resistivity in each cell of the discretized computational grid. An ensemble of 50 realizations of conductivity fields is generated using Gaussian indicator simulator in the Stanford SGeMS. The simulated ensemble is then parameterized by the DCT so that each high-dimensional hydraulic conductivity replicate can be represented by a corresponding set of truncated reduced-dimensional DCT coefficients. The prior ensemble is reconstructed from the simulated ensemble after DCT parameterization. The parameterization process is discussed in the following subsection. Five of the resulting replicates are shown in Figure 3-4(b). We can clearly see that the conductivity fields have high permeable and low permeable zones, which create pathways for solute transport. The resulting reconstructed ensemble is used in the experiments as the prior ensemble instead of the original ensemble.

A synthetic true conductivity fields is drawn from the same probabilistic distribution as the prior ensemble. As shown in Figure 3-4(a), the log conductivity field generated by the Gaussian indicator simulator is characterized by two high permeable channels in the middle of the domain. The true conductivity field is used in the simulations to generate noisy synthetic true measurements.

To quantify the quality of the ensemble mean of the EnKF updates during online simulations, a dissimilarity metric called Jaccard distance [47] is introduced to compare the similarity and diversity of the true conductivity field and its estimates. To

apply the Jaccard distance metric, the 2D conductivity fields are first converted to binary images. As shown in Figure 3-4(a), for the true conductivity field, the converted binary image has 1's in the cells with $\log(k)>1$, where k denotes the conductivity. All the other cells have zero values. This conversion emphasizes the similarity of channelized structures between the two different conductivity fields. For our application the Jaccard distance can be defined as

$$\chi(\kappa,\hat{\kappa})=1-\frac{|\kappa\cap\hat{\kappa}|}{|\kappa\cup\hat{\kappa}|} \tag{3.11}$$

where $\chi(\kappa,\hat{\kappa})$ is the Jaccard distance between two binary images κ and $\hat{\kappa}$. κ and $\hat{\kappa}$ are converted true conductivity field and the ensemble mean, respectively. $|\kappa\cap\hat{\kappa}|$ defines the size of the intersection of the two binary sets, which can be defined as the number of cells that both κ and $\hat{\kappa}$ denote as high permeable. $|\kappa\cup\hat{\kappa}|$ defines the size of the union of the two binary sets, which indicates the total number of cells that are denoted by either κ or $\hat{\kappa}$ as high permeable zones. By definition, a Jaccard distance of one denotes the largest dissimilarity between the true conductivity field and the ensemble mean of the EnKF updates, and lower Jaccard distance denote higher similarity between the true and the ensemble mean.

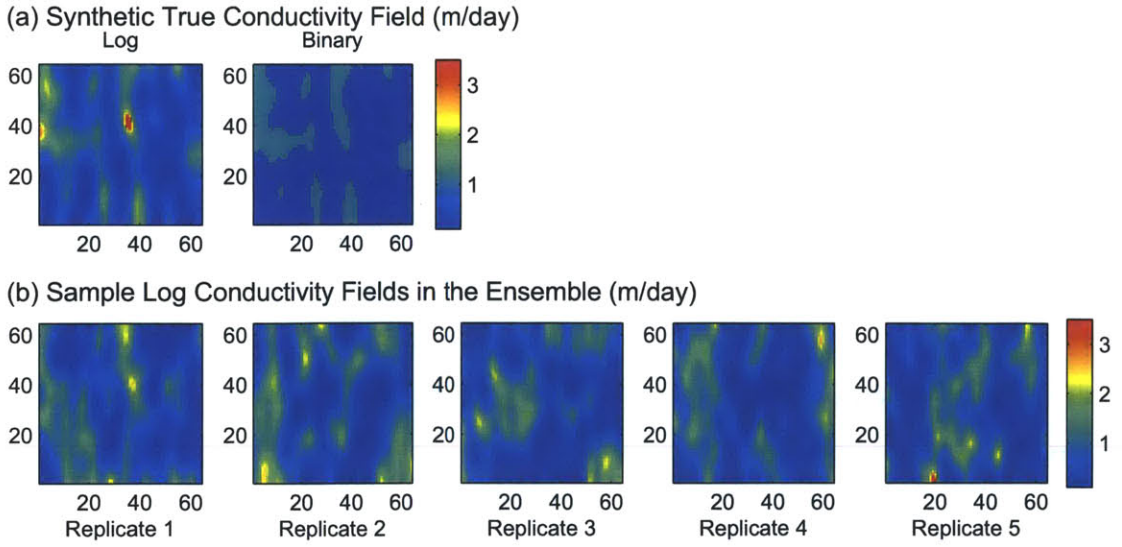

Figure 3-4: Samples of hydraulic conductivity. (a) The true conductivity field. (b) Five representative replicates from the prior ensemble.

3.3.2 Generation of the Reduced-Order Model

The reduced-order model uses reduced-dimensional DCT coefficients to represent high-dimensional hydraulic conductivity. The DCT is performed for the entire prior ensemble, and the resulting DCT coefficients are arranged in a descending order for each replicate in the ensemble. The DCT vectors correspond to the first few (about 30) largest coefficients of each replicate are retained and the others are discarded. Then all distinctive retained DCT vectors are combined to form the DCT projection matrix for the ensemble. The process results in about 3% DCT basis vectors in the projection matrix.

In the reduced-order model derivation 10 of the replicates in the ensemble are selected for off-line full order simulations. As discussed in Chapter 2, these provide snapshots of states at different times for each selected replicate. Also, derivatives of the head and velocity with respect to hydraulic resistivity are calculated and collected as part of the snapshots for 3 of the replicates. For each replicate, there are a total of 4096 columns of derivative vectors and thus the snapshot matrices are expanded significantly. POD projection matrices can then be obtained based on the snapshots to generate reduced representations of the states. To obtain a compact representation of the states, the POD expansion is truncated at the number of basis function terms that account for 99%, 93%, 93%, and 99% of the energy in the head, x velocity, y velocity and concentration, respectively. This gives reduced dimensions of 69, 113, 84, and 184, for these four variables, each of which originally has a full order dimension of about 4096. With the reduced representations of the parameters and states, a second order reduced-order model can then be constructed based on the expanded governing equations in (3.10). Detailed derivation of the reduced-order model and validation of its robustness for the ensemble can be found in Chapter 2.

The next two subsections present the results of two EnKF numerical experiments. In Experiment 1 the EnKF update is based on both head and concentration measurements. In Experiment 2, only head measurements are included. For both experiments, we compare the performance of the EnKF with the full order and reduced-order models used in the forecast step.

3.3.3 Experiment 1: EnKF Estimation with Head and Concentration Measurements

Figure 3-5 summarizes the EnKF estimation results for Experiment 1. Figure 3-5(a) presents the channelized true conductivity field. The EnKF conductivity ensemble means at different times are shown for the full- and reduced-order cases in each row of Figure 3-5(b). The Jaccard distance defined in equation (3.11) is presented at the top of each plot to illustrate the dissimilarity between the true conductivity filed and each ensemble mean. From the figure it is clear that the Jaccard distances gradually decrease and the channelized structures of the conductivity field are gradually recovered for both full order and reduced-order cases after the updates on day 200, 400, 600, and 800. The full order case illustrates the ability of the EnKF to identify channelized geological structures. This capability is mainly due to the strong correlations between measurements and uncertain conductivity, which help the EnKF updates converge to the true value, provided that the ensemble is sufficient to characterize the correlation information. The reduced-order case shows that the EnKF can also capture channelized structures in this case, indicating that the reduced-order model is sufficient and accurate enough to provide the information necessary for accurate EnKF updating. This illustrates that the reduced-order is a promising alternative during the forward simulations of the EnKF.

The Jaccard distances of the reduced-order case are smaller on day 600 and 800 than those of the full order case. This indicates that the EnKF can capture the high permeable zones better in the reduced-order case. The reason can be attributed to the fact that in the reduced-order case there are fewer unknowns that need to be updated

by the EnKF. The ratio between the number of the states in the reduced-order model and the full order model is about 1 to 40.

A close inspection reveals that it is difficult for the EnKF to capture the high permeable zones at the upper-left corner of the domain in both cases. This is due to the fact that there is no measurement information near the boundaries. In ideal cases that the ensemble is sufficient to capture the correlations, the head measurements can reveal more conductivity information for those cells near the measurement locations, while the concentration measurements can reveal more information for those cells within solute propagation paths.

Figure 3-5(c) shows snapshots of concentration predictions at different time instances for the true conductivity field. The four crosses with different colors indicate the locations of the four pumping wells. As illustrated by the figure, the plume is dragged to the wells by the pumping force such that each well has solute breakthrough over the simulation horizon. This insures that the concentration data can give sufficient information for the EnKF updating. Figure 3-5(d) shows the ensemble mean concentration snapshots in the full order and reduced-order cases. Compared to Figure 3-5(c), it is clear that in both cases the EnKF can capture the shapes of the plume at different time steps, especially on day 800 when the last update happens. On day 800, the shapes of the plume in both cases are very close to the one predicted by the true case. This is consistent with the fact that the filter performance improves over time, as more measurements are collected.

A close inspection of the plume shapes reveals that the ensemble mean in the reduced-order case is more consistent with the true plume than in the full order case. As shown in Figure 3-5(c), on day 200 the plume has a left tip pointing to Well P1 (indicated by the black cross), indicating a dragging force by well pumping. This is missing in the full order case, while in the reduced-order the EnKF successfully captures the tip. A similar observation can be made on day 400. This is due to the fact that the EnKF updates the reduced-order concentration vector, making it easier for the EnKF to capture the dominant spatial features of the concentration plume.

Although reduced-order modeling can better capture the shapes of the concentration plume, we can observe some wrinkles around the fronts of the plume estimated in the reduced-order case. The wrinkles are resulted from the prediction errors by the reduced-order model. However, this doesn't deteriorate the performance of the EnKF, provided that we properly select the concentration measurement error covariance. In principle, we need to make sure that the error covariance is adequately accounts for prediction errors.

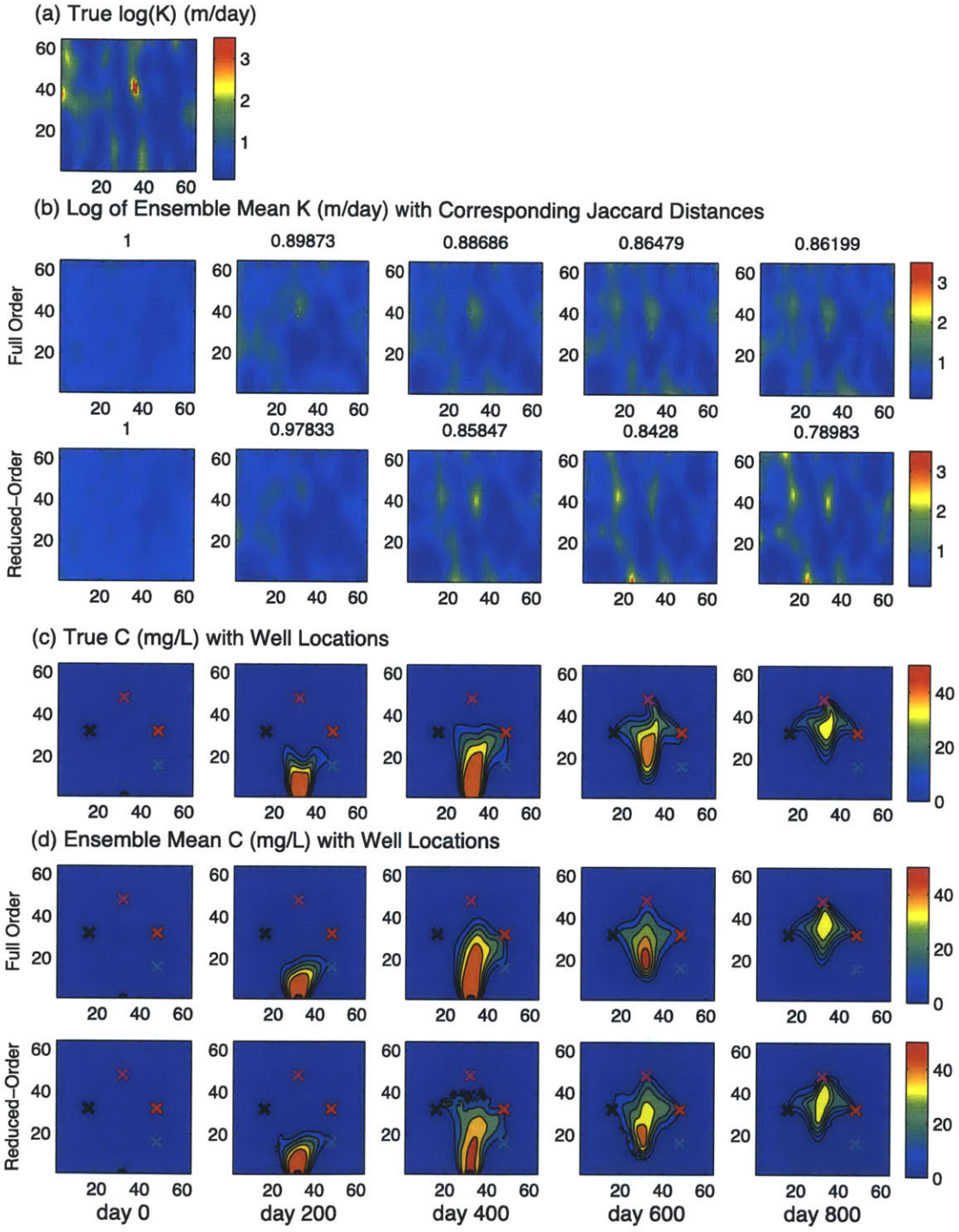

Figure 3-5: Results for Experiment 1: (a) the true log-conductivity field; (b) ensemble mean log-conductivity with corresponding Jaccard distances using the full- and reduced-order models; (c) concentration snapshots corresponding to the synthetic true conductivity field with well locations indicated by black (Well P1), red (Well P2),

cyan (Well P3), and magenta (Well P4) crosses; (d) ensemble mean concentration using the full- and reduced- order models with well locations indicated by crosses.

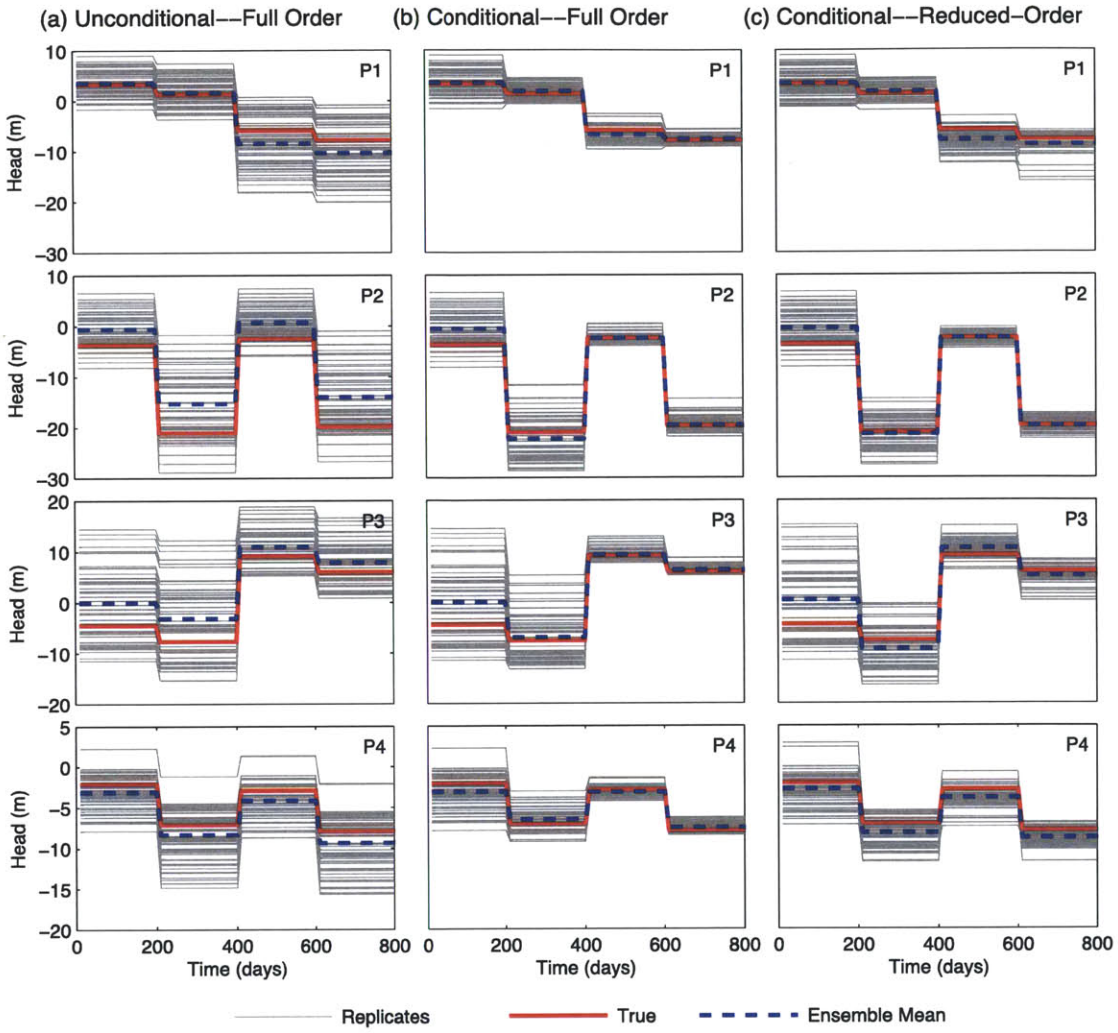

Figure 3-6: Time series of head predictions at the four well locations for replicates (gray lines), the true conductivity field (red lines), and the ensemble mean (blue lines) in Experiment 1: (a) predictions using the full order model for replicates in the prior ensemble without EnKF updating; (b) predictions using the full order model for the replicates in the ensemble with the EnKF updating the states and parameters at the end of each control step; (c) predictions using the reduced-order model for the replicates in the ensemble with the EnKF updating.

In this problem head predictions are related to energy consumption of pumping and the concentration predictions are related to water treatment cost in containment transport cases. Figure 3-6 and Figure 3-7 illustrate head and concentration predictions for replicates in the ensemble (gray lines), the true conductivity field (red lines),

and the mean over the ensemble members (blue lines) at the four pumping wells. Gray lines in Figure 3-6(a) and Figure 3-7(a) show predictions using the full order model for the prior ensemble without the EnKF updating. The spreads of the gray lines indicate the variability in the prior ensemble. Sufficient variability in the prior ensemble is needed to properly calculate the covariance used in the EnKF updating. In the plots we can also observe significant disparity between the ensemble mean (indicated by blue lines) and the true predictions (red lines). However, the true predictions fall inside the spreads of the ensemble. This suggests that the true predictions fall in the space spanned by the replicates.

Gray lines in Figure 3-6(b) and Figure 3-7(b) show ensemble predictions using the full order model with EnKF updates on day 200, 400, 600, and 800. In the plots the spreads of the ensemble shrinks noticeably over time compared to the unconditional case, indicating decreased variability or uncertainty in the ensemble. The ensemble mean (blue lines) gradually converges to the true values, indicating the ability of the EnKF to capture the dynamic of the true system.

Gray lines in Figure 3-6(c) and Figure 3-7(c) show predictions using the reduced-order model with EnKF updates on day 200, 400, 600, and 800. We can observe behavior similar to Figure 3-6(b) and Figure 3-7(b), indicating the ability of the reduced-order model to predict system behavior. One noticeable difference between plots in (b) and (c) is that the spreads in (c) can be larger than those in (b) over some control steps. This is primarily due to additional model errors introduced by the reduced-order model. For example, a close inspection of the concentration predictions at Well P1 in Figure 3-7(c) reveals that on day 400, there is a jump in the concentration curves of the replicates. This corresponds to the small wrinkles in Figure 3-5(d), which result from predictions errors.

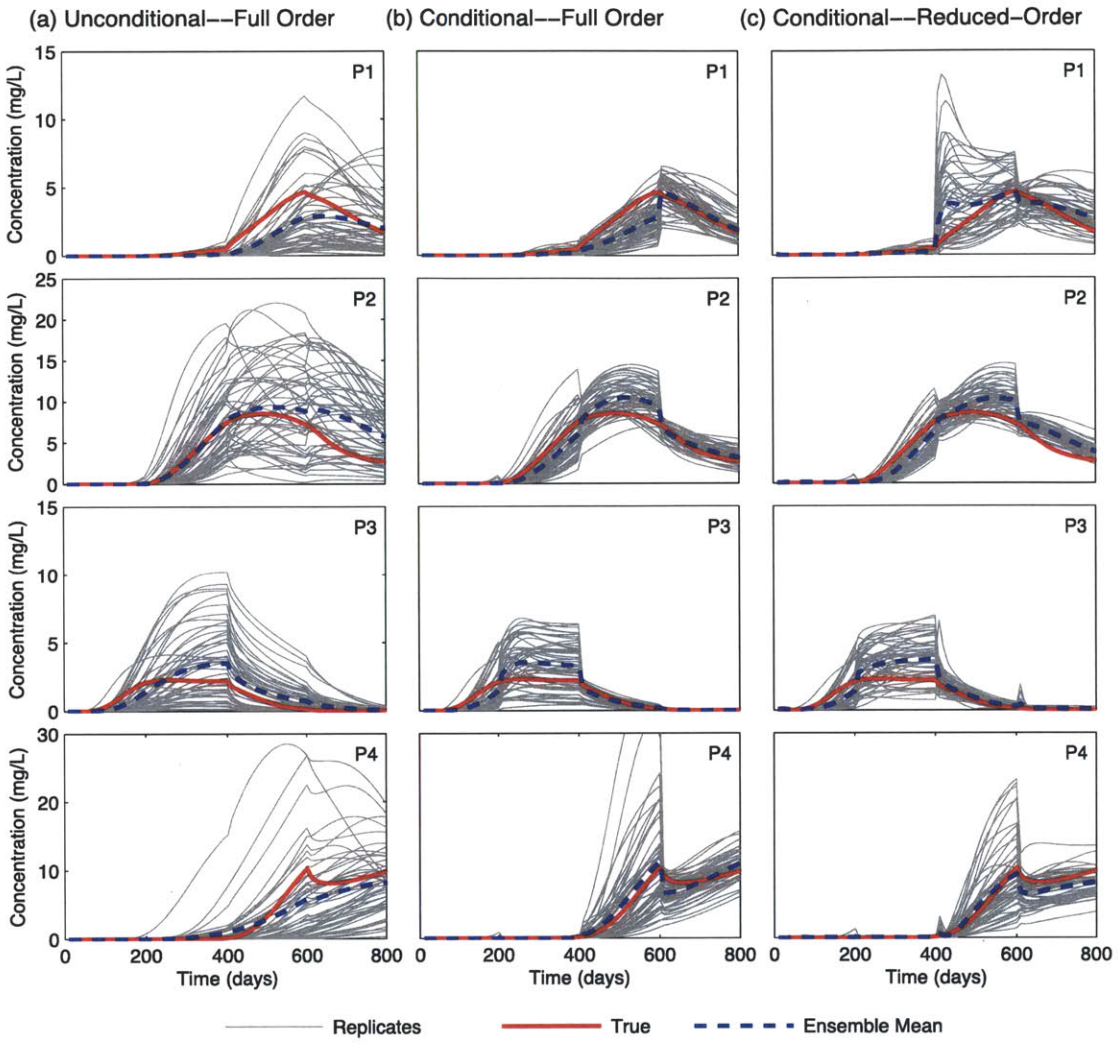

Figure 3-7: Time series of concentration predictions at the four well locations for replicates (gray lines), the true conductivity field (red lines), and the ensemble mean (blue lines) in Experiment 1: (a) predictions using the full order model for replicates in the prior ensemble without EnKF updating; (b) predictions using the full order model for the replicates in the ensemble with the EnKF updating the states and parameters at the end of each control step; (c) predictions using the reduced-order model for the replicates in the ensemble with the EnKF updating.

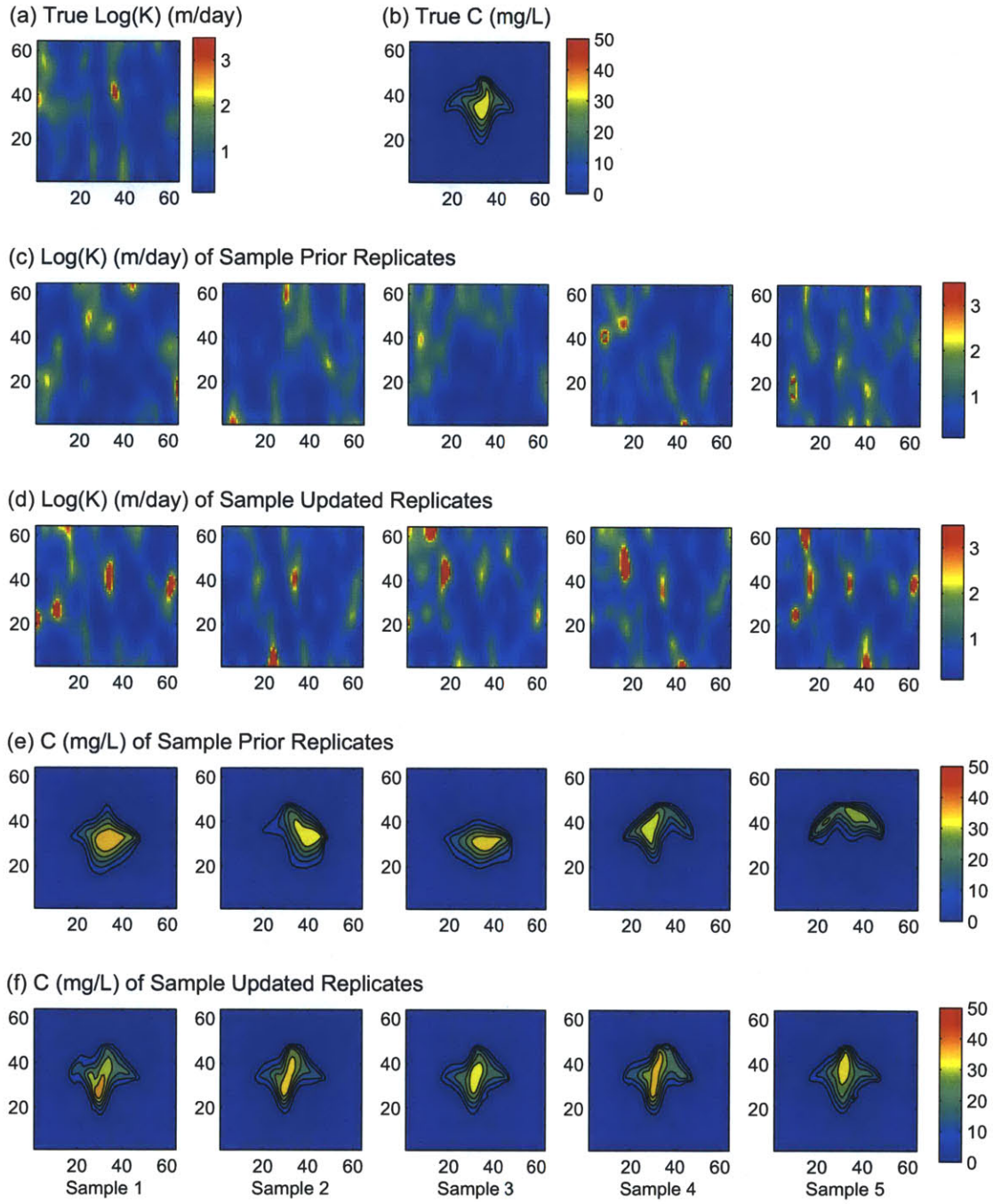

Figure 3-8: Updated conductivity and concentration replicates in the ensemble for Experiment 1: (a) the true log-conductivity field; (b) the snapshot of the concentration filed on day 800; (c) five replicates of the conductivity field in the prior ensemble; (d) corresponding updated conductivity replicates on day 800; (e) replicates of the plume on day 800 corresponding to predictions based on the five sample prior conductivity fields without the EnKF updating; (f) corresponding updated replicates of the plume on day 800.

Figure 3-8 illustrates some typical conductivity and concentration updated replicates on day 800. Figure 3-8(a) and (b) present the true conductivity field and the true plume shape on day 800. Figure 3-8(c) show five prior conductivity replicates and the plots in (d) show the corresponding five updated replicates, all on day 800. The updated replicates are more similar than the prior samples. Also, the updates display channels that are more similar to those observed in the true field. This illustrates the EnKF's ability to recover geological features. Similar behavior is shown in Figure 3-8(e) and (f). The update decreases the variability in the plumes displayed in these figures. The updated plumes are generally closer to the true plume of Figure 3-8(b) than the corresponding prior plumes.

From the aforementioned results it is clear that the reduced-order model is an accurate and effective alternative to the full order model during the forward simulations. Another advantage of using the reduced-order model is that the computation time has dropped dramatically from about 1500 seconds to about 100 seconds. This indicates that it should be possible to use a larger ensemble so as to reduce the adverse effects of sampling errors. Such errors arise in high dimensionality problems when computational constraints make it impractical to include an adequate number of samples in the ensemble.

3.3.4 Experiment 2: EnKF Estimation with Only Head Measurements

In this experiment we investigate the effect of excluding concentration measurements in the EnKF updating. This will demonstrate the importance of accurate predictions of concentration, which are more difficult for the reduced-order model.

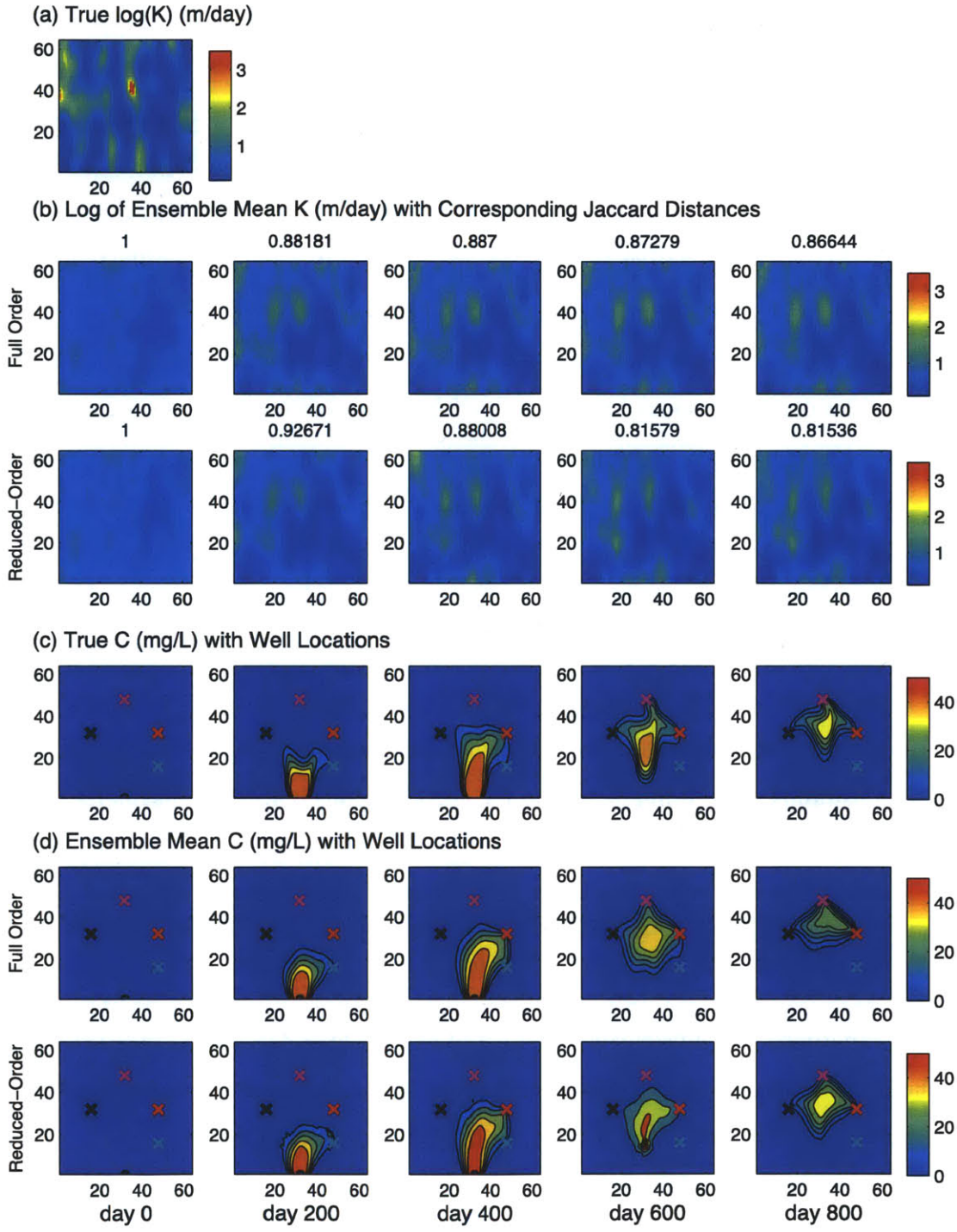

Figure 3-9: Results for Experiment 2: (a) the true log-conductivity field; (b) ensemble mean log-conductivity with corresponding Jaccard distances using the full- and reduced-order models; (c) concentration snapshots corresponding to the synthetic true conductivity field with well locations indicated by black (Well P1), red (Well P2),

cyan (Well P3), and magenta (Well P4) crosses; (d) ensemble mean concentration using the full- and reduced- order models with well locations indicated by crosses.

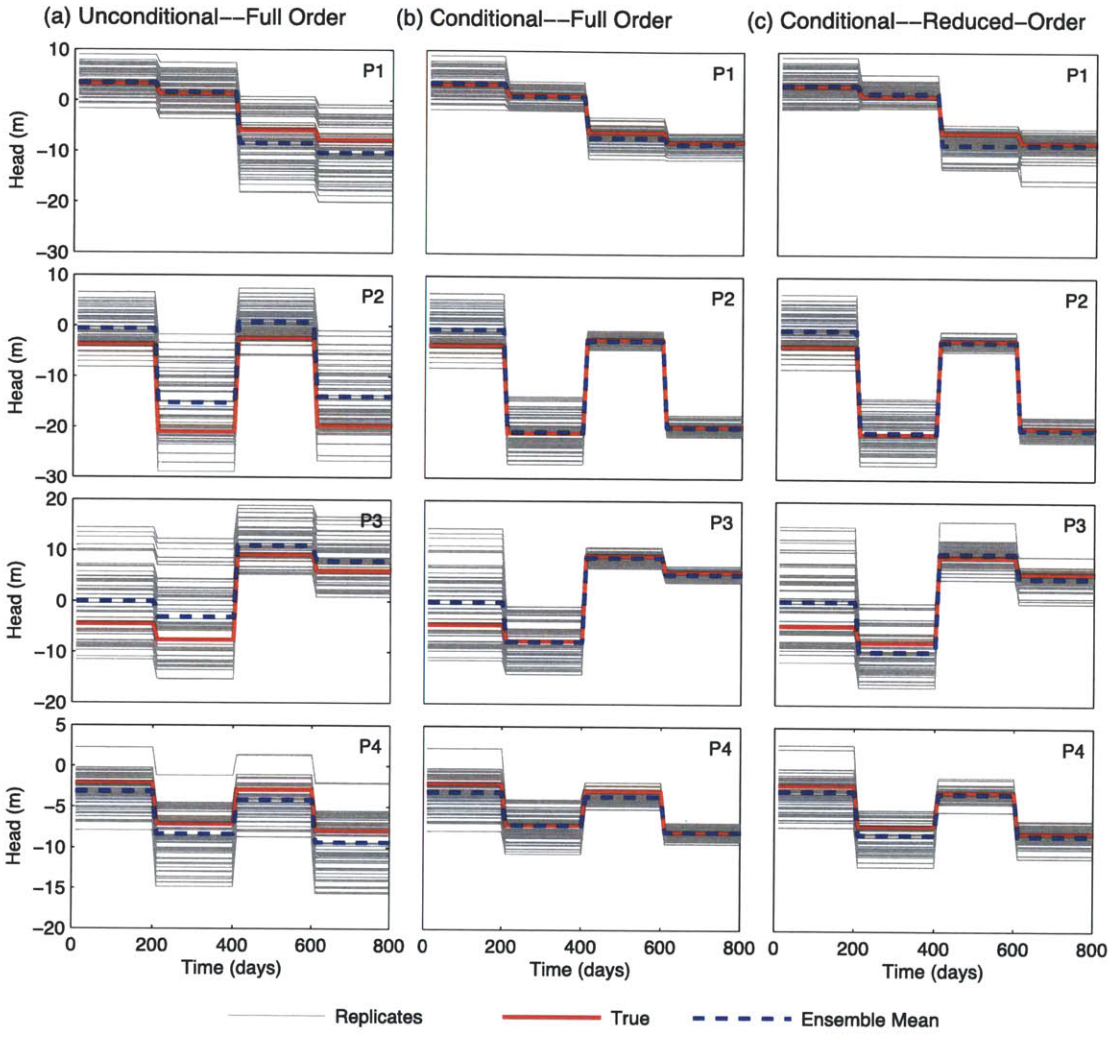

Figure 3-10: Time series of head predictions at the four well locations for replicates (gray lines), the true conductivity field (red lines), and the ensemble mean (blue lines) in Experiment 2: (a) predictions using the full order model for replicates in the prior ensemble without EnKF updating; (b) predictions using the full order model for the replicates in the ensemble with the EnKF updating the states and parameters at the end of each control step; (c) predictions using the reduced-order model for the replicates in the ensemble with the EnKF updating.

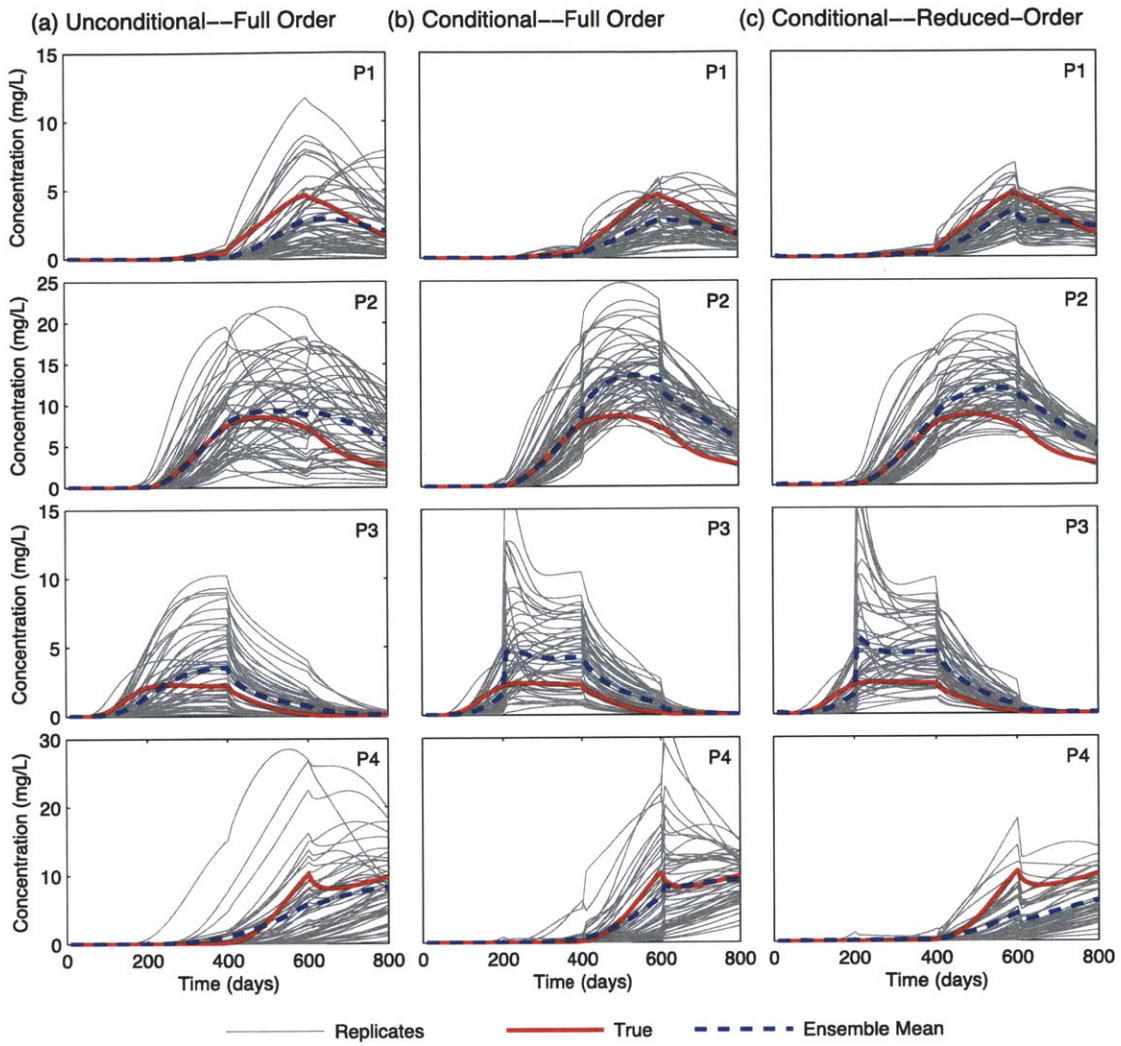

Figure 3-11: Time series of concentration predictions at the four well locations for replicates (gray lines), the true conductivity field (red lines), and the ensemble mean (blue lines) in Experiment 2: (a) predictions using the full order model for replicates in the prior ensemble without EnKF updating; (b) predictions using the full order model for the replicates in the ensemble with the EnKF updating the states and parameters at the end of each control step; (c) predictions using the reduced-order model for the replicates in the ensemble with the EnKF updating.

Figure 3-9 through Figure 3-11 summarize EnKF results for Experiment 2, using the same format as the results for Experiment 1. By comparing Figure 3-5(b) and Figure 3-9(b), we can observe that in both full order and reduced-order cases, although the EnKF can still capture the channelized structures in the true conductivity field, the geological features are not so well portrayed and thus the Jaccard distances are larger,

especially in the reduced-order case. This is expected since there are fewer measurements for the EnKF update. In Figure 3-9(c) and (d) we can also see that the EnKF cannot recover the plume distributions effectively, indicating head measurements are not sufficient to estimate the concentration propagation.

However, head and concentration predictions in Figure 3-10 and Figure 3-11 reveals an interesting fact that, although the EnKF can only recover some of the geological features of conductivity, the variability in head predictions of the ensemble decreases significantly during the EnKF updating and the ensemble mean is consistent with the true predictions. The variability in concentration replicates is still significant and individual replicates can differ significantly from the true value. It is possible that if we rely on only head measurements during the EnKF updating, we can obtain good agreement between the predicted and measured heads. However, the geological features and transport dynamics are not well captured and thus a performance evaluation based only on head predictions could be misleading.

3.4 Conclusion

In stochastic inversion methods, the ensemble Kalman filter is an effective and efficient alternative to traditional deterministic inverse methods. However, the computation burden of the EnKF can be a significant bottleneck in the application of the EnKF to large problems. For such problems a relatively small size of ensemble is typically used to obtain the statistical moments needed to update prior replicates with measurements. Unfortunately, the performance of the EnKF relies heavily on the ability of the ensemble to accurately represent the first and second moments of the probability distributions. Sampling errors due to small ensemble sizes will deteriorate the performance of the EnKF. Traditional approaches to deal with this problem include covariance inflation and localization. In this chapter we present a promising alternative solution to the sampling error problem by reducing the computation burden of the EnKF.

In the applications considered here the forecast step contributes most of the computation burden of the EnKF. Reduced-order modeling is an attractive option for decreasing the computation time during online forecast simulations. In this chapter, an efficient reduced-order model is implemented during online simulations. This reduced-order model replaces a much larger and more expensive full order model. The reduced-order model is derived from representative full order model snapshots to insure that it is valid over a reasonable range of parameter replicates. There is no need to update the reduced-order model during the online EnKF forecast steps. This reflects the fact that the reduced basis vectors adequately span the parameter spaces. In our example reduced-order modeling can decrease the online forecast computation time from 1500 seconds to 100 seconds. This opens up the possibility of applying the EnKF with reduced-order modeling to large-scale inversion problems.

Another advantage of combining reduced-order modeling with the EnKF is that the dimensions are reduced in both parameter and state spaces. The reduced-order model is intrinsically parameterized, and thus it can preserve geological features during the EnKF updating when an effective parameterization method such as DCT is implemented. Since the reduced-order EnKF only needs to update a small number of parameters and states compared to the full order EnKF, it is better able to capture complex geological structures and plume shapes, even though it relies on an approximation of the full-order model. Hence, model order reduction in both parameter and state spaces facilitates computational efficiency while also producing EnKF ensembles that give a more accurate description of reality.

The reduced-order model used here for ensemble updating can also be implemented in management problems when the optimization process is time-consuming so long as the reduce-order model is still valid over the range of control values encountered during optimization. Hence, it is possible to apply reduced-order modeling in a closed-loop control framework [48], which includes both parameter inversion and control optimization. This possibility is discussed in the next chapter.

3.5 References

[1] J. Carrera, A. Alcolea, A. Medina, J. Hidalgo, and L. J. Slooten, "Inverse problem in hydrogeology," *Hydrogeology Journal,* vol. 13, pp. 206-222, Mar 2005.

[2] G. de Marsily, J. P. Delhomme, A. Coudrain-Ribstein, and A. M. Lavenue, "Four decades of inverse problems in hydrogeology," *Theory, Modeling, and Field Investigation in Hydrogeology: A Special Volume in Honor of Shlomo P. Neuman's 60th Birthday,* pp. 1-17, 2000.

[3] G. Evensen, "Sequential Data Assimilation with a Nonlinear Quasi-Geostrophic Model Using Monte-Carlo Methods to Forecast Error Statistics," *Journal of Geophysical Research-Oceans,* vol. 99, pp. 10143-10162, May 15 1994.

[4] G. Evensen, "Sampling strategies and square root analysis schemes for the EnKF," *Ocean Dynamics,* vol. 54, pp. 539-560, 2004.

[5] S. I. Aanonsen, G. Naevdal, D. S. Oliver, A. C. Reynolds, and B. Valles, "The Ensemble Kalman Filter in Reservoir Engineering-a Review," *Spe Journal,* vol. 14, pp. 393-412, Sep 2009.

[6] J. I. Allen, M. Eknes, and G. Evensen, "An Ensemble Kalman Filter with a complex marine ecosystem model: hindcasting phytoplankton in the Cretan Sea," *Annales Geophysicae,* vol. 21, pp. 399-411, Jan 2003.

[7] M. Eknes and G. Evensen, "An Ensemble Kalman filter with a 1-D marine ecosystem model," *Journal of Marine Systems,* vol. 36, pp. 75-100, Jul 15 2002.

[8] G. Evensen, "The Ensemble Kalman Filter for Combined State and Parameter Estimation MONTE CARLO TECHNIQUES FOR DATA ASSIMILATION IN LARGE SYSTEMS," *Ieee Control Systems Magazine,* vol. 29, pp. 83-104, Jun 2009.

[9] V. Haugen, G. Naevdal, L. J. Natvik, G. Evensen, A. M. Berg, and K. M. Flornes, "History Matching Using the Ensemble Kalman Filter on a North Sea Field Case," *Spe Journal,* vol. 13, pp. 382-391, Dec 2008.

[10] N. Liu and D. S. Oliver, "Critical evaluation of the ensemble Kalman filter on history matching of geologic facies," *Spe Reservoir Evaluation & Engineering,* vol. 8, pp. 470-477, Dec 2005.

[11] J. A. Skjervheim, G. Evensen, S. I. Aanonsen, B. O. Ruud, and T. A. Johansen, "Incorporating 4D seismic data in reservoir simulation models using ensemble Kalman filter," *Spe Journal,* vol. 12, pp. 282-292, Sep 2007.

[12] B. Jafarpour and M. Tarrahi, "Assessing the performance of the ensemble Kalman filter for subsurface flow data integration under variogram uncertainty," *Water Resources Research,* vol. 47, May 26 2011.

[13] J. L. Anderson and S. L. Anderson, "A Monte Carlo implementation of the nonlinear filtering problem to produce ensemble assimilations and forecasts," *Monthly Weather Review,* vol. 127, pp. 2741-2758, Dec 1999.

[14] J. S. Whitaker and T. M. Hamill, "Ensemble data assimilation without perturbed observations," *Monthly Weather Review,* vol. 130, pp. 1913-1924, Jul 2002.

[15] T. M. Hamill, J. S. Whitaker, and C. Snyder, "Distance-dependent filtering of background error covariance estimates in an ensemble Kalman filter," *Monthly Weather Review,* vol. 129, pp. 2776-2790, 2001.

[16] P. L. Houtekamer and H. L. Mitchell, "A sequential ensemble Kalman filter for atmospheric data assimilation," *Monthly Weather Review,* vol. 129, pp. 123-137, 2001.

[17] E. Ott, B. R. Hunt, I. Szunyogh, A. V. Zimin, E. J. Kostelich, M. Corazza, E. Kalnay, D. J. Patil, and J. A. Yorke, "A local ensemble Kalman filter for atmospheric data assimilation," *Tellus Series a-Dynamic Meteorology and Oceanography,* vol. 56, pp. 415-428, Oct 2004.

[18] P. R. Oke, P. Sakov, and S. P. Corney, "Impacts of localisation in the EnKF and EnOI: experiments with a small model," *Ocean Dynamics,* vol. 57, pp. 32-45, Feb 2007.

[19] J. L. Anderson, "An adaptive covariance inflation error correction algorithm for ensemble filters," *Tellus Series a-Dynamic Meteorology and Oceanography,* vol. 59, pp. 210-224, Mar 2007.

[20] A. C. Antoulas, "An overview of approximation methods for large-scale dynamical systems," *Annual Reviews in Control,* vol. 29, pp. 181-190, 2005.

[21] E. Grimme, "Krylov Projection Methods for Model Reduction," PhD, University of Illinois at Urbana-Champaign, 1997.

[22] Z. J. Bai, "Krylov subspace techniques for reduced-order modeling of large-scale dynamical systems," *Applied Numerical Mathematics,* vol. 43, pp. 9-44, Oct 2002.

[23] K. Gallivan, E. Grimme, and P. Vandooren, "Pade Approximation of Large-Scale Dynamic Systems with Lanczos Methods," *Proceedings of the 33rd Ieee Conference on Decision and Control, Vols 1-4,* pp. 443-448, 1994.

[24] C. W. Rowley, "Model reduction for fluids, using balanced proper orthogonal decomposition," *International Journal of Bifurcation and Chaos,* vol. 15, pp. 997-1013, Mar 2005.

[25] B. C. Moore, "Principal Component Analysis in Linear-Systems - Controllability, Observability, and Model-Reduction," *Ieee Transactions on Automatic Control,* vol. 26, pp. 17-32, 1981.

[26] L. Sirovich, "Turbulence and the Dynamics of Coherent Structures .1. Coherent Structures," *Quarterly of Applied Mathematics,* vol. 45, pp. 561-571, Oct 1987.

[27] X. Ma and G. E. Karniadakis, "A low-dimensional model for simulating three-dimensional cylinder flow," *Journal of Fluid Mechanics,* vol. 458, pp. 181-190, May 10 2002.

[28] M. Bergmann, L. Cordier, and J. P. Brancher, "Optimal rotary control of the cylinder wake using proper orthogonal decomposition reduced-order model," *Physics of Fluids,* vol. 17, Sep 2005.

[29] L. Daniel, O. C. Siong, L. S. Chay, K. H. Lee, and J. White, "A multiparameter moment-matching model-reduction approach for generating geometrically parameterized interconnect performance models," *Ieee Transactions on Computer-Aided Design of Integrated Circuits and Systems,* vol. 23, pp. 678-693, May 2004.

[30] K. Kunisch and S. Volkwein, "Control of the Burgers equation by a reduced-order approach using proper orthogonal decomposition," *Journal of Optimization Theory and Applications,* vol. 102, pp. 345-371, Aug 1999.

[31] T. Bui-Thanh, K. Willcox, and O. Ghattas, "Parametric Reduced-Order Models for Probabilistic Analysis of Unsteady Aerodynamic Applications," *Aiaa Journal,* vol. 46, pp. 2520-2529, Oct 2008.

[32] T. Bui-Thanh, K. Willcox, and O. Ghattas, "Model Reduction for Large-Scale Systems with High-Dimensional Parametric Input Space," *SIAM Journal on Scientific Computing,* vol. 30, pp. 3270-3288, 2007.

[33] D. Amsallem and C. Farhat, "Interpolation method for adapting reduced-order models and application to aeroelasticity," *Aiaa Journal,* vol. 46, pp. 1803-1813, Jul 2008.

[34] J. Degroote, J. Vierendeels, and K. Willcox, "Interpolation among reduced-order matrices to obtain parameterized models for design, optimization and probabilistic analysis," *International Journal for Numerical Methods in Fluids,* vol. 63, pp. 207-230, May 20 2010.

[35] C. Lieberman, K. Willcox, and O. Ghattas, "Parameter and State Model Reduction for Large-Scale Statistical Inverse Problems," *Siam Journal on Scientific Computing,* vol. 32, pp. 2523-2542, 2010.

[36] R. Kalman, "A new approach to linear filtering and prediction problems," *J. Basic Eng.,* vol. 82, pp. 35-45, 1960.

[37] G. Evensen, "The Ensemble Kalman Filter: theoretical formulation and practical implementation," *Ocean Dynamics,* vol. 53, pp. 343-367, 2003.

[38] B. Jafarpour and D. B. McLaughlin, "Estimating Channelized-Reservoir Permeabilities With the Ensemble Kalman Filter: The Importance of Ensemble Design," *Spe Journal,* vol. 14, pp. 374-388, Jun 2009.

[39] C. H. Bishop, B. J. Etherton, and S. J. Majumdar, "Adaptive sampling with the ensemble transform Kalman filter. Part I: Theoretical aspects," *Monthly Weather Review,* vol. 129, pp. 420-436, 2001.

[40] J. L. Anderson, "An ensemble adjustment Kalman filter for data assimilation," *Monthly Weather Review,* vol. 129, pp. 2884-2903, 2001.

[41] D. M. Livings, S. L. Dance, and N. K. Nichols, "Unbiased ensemble square root filters," *Physica D-Nonlinear Phenomena,* vol. 237, pp. 1021-1028, Jun 15 2008.

[42] P. Sakov and P. R. Oke, "A deterministic formulation of the ensemble Kalman filter: an alternative to ensemble square root filters," *Tellus Series a-Dynamic Meteorology and Oceanography,* vol. 60, pp. 361-371, Mar 2008.

[43] L. Sirovich, "Turbulence and the dynamics of coherent structures. I: Coherent structures. II: Symmetries and transformations. III: Dynamics and scaling," *Quarterly of Applied Mathematics,* vol. 45, pp. 561-590, 1987.

[44] Y. Gu and D. S. Oliver, "An iterative ensemble Kalman filter for multiphase fluid flow data assimilation," *Spe Journal,* vol. 12, pp. 438-446, Dec 2007.

[45] Y. Chen, D. S. Oliver, and D. X. Zhang, "Data assimilation for nonlinear problems by ensemble Kalman filter with reparameterization," *Journal of Petroleum Science and Engineering,* vol. 66, pp. 1-14, May 2009.

[46] B. Jafarpour and D. B. McLaughlin, "Reservoir Characterization With the Discrete Cosine Transform," *Spe Journal,* vol. 14, pp. 182-201, Mar 2009.

[47] P.-N. Tan, M. Steinbach, and V. Kumar, *Introduction to data mining.* Boston: Pearson Addison Wesley, 2006.

[48] J. D. Jansen, S. D. Douma, D. R. Brouwer, P. M. J. v. d. Hof, O. H. Bosgra, and A. W. Heemink, "Closed-loop reservoir management," presented at the the 2009 SPE Reservoir Simulation Symposium, the Woodlands, Texas, 2009.

Chapter 4

Application of Reduced-Order Modeling to Ensemble Real-time Control

4.1 Introduction

One of the aims of subsurface flow modeling is to predict the response of variables such as pressure and concentration to external forcing, such as well pumping and injection. Simulation results from a subsurface flow model can provide important information for management of subsurface resources, including water, oil, and gas reservoirs. By controlling pumping and injection configurations, water, solutes, and other fluid components can be controlled to achieve a particular management goal such as minimizing containment concentrations [1], maximizing oil production [2], or optimizing carbon dioxide sequestration. In such applications a design tool is needed to determine the best well configurations and pumping strategies.

Modern design tools for subsurface management combine simulation models with optimization techniques [3]. This combination provides a framework to formulate the management problems rigorously. In the management of subsurface resources, the optimization problem is constrained by conservation laws and other relationships involving pressure, solute concentration, well pumping rates, etc. The optimization objective is typically the net benefit, defined as the difference between the economic

benefit of the resources extracted and the cost of well placement, energy consumption, etc.. This objective depends on the system's response to the control strategy, as reflected by system states such as pressure and saturation. The system model relates these states to the control variables. An open loop control [4] strategy derives optimal controls offline from predictions based only on information available before the controls are actually applied. By contrast, a closed-loop strategy derives controls on line, in real time. In this approach the control values applied at any control time depend on the current state of the system, as revealed by current measurements of variables such as saturation and pressure.

Since the parameters used to predict the response of subsurface system are uncertain open loop control strategies can perform poorly. The system states derived from estimated parameters gradually diverge from the true values, leading to optimization solutions that do not actually maximize actual net benefits. Closed-loop control [2, 5-7] usually performs better in practical applications because the controls are continually adjusted in real time to respond to the information conveyed by new measurements. In effect, the optimization problem is resolved and the control strategy is adjusted whenever a new measurement becomes available.

In recent years, a lot of work has been done on deterministic closed-loop control of subsurface flow systems. Early studies carried out by Birnovskii [8] and Virnovsky [9] investigated a thorough optimization of the well location, well type, water flooding efficiency, etc., for multiphase flow in 2D reservoirs. In their studies the fluids were incompressible and the gravity was neglected. They found that the optimal flow rates were lower for wells in high permeable areas. Also, their optimization procedure adjusted controls to produce a uniform displacement front. Some studies have also considered optimization of switching times (pumping schedules) as well as pumping rates [10-12].

Control strategies derived from a deterministic description of the system do not account for parameter and state uncertainties, which are significant in subsurface applications. As a result, such strategies tend to be "over confident", applying controls

that do not work as expected because the real system has properties that are different than those assumed in the control derivation. Although the closed-loop provides a way to address this problem it is still important to account for uncertainty when deriving closed-loop controls. Robust optimization [13-15] deals with this problem by utilizing the ensemble representation of the system uncertainty and optimizing over the whole ensemble. Water flooding examples in the studies by Chen et al. [15], Chen et al. [14], and van Essen et al. [13] showed that the net present value obtained by using robust optimization was comparable to the net present value obtained from the optimization based on known geology.

Here, we apply an ensemble-based closed-loop control strategy to a subsurface system with uncertain physical properties. Uncertainty in these properties is initially represented by an ensemble of realizations that describes a prior probability distribution. As time passes and measurements of the system response are collected the ensemble is updated to account for new information. Here the updates are based on the Bayesian formulation described in Chapter 3. In particular, the prior (or unconditional) replicates are adjusted with an ensemble Kalman filter to obtain a set of a posteriori (conditional) replicates that follow the a posteriori distribution specified by Bayes theorem. These posterior replicates provide a description of the likely range of parameter values that can be expected, given available measurements and prior information.

As indicated by Figure 4-1, the whole closed-loop procedure includes two key loops, i.e. the optimization loop and the ensemble-updating loop. The ensemble-updating loop updates current states and uncertain model parameters based on measurements collected on the current time step. The optimization loop derives controls for the next control step by maximizing expected net benefits, averaged over the a posteriori ensemble of updated states and model parameters. These controls are then applied to the subsurface system.

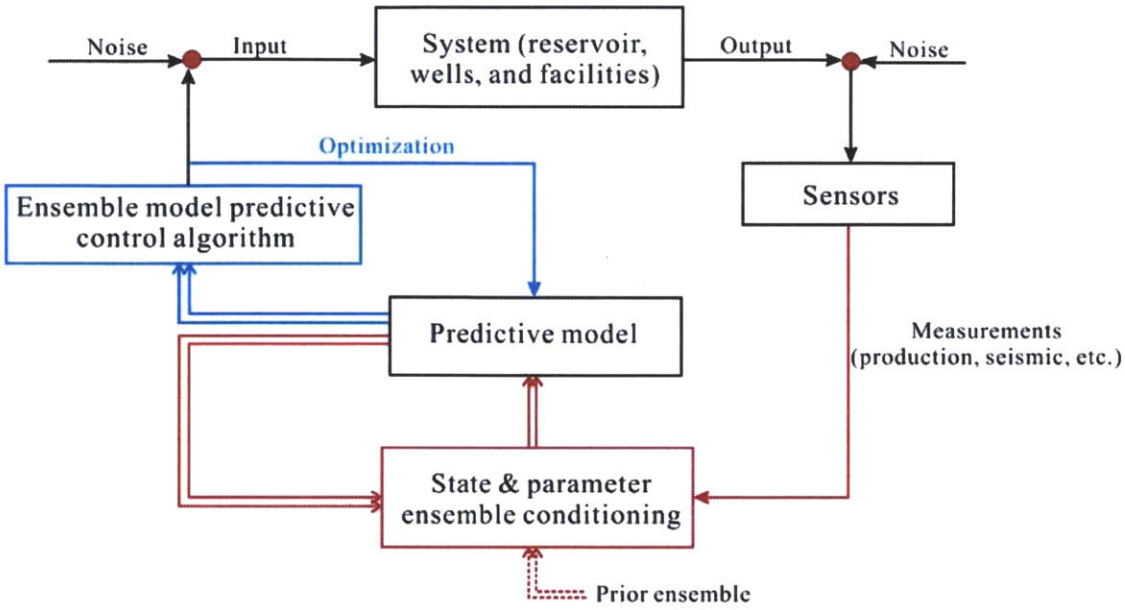

Figure 4-1: Flowchart showing the ensemble-based closed-loop control approach (after [6]). Double lines indicate that the specific operation is performed for each replicate in the ensemble.

The ensemble Kalman filter (EnKF) [16-18] has been introduced to the petroleum industry recently [19] and has been implemented and tested by many authors [20-24]. Although the EnKF is easy to use, its accuracy depends on the ensemble size. Normally, a large ensemble is needed to obtain a good representation of geological uncertainty. This increases the computational burden for large-scale subsurface problems.

To facilitate real-time ensemble updating and control optimization, an efficient parameterization algorithm is required for efficient representation of the uncertain geological parameters. Parameterization aims to remove redundancy in the geological description by taking advantage of spatial correlation between parameter values in adjacent cells. The simplest parameterization method is zonation of the reservoir into regular homogeneous zones [25]. An improvement of this technique is to use a multi-scale technique to condition the dynamic data by history-matching a coarse model [26]. The coarse model is then successively refined using a combination of downscaling and history matching until the data matches the model at the finest scale.

An alternative approach is the Karhunen-Loéve (K-L) expansion or linear principle component analysis (PCA), which was introduced to the petroleum field by Ga-

valas et al. [27]. This method projects a high-dimensional grid cell-based parameter vector onto a lower dimensional space spanned by the leading eigenvectors of the parameter spatial covariance matrix. The truncated Karhunun-Loeve parameterization has used by many other authors [28, 29]. However, the K-L expansion has three major limitations. First, it needs requires knowledge of the parameter covariance. Second, it presumes that this covariance adequately characterizes spatial variability, an assumption which implicitly supposes the parameter is multivariate Gaussian. This may not be justified in many geological setting such as channelized formations. Third, eigen-decomposition of the covariance matrix is prohibitively expensive for practical high-dimensional problems.

As an alternative, Jafarpour and McLaughlin [30] introduced the discrete cosine transform (DCT) for parameterization of subsurface properties. Compared to the K-L expansion, the DCT provides a robust parameterization alternative that doesn't require specification of a covariance or other statistics. Since the DCT basis vectors and the associated transformation matrix are constant, there is no need for extra computation to derive the basis. It has been shown that the DCT is a flexible and effective method for describing structural geological fields [30, 31].

Any of the aforementioned parameterizations can be included in the ensemble closed-loop control framework as shown in Figure 4-1. Lorentzen et al. [32] performed an ensemble closed-loop control study on a large-scale oil reservoir model with about 60, 000 grids. In their study the EnKF was used for ensemble updating and a sequential quadratic programming method was used for the step. An ensemble size of 104 was used to represent uncertainty in geological properties. However, only ten of the replicates in the ensemble were chosen to calculate the expected value of the objective function during the optimization. This is because the large-scale model needs to be run for each replicate for each iteration of the optimization search, which makes the computation prohibitively expensive.

Reduced-order modeling (ROM) is a promising option for improving the efficiency of forward simulations significantly so that robust real-time control can be made

practical for high-dimensional subsurface management problems. With reduced-order modeling, it is possible to use a larger size of ensemble for both ensemble updating and robust optimization. Chapter 2 describes a reduced-order subsurface flow and transport model that works well over a range of spatially variable parameter fields. This reduced-order model relies on projections onto low-dimensional state and parameter subspaces. In Chapter 3, the reduced-order model is used to greatly decrease the computational effort of an EnKF forecast step. This creates the possibility of using a large ensemble size for high-dimensional problems, so that sampling error and related filter divergence issues can be resolved.

In this chapter, we extend the reduced-order model so that it works well over a range of different control strategies as well as a range of different parameter replicates. This extension enables us to apply reduced-order modeling in both ensemble-updating loop and optimization loop of the real-time control procedure. In our approach the parameter space is reduced with the discrete cosine transform (DCT), while the state space is reduced with the proper orthogonal decomposition (POD). The DCT is used to preserve geological features and thus can facilitate model-updating procedure. The POD basis vectors are based on snapshots of model states as well as the derivatives of states with respect to parameters. These snapshots are generated by evaluating the full order model for several realizations of model parameters. The effectiveness of a particular set of POD basis vectors depends on the information contained in the snapshots. In Chapter 3 it is shown that a combined snapshot set of states and derivatives contains sufficient information to derive robust POD basis vectors over an entire ensemble of realizations consisting of either prior or updated replicates.

In order to extend the reduced-order model so that it works over a range of control inputs it is important to ensure that the state space POD basis vectors account for a realistic range of possible control sequences. Several techniques have been proposed to improve the POD basis to account for control variability. In the field of fluid control, Gunes and Rist [33] used POD basis vectors extracted from the dynamics of un-

controlled flow but corrected the dynamics of the reduced-order model based on new snapshots of controlled flow. Another approach is to use so-called shift modes [34], which are derived from the difference between the time-averaged flow under prescribed control conditions and the corresponding steady flow solutions, to complement the uncontrolled flow POD basis such that a better representation of the controlled flow dynamics can be achieved.

The POD basis can also be updated online in response to changes of control strategies during the optimization procedure. One way to do that is to use an adaptive procedure that improves the reduced-order model by successively updating the snapshots when the existing POD reduced model is considered to be insufficient [35]. Another approach is so-called trust-region proper orthogonal decomposition (TRPOD) approach [36] in which a trust region in the control space is defined. The reduced-order model is deemed to be representative of the controlled dynamics in the trust region. Whenever the control strategy leaves the trust region, the reduced-order must be updated to better account for the system dynamics in the actual range of operating conditions.

Although the methods described above have been shown to be effective in certain applications, they are either heuristic or require additional on-line computation effort. Here we seek a reduced-order model that does not need to be updated during online simulations. To achieve this, the POD basis must rely on snapshots that adequately portray the range of likely control sequences. A straightforward way to achieve this is to sample in the control space a priori to generate a snapshot set as rich as possible. Centroidal Voronoi Tessellations [37] is an intelligent method to sample the control space. This method essentially selects snapshots that are sufficiently representative of the system dynamics in some neighborhood of the control range and discard those that are less representative. However, this method requires a large number of samples to enrich the snapshot set.

In ensemble-based control, the offline training procedure relies on evaluations of the full order model for each replicate in the ensemble. In order to account for the ef-

fect of control variability we solve a deterministic control problem for several of the realizations in the ensemble. Each of these solutions represents a plausible control sequence that is associated with a particular parameter replicate. If the selected realizations are sufficiently representative of the dynamics of the prior parameter ensemble the derived control set should span the neighborhood of the actual control sequence derived from the real-time control procedure.

Section 4.2 summarizes the various techniques used in the ensemble closed-loop control, including the adjoint method to derive the gradients used in the optimization algorithm and the EnKF method for updating model states and parameters. Derivation of the reduced-order model, including sampling in both the control and parameter spaces, is also discussed in Section 4.2. In Section 4.3 a 2D solute transport control example is introduced to validate the reduced-order model. Section 4.4 concludes this work.

4.2 Methodology

4.2.1 The Subsurface Transport Model

Here we investigate 2D solute transport in a thin layer of isotropic saturated aquifer. We assume a constant layer height. Pressure head and solute concentration are vertically uniform so the vertical flux and gravity can be neglected. The simulation model presented here assumes transient nonreactive single species solute transport and predicts head and solute concentration at particular locations and times in response to a particular set of pumping rates at several well locations. The predicted concentration is then used to evaluate the performance of the specific control strategies.

Based on the conservation of mass and momentum and with relevant initial and boundary conditions, the discretized forward model for 2D non-gravitational solute transport in saturated porous media can be written in an implicit form as:

$$\mathbf{F}_{t-1}\left(\mathbf{x}_t, \mathbf{x}_{t-1}, \mathbf{u}_{t-1}, \boldsymbol{\alpha}\right) = 0 \tag{4.1}$$

Here $\mathbf{x}_t$ are vectors of state solutions that including head, velocity, and concentration, evaluated $t = 1,\ldots,N_T$. The vector $\mathbf{u}_{t-1}$ is composed of controls (pumping rates) at specific wells, at time $t-1$. The vector $\boldsymbol{\alpha}$ is a vector of model parameters defined at the discretized computational grid cells. In this work $\boldsymbol{\alpha}$ is specifically referred to as hydraulic conductivity or its inverse, i.e. hydraulic resistivity. As shown in Chapter 2, the vector functions $\mathbf{F}_{t-1}$ are bilinear functions in $\mathbf{x}$ and $\boldsymbol{\alpha}$ if the flow equations are discretized using the mixed finite element scheme, and the transport equation is discretized using the upwind finite difference scheme.

In this work we assume there is uncertainty in the parameter vector $\boldsymbol{\alpha}$, and the uncertainty will eventually result in uncertainty in predictions of $\mathbf{x}$. The ensemble closed-loop control framework presented here uses an ensemble of realizations $\left\{\boldsymbol{\alpha}^j\right\}_j^M$ to represent the probabilistic distribution of $\boldsymbol{\alpha}$, where M is the number of realizations in the ensemble. The propagation of the state variable $\mathbf{x}_t^j$ for the realization $\boldsymbol{\alpha}^j$ is determined by

$$\mathbf{F}_{t-1}^j\left(\mathbf{x}_t^j, \mathbf{x}_{t-1}^j, \mathbf{u}_{t-1}, \boldsymbol{\alpha}^j\right) = 0 \tag{4.2}$$

The feedback from the real system consists of measurements of the states, in particular head and concentration at a few monitoring well locations. The relationship between the measurement vector $\mathbf{z}$ and the state vector $\mathbf{x}$ can be written as

$$\mathbf{z}_t = \mathbf{g}\left(\mathbf{x}_t\right) + \mathbf{v}_t \tag{4.3}$$

where $\mathbf{v}_t$ is a vector of measurement noise. Since $\mathbf{z}$ is a vector of measured state variables at particular locations, $\mathbf{g}$ is a linear function that simply identifies the measurement locations. For realization $\boldsymbol{\alpha}^j$, the measured output can be written as

$$\mathbf{z}_t^j = \mathbf{g}\left(\mathbf{x}_t^j\right) + \mathbf{v}_t^j \tag{4.4}$$

4.2.2 Formulations of the Real-time Control Problem

In the example considered here the objective of solute transport control is to minimize the total cost associated with aquifer cleanup. This includes 1) the cost of remedial well pumping needed to remove solute, 2) ex situ treatment of the pumped groundwa-

ter, and 3) a penalty cost related to the solute concentration at a target (e.g. municipal water supply) well. Formally, the real-time stochastic control problem can be formulated as a minimization problem in the form of:

$$\underset{\mathbf{u}_{t:N_T-1}}{\text{minimize}}\, E\left[J_t \mid \mathbf{z}_{1:t}, \mathbf{u}_{1:t-1}\right] \tag{4.5}$$

where

$$J_t = \sum_{\tau=t}^{N_T-1} J'_\tau(\mathbf{x}_\tau, \mathbf{u}_\tau, \boldsymbol{\alpha}) \tag{4.6}$$

Here, J'_τ is the contribution to the optimization objective function J_t at the time step $\tau \geq t$. Note that $J'_\tau(\mathbf{x}_\tau, \mathbf{u}_\tau, \boldsymbol{\alpha})$ is are random by virtue of its dependence on the random parameter $\boldsymbol{\alpha}$ and the random states $\mathbf{x}_\tau$. The notation $J_t \mid \mathbf{z}_{1:t}, \mathbf{u}_{1:t-1}$ indicates that the expectation in (4.5) is conditional on knowledge of all previous controls and all measurements available through time t. Equation (4.6) recognizes that J_t depends on $\mathbf{x}_\tau$ and $\boldsymbol{\alpha}$ implicitly, through the model constraints (4.1).

The complete set of optimization problem constraints include the model constraints expressed in equation (4.1), as well as upper and lower bounds on $\mathbf{u}_\tau$:

$$\mathbf{u}_\tau^l \leq \mathbf{u}_\tau \leq \mathbf{u}_\tau^u \qquad \tau = t, \ldots, N_T - 1 \tag{4.7}$$

For deterministic control $\boldsymbol{\alpha}$ is assumed to be perfectly known. There is no need to condition on measurements, and the expectation operation drops out. The control problem is then to seek a set of well pumping configurations $\{\mathbf{u}_\tau\}_{\tau=t}^{N_T-1}$ to minimize the cost expressed in equation (4.6) for a particular known hydraulic conductivity distribution, subject to constraints expressed in equation (4.1) and (4.7), as well as initial conditions. For open loop control, $\boldsymbol{\alpha}$ is assumed to be random with a known probability distribution (or known statistical moments) but there is no measurement conditioning. In the deterministic and open loop cases, the entire control sequence can be computed off-line, before the initial control time. For closed loop control, $\boldsymbol{\alpha}$ is assumed to be random with a known probability distribution (or known statistical moments) and there is measurement conditioning. In this case, the control must be computed on-line, as new measurements become available.

Gorelick et al. [38] describe an approach for solving a deterministic subsurface control problem. Their objective is to minimize the total pumping rates subject to solute concentration constraints at some specific locations. However, this approach

doesn't account for uncertainty in $\boldsymbol{\alpha}$, and thus lacks robustness in real field applications. Wagner and Gorelick [39] describe two alternative formulations for determining optimal well pumping configurations with uncertain conductivity. In this case the objective is to minimize total pumping rates subject to so-called chance constraints on the concentrations at specific locations. In this work the objective is a deterministic function of the pumping rates, while the constraints are stochastic and dependent on specific realizations of conductivity. In the first approach they generated an ensemble of conductivity realizations and then minimized the objective function while simultaneously enforcing constraints for all realizations in the ensemble simultaneously. Since the constraints must be satisfied for all replicates, including the most unfavorable one optimal strategies from this formulation are conservative. The second approach is to solve the aforementioned deterministic optimization problem for each of the realizations. If there are M realizations in the ensemble, this approach will result in M sets of control strategies. For a single control variable, this approach can give a probabilistic distribution of possible optimal control values, and thus the applied control value can then be determined by a specific reliability level. However, for multiple control variables, there is no monotonic relationship between control variables and reliability levels. The "optimal" control is then ambiguous.

In the problem considered here the objective is stochastic since it depends implicitly on the random parameter $\boldsymbol{\alpha}$ through the flow and transport model equations. The expectation in the objective function can be approximated by the average taken over all replicates in the ensemble:

$$\begin{aligned} E\left[J_t \mid \mathbf{z}_{1:t}, \mathbf{u}_{1:t-1}\right] &= E\left[\sum_{\tau=t}^{N_T-1} J'_\tau\left(\mathbf{x}_{\tau|t}, \mathbf{u}_\tau, \boldsymbol{\alpha}_{\tau|t}\right)\right] \\ &\approx \frac{1}{M}\sum_{j=1}^{M}\sum_{\tau=t}^{N_T-1} J'_\tau\left(\mathbf{x}^j_{\tau|t}, \mathbf{u}_\tau, \boldsymbol{\alpha}^j_{\tau|t}\right) \end{aligned} \tag{4.8}$$

where $\mathbf{x}^j_{\tau|t}$ is the state obtained by solving (4.2) with the parameter replicate $\boldsymbol{\alpha}^j_{\tau|t}$. The notation $\tau \mid t$ indicates that the state and parameter replicates at time τ have been up-

dated using measurements available through t. If $\tau > t$ the state or parameter is a forecast obtained from the augmented model equations.

The control solution obtained by solving this optimization problem is deterministic if there is only one perfectly known replicate and there is no measurement conditioning, so $t = 0$, $\mathbf{x}_{\tau|t}^{j} = \mathbf{x}_{\tau}$, and $\boldsymbol{\alpha}_{\tau|t}^{j} = \boldsymbol{\alpha}$. If the control is open loop, there is an ensemble of prior replicates to represent uncertain parameters but no measurement conditioning, so $\mathbf{x}_{\tau|t}^{j} = \mathbf{x}_{\tau}^{j}$, and $\boldsymbol{\alpha}_{\tau|t}^{j} = \boldsymbol{\alpha}^{j}$.

Equation (4.8) assumes realizations in the ensemble are equiprobable. The complete real-time stochastic optimization problem at time t can be defined as

$$\min_{\mathbf{u}_{t:N_T-1}} \frac{1}{M} \sum_{j=1}^{M} \sum_{\tau=t}^{N_T-1} J_{\tau}' \left(\mathbf{x}_{\tau|t}^{j}, \mathbf{u}_{\tau}, \boldsymbol{\alpha}_{\tau|t}^{j} \right) \tag{4.9}$$

subject to

$$\begin{aligned} \mathbf{F}_{\tau}^{j} \left(\mathbf{x}_{\tau+1|t}^{j}, \mathbf{x}_{\tau|t}^{j}, \mathbf{u}_{\tau}, \boldsymbol{\alpha}_{\tau|t}^{j} \right) &= 0 \\ \mathbf{u}_{\tau}^{l} \le \mathbf{u}_{\tau} \le \mathbf{u}_{\tau}^{u} & \end{aligned} \tag{4.10}$$

where $j = 1, \ldots, M$, and $\tau = t, \ldots, N_T - 1$. After the optimization has been carried out only the first control $\mathbf{u}_t$ is retained. All future controls $\mathbf{u}_{t+1:N_T-1}$ are discarded since they will be re-computed with new measurements on subsequent time steps. This approach to real-time control is a stochastic extension of Model Predictive Control (MPC).

At any given time t the real-time control problem then seeks an pumping rate vector $\mathbf{u}_t$ that minimizes the objective function defined in equation (4.9), subject to model constraints and upper and lower bounds imposed for each realization in the ensemble. The new objective in equation (4.9) is one particular way to account for the impact of uncertainty within the optimization problem. There are other objectives that can be implemented under this framework, such as objectives that incorporates the variance of the cost over all replicates or objectives that focus on worst-case costs. In this work, however, we limit ourselves to the expected objective.

4.2.3 The Adjoint Model for Calculating Gradients

The ensemble optimization problem can be solved using gradient-based methods, such as Newton's method, conjugate gradient methods, or the steepest descent method. Here we utilize the *fmincon* function in MATLAB with the interior point method [40], which requires the gradients of the objective with respect to the control variables, i.e.

$$\frac{dJ_t}{d\mathbf{u}} = \frac{1}{M}\sum_{j=1}^{M}\frac{dJ_t^j}{d\mathbf{u}} \tag{4.11}$$

where $\mathbf{u}$ is a vector containing all controls $\mathbf{u}_{t:N_T-1}$. Here we define

$$\begin{aligned} \left(J_\tau'\right)^j &= J_\tau'\left(\mathbf{x}_{\tau|t}^j, \mathbf{u}_\tau, \boldsymbol{\alpha}_{\tau|t}^j\right) \\ J_t^j &= \sum_{\tau=t}^{N_T-1}\left(J_\tau'\right)^j \end{aligned} \tag{4.12}$$

The gradients are essentially an average of the gradients $dJ_t^j / d\mathbf{u}$ over the entire ensemble.

We need to calculate individual $dJ_t^j / d\mathbf{u}$ first. These gradients can be evaluated using the finite difference method. However, this requires additional forward simulations of the system model for each realization, and to obtain $dJ_t^j / d\mathbf{u}$ the total number of evaluations equals the number of control steps remaining multiplied by the number of realizations in the ensemble. For large problems, this approach is prohibitively expensive. A more efficient way to calculate the gradients $dJ_t^j / d\mathbf{u}$ is achieved by the use of an adjoint model [41]. The derivation of the adjoint model is closely connected to the classical way to solve a constrained optimization problem.

Setting aside the lower and upper bound constraints, a new objective augmented by the model constraints in (4.2) through the Lagrange multipliers $\boldsymbol{\lambda}_\tau^j$ for realization j can be written as

$$\ell_t^j = \sum_{\tau=t}^{N_T-1} J_\tau'\left(\mathbf{x}_{\tau|t}^j, \mathbf{u}_\tau, \boldsymbol{\alpha}_{\tau|t}^j\right) + \left(\boldsymbol{\lambda}_{\tau+1}^j\right)^T \cdot \mathbf{F}_\tau^j\left(\mathbf{x}_{\tau+1|t}^j, \mathbf{x}_{\tau|t}^j, \mathbf{u}_\tau, \boldsymbol{\alpha}_{\tau|t}^j\right) \tag{4.13}$$

Here the vectors $\boldsymbol{\lambda}_{\tau+1}^{j}$ are Lagrange multipliers for model constraints. Treatment of other types of constraints is similar and thus omitted here. The first variation of the augmented objective is then

$$\begin{aligned}\delta\ell_t^j = &\left(\frac{\partial\left(J_t'\right)^j}{\partial\mathbf{x}_{t|t}^j}+\left(\boldsymbol{\lambda}_{t+1}^j\right)^T\frac{\partial\mathbf{F}_t^j}{\partial\mathbf{x}_{t|t}^j}\right)\cdot\delta\mathbf{x}_{t|t}^j\\ &+\sum_{\tau=t+1}^{N_T-1}\left(\frac{\partial\left(J_\tau'\right)^j}{\partial\mathbf{x}_{\tau|t}^j}+\left(\boldsymbol{\lambda}_{\tau+1}^j\right)^T\frac{\partial\mathbf{F}_\tau^j}{\partial\mathbf{x}_{\tau|t}^j}+\left(\boldsymbol{\lambda}_\tau^j\right)^T\frac{\partial\mathbf{F}_{\tau-1}^j}{\partial\mathbf{x}_{\tau|t}^j}\right)\cdot\delta\mathbf{x}_{\tau|t}^j\\ &+\left(\boldsymbol{\lambda}_{N_T}^j\right)^T\frac{\partial\mathbf{F}_{N_T-1}^j}{\partial\mathbf{x}_{N_T|t}^j}\cdot\delta\mathbf{x}_{N_T|t}^j+\sum_{\tau=t}^{N_T-1}\left(\delta\boldsymbol{\lambda}_{\tau+1}^j\right)^T\cdot\mathbf{F}_\tau^j+\sum_{\tau=t}^{N_T-1}\left(\frac{\partial\left(J_\tau'\right)^j}{\partial\mathbf{u}_\tau}+\left(\boldsymbol{\lambda}_{\tau+1}^j\right)^T\frac{\partial\mathbf{F}_\tau^j}{\partial\mathbf{u}_\tau}\right)\cdot\delta\mathbf{u}_\tau\end{aligned} \tag{4.14}$$

where there are no variations of $\boldsymbol{\alpha}_{\tau|t}^j$ due to the fact that $\boldsymbol{\alpha}_{\tau|t}^j$ is independent of $\mathbf{u}_\tau$. To achieve optimality the terms involving $\delta\mathbf{x}_{\tau|t}^j$, $\delta\boldsymbol{\lambda}_{\tau+1}^j$, and $\delta\mathbf{u}_\tau$ should all vanish. Note that the first term in equation (4.14) automatically vanishes due to the fact that a change in inputs does not affect the initial condition $\mathbf{x}_{t|t}^j$. The fourth term in equation (4.14) vanishes due to the fact that $\mathbf{F}_\tau^j=0$. The terms involving $\delta\mathbf{x}_{\tau|t}^j$ and $\delta\mathbf{x}_{N_T|t}^j$ will vanish if the following conditions are satisfied:

$$\begin{aligned}\left(\boldsymbol{\lambda}_\tau^j\right)^T &= -\left[\frac{\partial\left(J_\tau'\right)^j}{\partial\mathbf{x}_{\tau|t}^j}+\left(\boldsymbol{\lambda}_{\tau+1}^j\right)^T\frac{\partial\mathbf{F}_\tau^j}{\partial\mathbf{x}_{\tau|t}^j}\right]\left(\frac{\partial\mathbf{F}_{\tau-1}^j}{\partial\mathbf{x}_{\tau|t}^j}\right)^{-1} \qquad \tau=t+1,\ldots,N_T-1\\ \left(\boldsymbol{\lambda}_{N_T}^j\right)^T &= \mathbf{0}^T\end{aligned} \tag{4.15}$$

Equation (4.15) defines the adjoint model for realization j. To calculate the Lagrange multipliers $\boldsymbol{\lambda}_t^j$ the adjoint model must be solved backwards in time. If the adjoint model is satisfied then equation (4.14) can be written as

$$\delta\ell_t^j=\sum_{\tau=t}^{N_T-1}\left(\frac{\partial\left(J_\tau'\right)^j}{\partial\mathbf{u}_\tau}+\left(\boldsymbol{\lambda}_{\tau+1}^j\right)^T\frac{\partial\mathbf{F}_\tau^j}{\partial\mathbf{u}_\tau}\right)\cdot\delta\mathbf{u}_\tau \tag{4.16}$$

Thus the gradients of the objective with respect to the controls are then

$$\frac{dJ_t^j}{d\mathbf{u}_\tau}=\frac{d\ell_t^j}{d\mathbf{u}_\tau}=\frac{\partial\left(J_\tau'\right)^j}{\partial\mathbf{u}_\tau}+\left(\boldsymbol{\lambda}_{\tau+1}^j\right)^T\frac{\partial\mathbf{F}_\tau^j}{\partial\mathbf{u}_\tau} \qquad \forall\tau=t,\ldots,N_T-1 \tag{4.17}$$

Detailed derivation could be found, for example, in [42]. For each realization, equation (4.15) and (4.17) can be used to calculate the necessary gradients. The gradients of the objective for the whole ensemble then can be calculated using equation (4.11). The interior point method is implemented to search for the optimal control strategies until all gradients are sufficiently close to zero. This is a very efficient approach compared to the finite difference approximation. For each realization, only one backward simulation of the adjoint model is needed to calculate the gradients.

Note that additional derivatives $\partial \mathbf{F}_{\tau-1}^{j} / \partial \mathbf{x}_{\tau}^{j}$, $\partial \mathbf{F}_{\tau}^{j} / \partial \mathbf{x}_{\tau}^{j}$, and $\partial \mathbf{F}_{\tau}^{j} / \partial \mathbf{u}_{\tau}$ are needed to calculate the gradients. As shown in Chapter 2, the second-order expansion of the discretized equations during the derivation the reduced-order model has already included those derivatives, and thus there is no additional effort to calculate these derivatives.

4.2.4 The EnKF for Ensemble Model Updating

An essential component of the closed-loop control framework is the model-updating part, i.e., conditioning of the states and model parameters to measured data. Here we utilize the ensemble Kalman filter to update the states and model parameters. There are several advantages using the EnKF within the ensemble closed-loop control framework. First, it is natural and efficient to use the EnKF here since we use the ensemble to represent uncertainty in model parameters and the EnKF can update the whole ensemble collectively. Second, the EnKF is able to characterize uncertainty propagation for large-scale nonlinear systems. Third, with appropriate parameterization methods, geological features are readily preserved during the EnKF updating.

The EnKF can be divided into two stages at each time step: the forecast of new states $\mathbf{x}_{\tau+1|t}^{j}$ for replicate j at current time $\tau+1$ based on updated states $\mathbf{x}_{\tau|t}^{j}$ and parameters $\boldsymbol{\alpha}_{\tau|t}^{j}$ at time τ using the system model; and updating of the predicted states $\mathbf{x}_{\tau+1|t}^{j}$ and model parameters $\boldsymbol{\alpha}_{\tau+1|t}^{j}$ to obtain conditional replicates $\mathbf{x}_{\tau+1|\tau+1}^{j}$ and $\boldsymbol{\alpha}_{\tau+1|\tau+1}^{j}$ based on the Kalman gain and perturbed observation ensemble $\left\{\mathbf{z}_{\tau+1|t}^{j}\right\}_{j=1}^{M}$ at time $\tau+1$. The forecast step proceeds by applying the system equations to each of the replicates

$$\begin{aligned} \mathbf{F}_{\tau}^{j}\left(\mathbf{x}_{\tau+1|t}^{j}, \mathbf{x}_{\tau|t}^{j}, \mathbf{u}_{\tau}, \boldsymbol{\alpha}_{\tau|t}^{j}\right) &= 0 \\ \boldsymbol{\alpha}_{\tau+1|t}^{j} - \boldsymbol{\alpha}_{\tau|t}^{j} &= 0 \end{aligned} \tag{4.18}$$

where $\mathbf{x}_{\tau+1|t}^{j}$ indicate predicted states at time $\tau+1$ based on information available at time τ, i.e. states and model parameters at time τ. $\mathbf{x}_{\tau|t}^{j}$ and $\boldsymbol{\alpha}_{\tau|t}^{j}$ denote state and parameter forecasts at time τ conditioned on measurements at time t. The second equation in (4.18) is an augmented equation to propagate static parameters forward in time. The augmented equation is needed due to the fact that the states are augmented by model parameters in the updating step such that the states and parameters can be updated simultaneously. This can be easily accomplished by augmenting the state vector with uncertain parameters, that is

$$\left(\mathbf{x}_{\tau|t}^{j}\right)^{\text{aug}} = \begin{bmatrix} \mathbf{x}_{\tau|t}^{j} \\ \boldsymbol{\alpha}_{\tau|t}^{j} \end{bmatrix} \tag{4.19}$$

At the model updating step the predicted states and model parameters in equation (4.18) can be updated using the following equation [43]

$$\left(\mathbf{x}_{\tau+1|\tau+1}^{j}\right)^{\text{aug}} = \left(\mathbf{x}_{\tau+1|t}^{j}\right)^{\text{aug}} + \text{Cov}\left(\left(\mathbf{x}_{\tau+1|t}^{j}\right)^{\text{aug}}, \mathbf{z}_{\tau+1|t}^{j}\right) \cdot \text{Cov}^{-1}\left(\mathbf{z}_{\tau+1|t}^{j}, \mathbf{z}_{\tau+1|t}^{j}\right) \cdot \left(\mathbf{d}_{\tau+1} - \mathbf{z}_{\tau+1|t}^{j}\right) \tag{4.20}$$

where $\text{Cov}(\cdot,\cdot)$ denotes the covariance between two arguments, and $\mathbf{d}_{\tau+1}$ is the measurement vector for the true system. $\mathbf{z}_{\tau+1|t}^{j}$ are predicted measurements for realization j, which follow

$$\mathbf{z}_{\tau+1|t}^{j} = \mathbf{g}\left(\mathbf{x}_{\tau+1|t}^{j}\right) + \mathbf{v}_{\tau+1}^{j} \tag{4.21}$$

where $\mathbf{v}_{\tau+1}^{j}$ is the measurement noise for realization j.

To complete the updating procedure, the following initial conditions are needed:

$$\begin{aligned} \mathbf{x}_{0|0}^{j} &= \mathbf{x}_{0}^{j} \\ \boldsymbol{\alpha}_{0|0}^{j} &= \boldsymbol{\alpha}_{0}^{j} \end{aligned} \tag{4.22}$$

4.2.5 Ensemble Open loop and Closed-loop Control Strategies

The characteristic of open-loop control is that it does not use the feedback to determine whether or not the system output has achieved the desired goal. For the subsur-

face transport control, the desired goal is the objective defined in equation (4.6). Applied pumping rates are intended for achieving cost minima. However, due to uncertainty in model parameters, open-loop control strategies often fail to achieve this goal in practice. To improve the robustness of open loop control strategies, an ensemble that characterizes probabilistic distribution of uncertain model parameters can be used to derive the optimal controls [13]. Formally, the ensemble open loop control strategies are solutions to the following optimization problem:

$$\min_{\mathbf{u}_{0:N_T-1}} \frac{1}{M}\sum_{j=1}^{M}\sum_{\tau=0}^{N_T-1} J'_\tau\left(\mathbf{x}^j_{\tau|0}, \mathbf{u}_\tau, \boldsymbol{\alpha}^j_{\tau|0}\right) \tag{4.23}$$

subject to

$$\begin{gathered}\mathbf{F}^j_\tau\left(\mathbf{x}^j_{\tau+1|0}, \mathbf{x}^j_{\tau|0}, \mathbf{u}_\tau, \boldsymbol{\alpha}^j_{\tau|0}\right) = 0 \\ \mathbf{u}^l_\tau \le \mathbf{u}_\tau \le \mathbf{u}^u_\tau\end{gathered} \tag{4.24}$$

where $\tau = 0,\ldots,N_T-1$, and $j = 1,\ldots,M$. Note that there is no model updating at time 0, and thus $\mathbf{x}^j_{\tau|0} = \mathbf{x}^j_\tau$ and $\boldsymbol{\alpha}^j_{\tau|0} = \boldsymbol{\alpha}^j$. The ensemble open loop control strategy $\mathbf{u}_{0:N_T-1}$ is essentially derived at the initial time step based on the prior ensemble.

The closed-loop control utilizes feedback information to adjust current controls in real time. In this implementation, the feedback information includes measurement data for the true system. Assume at time t the states and model parameters have been updated using equation (4.20) based on measured data available at time t. The new controls for current time step t can be obtained by solving the following optimization problem:

$$\min_{\mathbf{u}_{t:N_T-1}} \frac{1}{M}\sum_{j=1}^{M}\sum_{\tau=t}^{N_T-1} J'_\tau\left(\mathbf{x}^j_{\tau|t}, \mathbf{u}_\tau, \boldsymbol{\alpha}^j_{\tau|t}\right) \tag{4.25}$$

subject to

$$\begin{gathered}\mathbf{F}^j_\tau\left(\mathbf{x}^j_{\tau+1|t}, \mathbf{x}^j_{\tau|t}, \mathbf{u}_\tau, \boldsymbol{\alpha}^j_{\tau|t}\right) = 0 \\ \mathbf{u}^l_\tau \le \mathbf{u}_\tau \le \mathbf{u}^u_\tau\end{gathered} \tag{4.26}$$

where $\tau = t,\ldots,N_T-1$ and $j=1,\ldots,M$. The new optimal controls $\mathbf{u}_t$ for current time step are then applied to the system. All future controls $\mathbf{u}_{t+1:N_T-1}$ are discarded since they will be re-computed with new measurements on subsequent time steps.

4.2.6 Ensemble Closed-loop Control with Reduced-Order Modeling

The ensemble closed-loop control requires evaluations of the system model during the forecast step of the EnKF for each realization. Moreover, during the optimization procedure, there are usually a significant number of search steps, and for each step, the system model is evaluated for each realization. Hence, for large-scale problems, the ensemble closed-loop control is prohibitively expensive. In this work, we use a reduced-order to substitute the expensive full order model during forward simulations. This create the possibility of apply the ensemble closed-loop control to large-scale subsurface control problems.

A robust, efficient second order reduced-order model for 2D subsurface solute transport has been derived and validated in Chapter 2. In this work, we implement the reduced-order model in the forward simulations of the closed-loop control. The reduced-order system model can be written as

$$\hat{\mathbf{F}}_\tau^j\left(\hat{\mathbf{x}}_{\tau+1|t}^j,\hat{\mathbf{x}}_{\tau|t}^j,\mathbf{u}_\tau,\hat{\boldsymbol{\alpha}}_{\tau|t}^j\right)=0 \tag{4.27}$$

where $\hat{\mathbf{F}}$ denote reduced-order system equations. $\hat{\mathbf{x}}_{\tau|t}^j$ and $\hat{\boldsymbol{\alpha}}_{\tau|t}^j$ are reduced representations of the states and model parameters, which follow

$$\begin{aligned}\mathbf{x}_{\tau|t}^j &\approx \boldsymbol{\Phi}_{\mathbf{x}}^T\hat{\mathbf{x}}_{\tau|t}^j\\ \boldsymbol{\alpha}_{\tau|t}^j &\approx \boldsymbol{\Phi}_{\boldsymbol{\alpha}}^T\hat{\boldsymbol{\alpha}}_{\tau|t}^j\end{aligned} \tag{4.28}$$

Here, $\boldsymbol{\Phi}_{\mathbf{x}}$ is the projection matrix for the states and is derived from the POD method, while $\boldsymbol{\Phi}_{\boldsymbol{\alpha}}$ is the projection matrix for model parameters and is actually drawn from the constant DCT matrix. Detailed introduction to the reduced-order model could be found in Chapter 2 and thus omitted here.

The key step to apply reduced-order modeling to the ensemble closed-loop control is to replace model constraints in equation (4.26) with equation (4.27) and propagate

the reduced-order states $\hat{\mathbf{x}}_{\tau|t}^{j}$ instead of the full order states in time. During the model-updating step, the reduced representations $\hat{\mathbf{x}}_{\tau|t}^{j}$ and $\hat{\boldsymbol{\alpha}}_{\tau|t}^{j}$ are updated using the EnKF instead of the full order states and model parameters. For the optimization loop, the objective function can now be evaluated as

$$\begin{aligned} J_t &\approx \frac{1}{M}\sum_{j=1}^{M}\sum_{\tau=t}^{N_T-1} J_\tau'\left(\boldsymbol{\Phi}_{\mathbf{x}}^{T}\hat{\mathbf{x}}_{\tau|t}^{j}, \mathbf{u}_\tau, \boldsymbol{\Phi}_{\boldsymbol{\alpha}}^{T}\hat{\boldsymbol{\alpha}}_{\tau|t}^{j}\right) \\ &= \frac{1}{M}\sum_{j=1}^{M}\sum_{\tau=t}^{N_T-1} \hat{J}_\tau'\left(\hat{\mathbf{x}}_{\tau|t}^{j}, \mathbf{u}_\tau, \hat{\boldsymbol{\alpha}}_{\tau|t}^{j}\right) \end{aligned} \tag{4.29}$$

The adjoint model is then derived based on $\hat{\mathbf{x}}_{\tau|t}^{j}$ and reduced model constraints defined in equation (4.27). However, the procedure of derivation is exactly the same as the full order case and thus is omitted here.

The objective, model constraints, and model-updating equations can all be expressed in terms of the reduced representations of the states and model parameters. This is much more efficient that the full order case as long as the reduced-order model is sufficiently robust. As shown in Chapter 2, the accuracy of the reduced-order model mainly depends on the ability of the DCT basis vectors to span the relevant parameters space as well as the ability of the POD basis vectors to span the relevant state space. The DCT representation is sufficient as long as it can characterize the geological features properly, while the ability of POD basis vectors depends on the snapshots of states used to generate the basis. It is crucial to enrich the POD basis vectors sufficiently such that the reduced-order model is accurate enough during the closed-loop control procedure.

In previous chapters, a combined snapshot set of states and derivatives of the states with respect to model parameters for several selected parameter configurations in the ensemble is used to generate the basis vectors to ensure that the reduced-order model is valid over the ensemble. In this work, it is necessary to ensure the POD basis vectors to span the space corresponding to both parameter and control changes. To this end, several control configurations are selected for the training runs of the full order model to generate necessary snapshots. Those training control configurations

are not arbitrary. Instead, to increase the possibility that the training control configurations are close to the optimal control configurations for the true system, those training control configurations are actually optimal for the selected parameter configurations. That is, each of the training control configurations corresponds to minimum cost for a particular parameter configuration. If the training parameter configurations have optimal control configurations close enough to the optimal control configurations for the true system, then, as the ensemble tends to converge to the true system with model updating, the POD basis vectors are then sufficient to span the state space relevant to the optimization procedure. Generally the true optimal control strategies are not identical to the ensemble closed-loop control strategies. Here we assume there are close to each other. This is especially true for a convex optimization problem where only one optimum exists.

4.2.7 **Implementation Issues**

Figure 4-2 illustrates the procedure of the ensemble closed-loop control with reduced-order modeling. The whole process can be divided into two stages: offline training and online closed-loop control. The offline training process of generating a robust reduced-order model has been elaborated in Chapter 2. Note that the training runs to generate snapshots of states are performed for combinations of selected parameter configurations and control configurations such that the POD basis vectors are sufficiently enriched. The resulting second order reduced-order is deemed to be robust during the ensemble closed-loop procedure and thus there is no updating of the reduced-order model during online simulations.

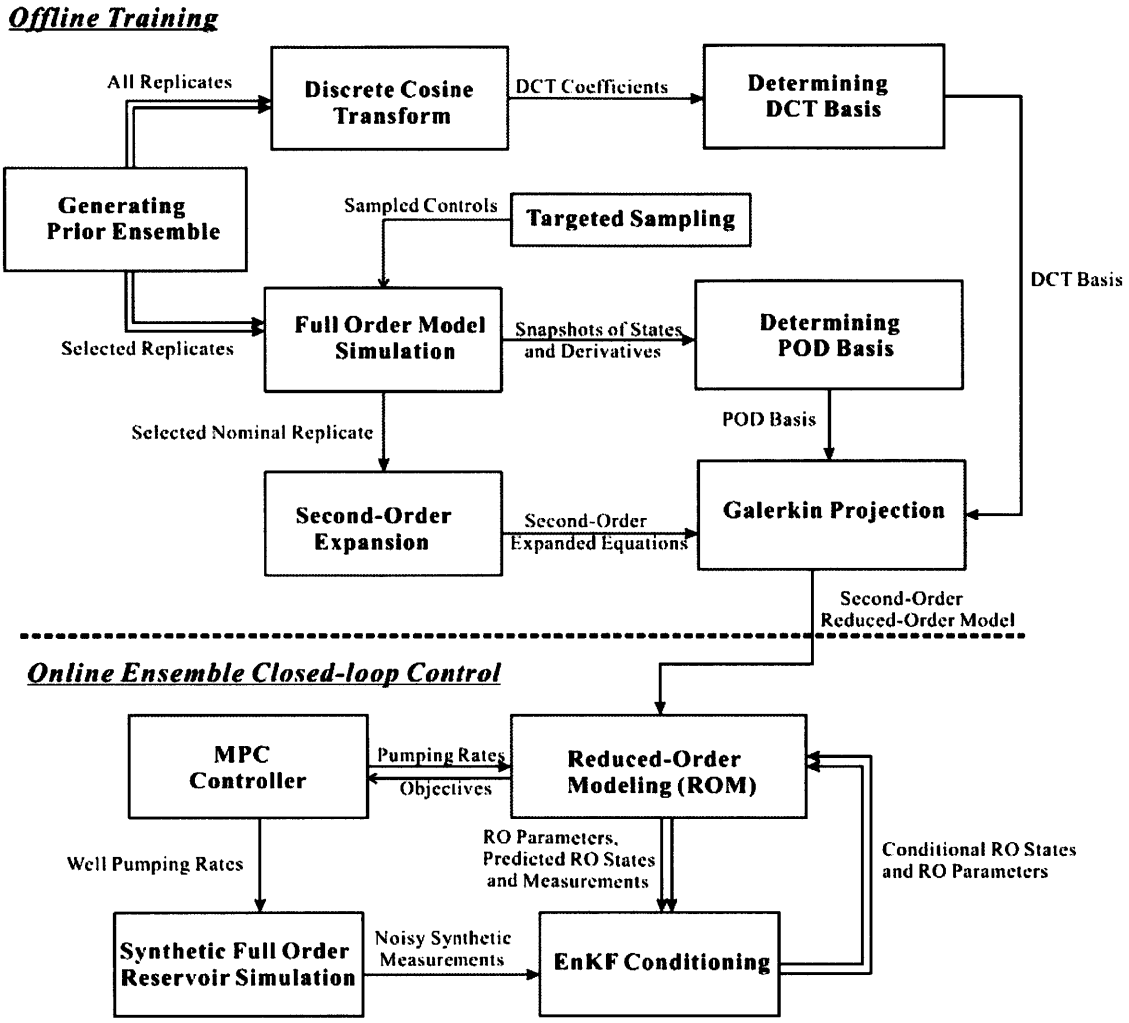

Figure 4-2: Flowchart showing offline ensemble-based generation of a robust reduced-order model with order reduction in both parameter and state spaces, and online closed-loop control of the system with ensemble updating of uncertain reduced-order (RO) states and reduced-order (RO) parameters. Double lines indicate multiple operations on replicates in the ensemble.

During online simulations, the controller solves an optimization problem defined in equation (4.25) and (4.26) to obtain optimal pumping rates for the current time step. Note that with reduced-order modeling now the objective is defined using the reduced representations and the model constraints are substituted by equation (4.27). The optimal control strategies are applied to the ensemble to generate necessary forecasts for the EnKF. Also, the optimal control strategies are applied to the true system to generate measurement data. The EnKF then updates reduced representations of

model states and model parameters. The conditional model states and parameters can then be used to solve for optimal control strategies for the next time step by the controller. In this ensemble closed-loop control loop, the EnKF updates uncertain model states and parameters sequentially based on feedback from the true system, while the controller adjust controls accordingly to steer the true system to approach minimum cost.

4.3 Numerical Experiments

4.3.1 Experimental Setup

In this synthetic example, a 320 m×320 m×1 m porous domain is discretized into a 2D 32×32×1 uniform grid cell system. The size of each cell is 10 m×10 m×1 m. The whole domain has the constant porosity of 0.2. Figure 4-3 shows the simulation domain and the locations of 4 pumping wells. The length of the simulation horizon is 400 days, which is divided into 4 constant intervals. Each of the intervals represents a control step. The solute is injected into the domain at the mid-lower cells with a constant rate of 5 m^3/day and constant concentration of 50 mg/L for the first 200 days. Here specific storage $s = 0$ is used to represent steady-state flow conditions so the head is constant over each control step. The flow equation has no water flux boundaries on the east and west sides and constant head boundaries of 10 m and 0 m on the south and north sides. The transport equation also has no solute flux boundaries on the east and west sides, but has prescribed zero solute concentration boundary conditions on the south and north sides. The dispersion coefficient is assumed to be constant over the whole domain in all direction, and thus the transport equation is linear for each control step.

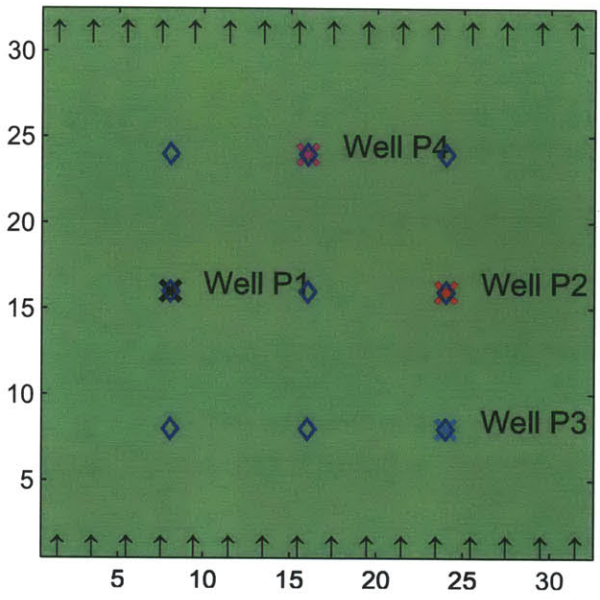

Figure 4-3: Experimental setup: simulation domain with 9 measurement locations (blue diamonds) and 4 pumping well locations: Well P1 (black cross), Well P2 (red cross), Well P3 (cyan cross), and Well P4 (magenta cross).

The measurements at the data assimilations step include head and pressure information at 9 measurement locations indicated by the blue diamonds in Figure 4-3. The measurements are taken at the end of control steps, which are day 100, 200, 300, and 400, and thus there are four EnKF updates during the simulations. In this study, the measurements are from full order simulations using a synthetic true conductivity field.

In this experiment, only well P1, P2, and P3 can be controlled, while well P4 is used for drinking purpose and has a constant pumping rate of 10 m^3/day. The control objective for time step τ is defined as

$$J'_\tau\left(\mathbf{x}^j_{\tau|t}, \mathbf{u}_\tau, \boldsymbol{\alpha}^j_{\tau|t}\right) = \sum_{i=1}^{3} u^2_{\tau,i} + w \cdot c_{\tau,4|t} \tag{4.30}$$

where $u_{\tau,i}$ is the pumping rate for the i-th well at time step τ, w is a weighting coefficient, and $c_{\tau,4|t}$ is the solute concentration for well P4 at time step τ. The first term in (4.30) represents cost incurred by pumping while the second term penalizes the amount of solute pumped out from well P4. The lower and upper bounds for pumping rates are

$$-50\ \mathrm{m}^3/\mathrm{day} \le u_{r,i} \le 0 \qquad i = 1,2,3 \tag{4.31}$$

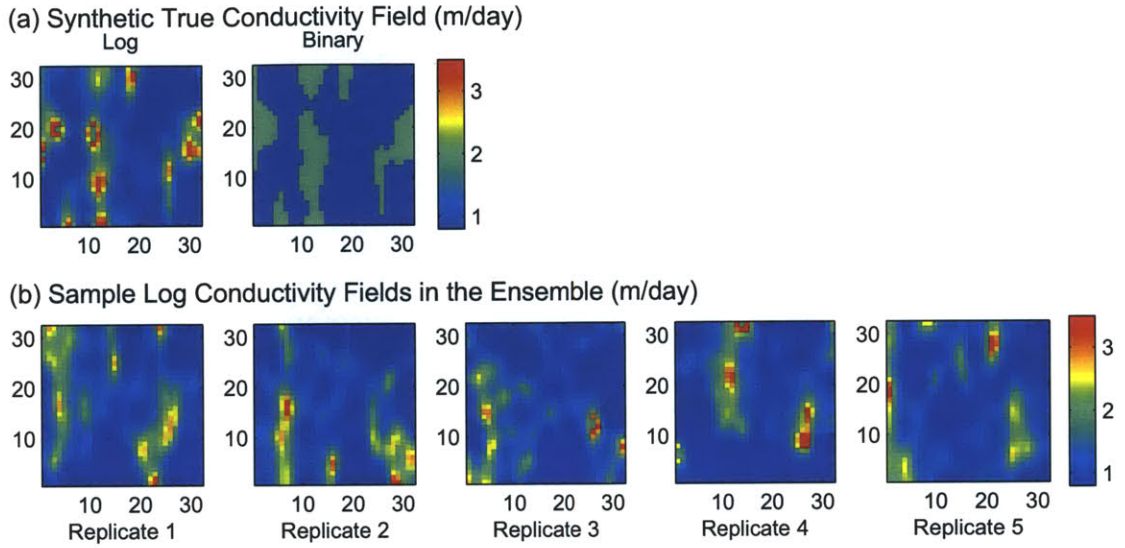

Figure 4-4: Samples of hydraulic conductivity. (a) The true conductivity field. (b) Five representative replicates in the prior ensemble.

The unknown parameters are the hydraulic resistivity for each cell of the discretized domain. A synthetic true conductivity fields is generated using Gaussian indicator simulator in the Stanford SGeMS. As shown in Figure 4-4(a), the true conductivity generated by the Gaussian simulator is characterized by one high permeable channel in the middle. The true conductivity field is used in the simulations to generate noisy synthetic true measurements. The true conductivity field is also converted to a binary image for the purpose of calculating Jaccard distances. As shown in Figure 4-4(a), for the true conductivity field, the converted binary image has 1's in the cells with $\log(k) > 1.5$, where k denotes the conductivity. All the other cells have zero values. The channelized structures are retained after this conversion.

Reasonable probabilistic models of the conductivity field need to be constructed before a successful EnKF implementation. An ensemble of 50 realizations of conductivity fields, which has the same probability distribution as the true conductivity field, is generated using Gaussian indicator simulator in the Stanford SGeMS. The prior ensemble used in experiments is a reconstructed ensemble from the simulated ensemble

using DCT parameterization. The parameterization process is described in the following subsection. Five of the resulting realizations are shown in Figure 4-4(b). We can clearly see that the conductivity fields have high permeable and low permeable zones, which create pathways for solute transport

4.3.2 Generation of the Reduced-Order Model

The reduced-order model uses reduced-dimensional DCT coefficients to represent high-dimensional hydraulic conductivity. The DCT is performed for the entire prior ensemble, and the resulting DCT coefficients are arranged in a descending order for each replicate in the ensemble. The DCT vectors correspond to the first few (about 20) largest coefficients of each replicate are retained and the others are discarded. Then all distinctive retained DCT vectors are combined to form the DCT projection matrix for the ensemble. The process results in about 10% DCT basis vectors in the projection matrix.

In the reduced-order model derivation 10 of the replicates in the ensemble are selected for off-line full order simulations under 10 different control sequences. Each control configuration corresponds to optimal control solutions for one of the replicate. The simulations are done for each combination of the replicates and control configurations, and thus a total of 100 training runs are needed. As discussed in Chapter 2, these provide snapshots of states at different times for each selected replicate. Also, derivatives of the head and velocity with respect to hydraulic resistivity are calculated and collected as part of the snapshots for one of the replicates under 10 different control sequences. There are a total of 1024 columns of derivative vectors and thus the snapshot matrices are expanded significantly. POD projection matrices can then be obtained based on the snapshots to generate reduced representations of the states. To obtain a compact representation of the states, the POD expansion is truncated at the number of basis function terms that account for 99%, 93%, 93%, and 99% of the energy in the head, x velocity, y velocity and concentration, respectively. This gives reduced dimensions of 56, 103, 97, and 194, for these four variables, each of which

has a full order dimension of about 1024. Detailed derivation of the reduced-order model and validation of its robustness for the ensemble can be found in Chapter 2.

4.3.3 Control Comparison

This and the next subsections present concentration evolutions for the true conductivity field under various control sequences. There are several cases discussed here. The first case is an uncontrolled case, where there is no pumping at Well P1, P2, and P3, while Well P4 maintains the constant pumping rate. This is the reference case, indicating how the plume behaviors under head gradients incurred by boundary conditions as well as pumping at Well P4. In the second case the true field is under optimal controls derived by solving a deterministic optimization problem with perfect conductivity knowledge. This case illustrates the best performance that can be achieved under all scenarios. In the third case the plume is controlled by optimal pumping rates derived by solving the ensemble closed-loop optimization problem defined in equation (4.25) with full order model constraints. During the control process, the ensemble is updated using the EnKF based on measured head and concentration. This case illustrates the benefits of taking feedback to control the true system under uncertainty. Similarly, in the fourth case the plume is controlled under ensemble closed-loop control strategies, with reduced-order, instead of full order model constraints. This case can evaluate the efficiency and robustness of applying reducing order modeling to the ensemble closed-loop control framework. In the last case the control sequence is derived by solving the optimization problem defined in equation (4.23) with full order constraints. This is the ensemble open loop control case, where there is no EnKF updating and the controls are purely based on the prior ensemble.

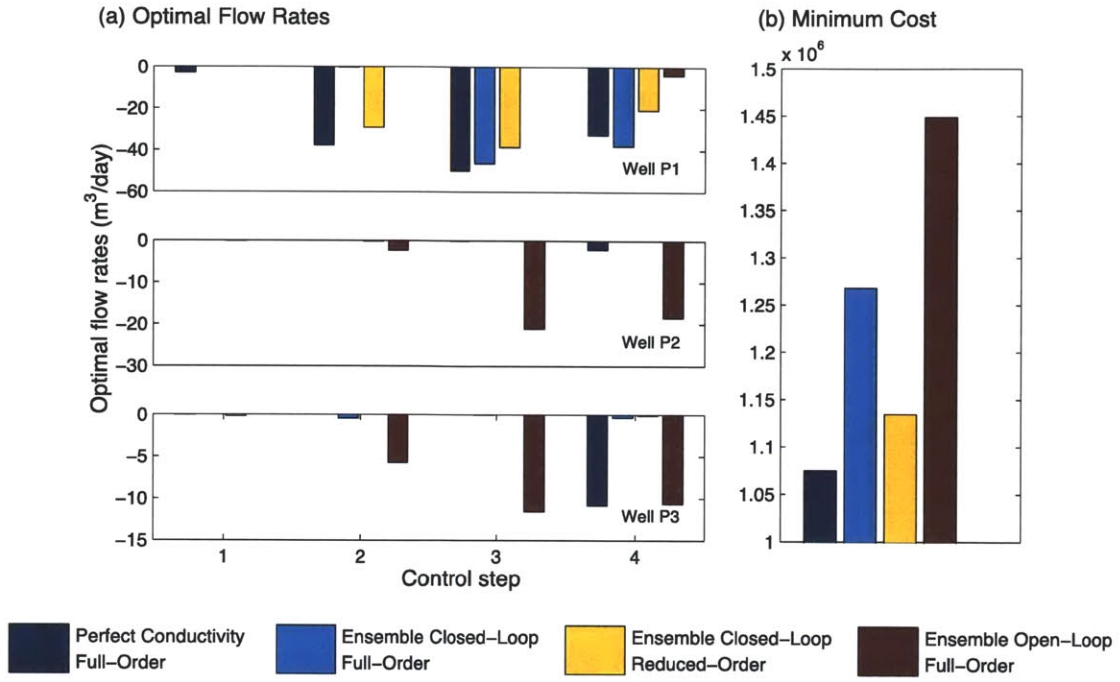

Figure 4-5: Comparison of various control strategies with dark blue indicating optimal controls based on perfect conductivity knowledge, cyan indicating ensemble closed-loop controls with EnKF updating using full order modeling, yellow indicating ensemble closed-loop controls with EnKF updating using reduced-order modeling, and brown indicating ensemble open-loop controls without EnKF updating using full order modeling: (a) various optimal control strategies for Well P1, P2, and P3; (b) corresponding minimum cost under various control strategies.

Figure 4-5 presents optimal control strategies under various scenarios. In Figure 4-5(a) the dark blue corresponds to the deterministic case where the true conductivity field is known perfectly. It is shown that the pumping rates increase first then decrease at Well P1, which is located within the high permeable channel (cf. Figure 4-3). There is almost no pumping at Well P2, while there is a noticeable amount of pumping at the last control step at Well P3. This indicates that the optimal control is trying to drag the plume to the high permeable channel and then pump the solute from Well P1. The cyan illustrates the ensemble closed-loop controls with full order modeling. Generally, the ensemble closed-loop control also tries to drag the plume to the channel. However, there is no pumping at Well P1 during the second control step. This is due to the fact that the EnKF hasn't recover the channelized structure and thus the controller determine there is no pumping for Well P1. This will be illustrated more

clearly in the estimation subsection. On the contrary, the ensemble closed-loop controller with reduced-order model constraints (yellow) suggests that Well P1 should be pumped during the second control step and thus the strategies are closer to those in the deterministic case. This is due to the fact that with reduced-order modeling, the channelized structure is recovered earlier than the full order case (cf. Figure 4-9). The brown illustrates the open loop control strategies derived by solving the optimization problem defined in equation (4.23). Since it is purely based on the prior ensemble and thus it is expected that the strategies are different from the previous cases where feedback is utilized.

Figure 4-5(b) presents the minimum costs corresponding to the aforementioned control scenarios. Obviously, with perfect conductivity knowledge, the performance is best in the sense that the defined cost in equation (4.30) is minimum. With uncertainty in conductivity, the ensemble closed-loop control can achieve comparable performance to the deterministic case. Note that the reduced-order case outperforms the full order case for it can derive more comparable controls than the full order case (cf. Figure 4-5(a)). The ensemble open loop controller has the worst performance due to the fact that it doesn't take advantage of the feedback from the true system.

Another trivial way, which is called Monte Carlo approach [39], to derive control strategies for the true system is based on individual replicate in the ensemble. This approach solves a series of individual optimization problems, each with a single realization from the prior ensemble of conductivity. Hence, there are a total of 50 optimization problems to be solved. The resulting 50 sets of optimal controls are then applied to the true system to evaluate their performance. Figure 4-6 illustrates the cost histogram for the true system after applying the 50 sets of controls. Obviously, the resulting costs are quite diverse. None of the 50 sets of controls can outperform the true optimal controls (indicated by the blue line). A few sets can outperform the ensemble closed-loop controls (indicated by the cyan and yellow lines), while most of them can outperform the open loop controls (indicated by the brown line). The results

indicate that the ensemble closed-loop controls are more robust than the open loop controls.

Note that although some of the 50 control sets have comparable performance to the true optimal controls, it is hard to determine which control sets will achieve the desired low cost. This is because there are a total of 12 controls in one single set and thus it is impossible to set up a direct map from controls to costs for the ensemble.

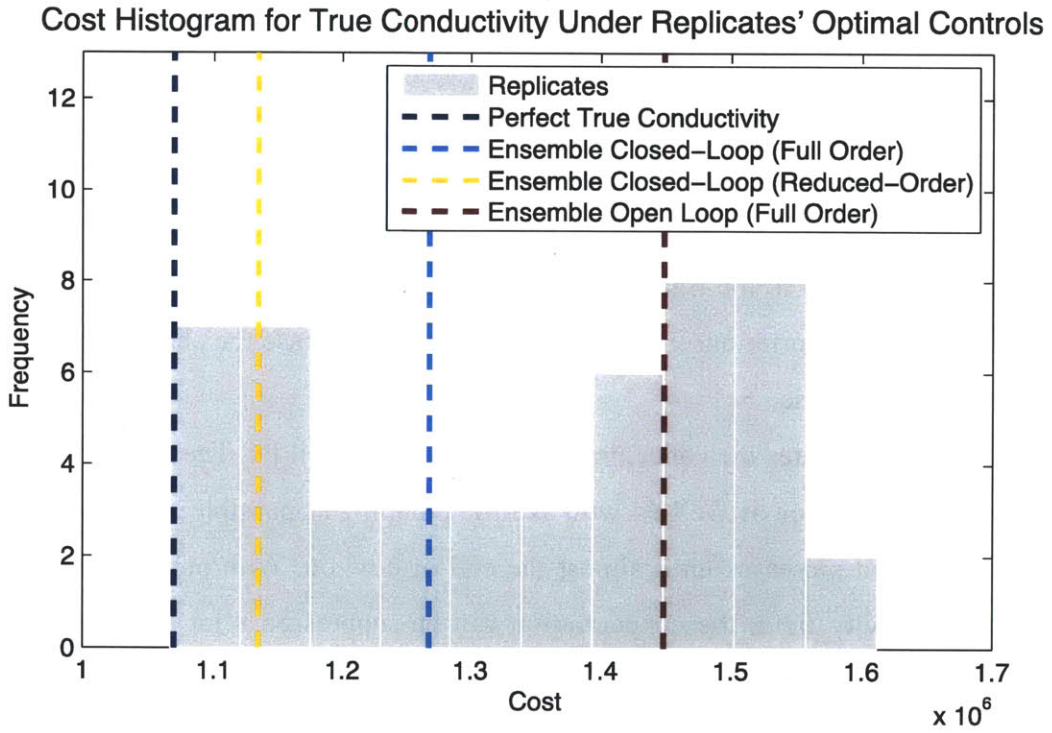

Figure 4-6: Cost histogram for the true conductivity field under individual replicates' optimal controls with dark blue indicating minimum cost based on perfect conductivity knowledge, cyan indicating cost under ensemble closed-loop controls with EnKF updating using full order modeling, yellow indicating cost under ensemble closed-loop controls with EnKF updating using reduced-order modeling, and brown indicating cost under ensemble open-loop controls without EnKF updating using full order modeling.

4.3.4 Controlled Concentration Evolutions

Figure 4-7 illustrates how the plume evolves under various control strategies. Figure 4-7(a) illustrates the uncontrolled case, i.e. the reference case. Without pumping at

Well P1, P2, and P3, the plume is swept from the bottom to the top due to head gradients. Figure 4-7(b) illustrates the optimal control case with perfect conductivity knowledge. In this case the plume is dragged to the channel and pumped out from Well P1 (cf. Figure 4-5(a)). Figure 4-7(c) illustrates the ensemble closed-loop control case with full order modeling. Generally the situation is close to the deterministic case, suggesting that with feedback the controller achieve comparable performance. A noticeable feature of the plume on day 200 is that the front of the plume reaches Well P4. This is due to this no pumping at Well P1 during the second control step. On the contrary, in Figure 4-7(c) where the reduced-order model is utilized, the front of the plume is dragged to Well P1 due to pumping. Figure 4-7(d) illustrates the ensemble open loop control case. The controls are quite different from the previous three cases. The plume is dragged to the right instead of the channel on the left. This is due to the fact the based on the prior ensemble the controller cannot sense the channelized structure on an average base.

Figure 4-8 illustrates the concentration time series at Well P4. The controller seeks minimum concentration at Well P4 with as little pumping as possible. Without control, the concentration increases until almost the end of horizon. With perfect knowledge of the conductivity field, the concentration can be suppressed a lot (compared dark and dark blue lines) with affordable pumping rates. With ensemble closed-loop control and full order modeling, from day 0 to day 200 the concentration still increases since there is no pumping for the first two control steps. After day 200, the concentration decreases a lot due to pumping. For the reduced-order case, the concentration has already decreased during the second control step due to pumping. However, the concentration increases significantly after day 300 due to decrease in pumping rates. This is due to the fact that the EnKF underestimates the concentration over this period (cf. Figure 4-12), and there is a compromise between increasing pumping rates and decreasing concentration during this period. In the ensemble open loop control case, the concentration decreases after day 250.

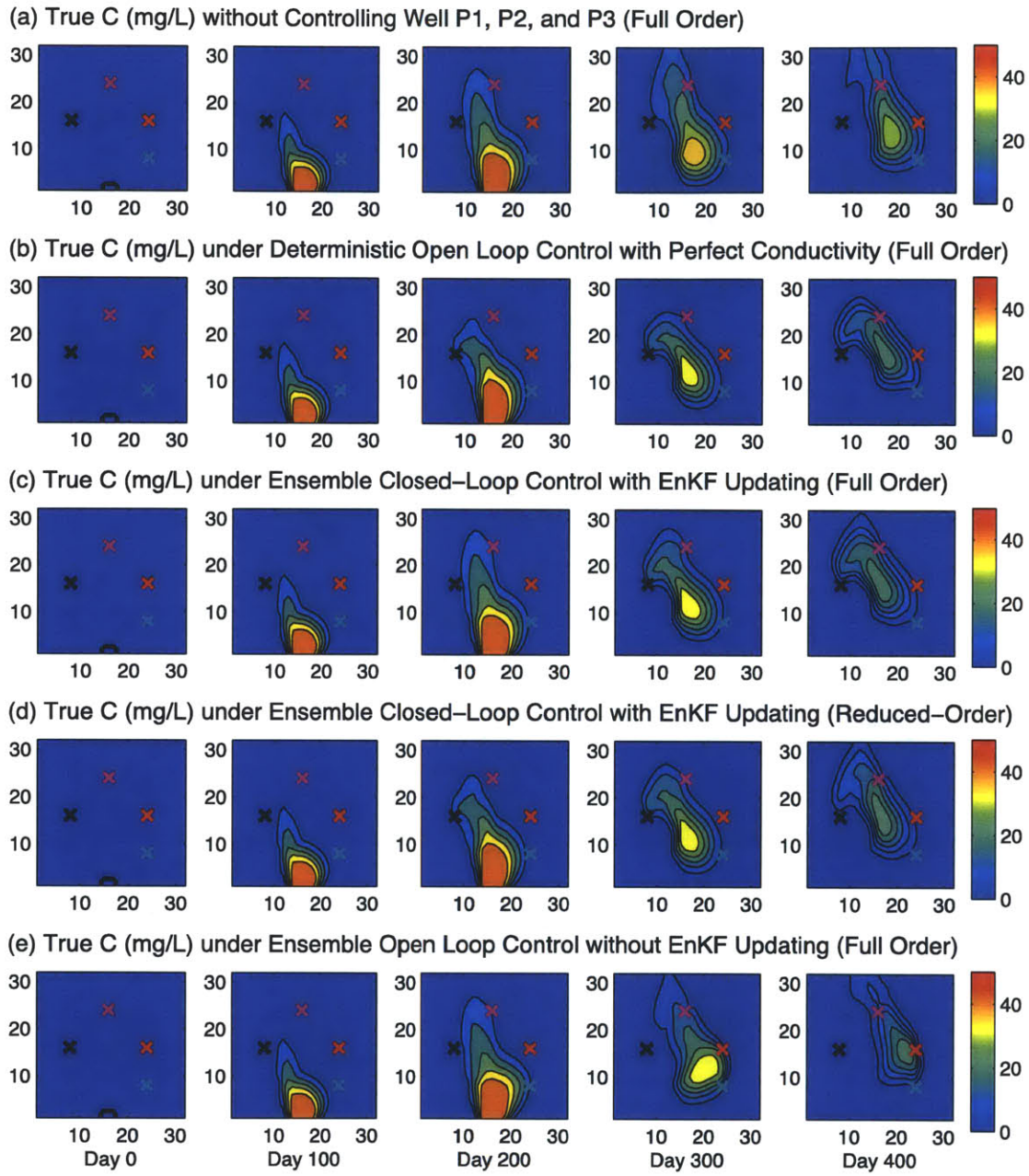

Figure 4-7: Concentration evolutions under various control strategies with well locations indicated by black (Well P1), red (Well P2), cyan (Well P3), and magenta (Well P4) crosses: (a) uncontrolled plume (no pumping at Well P1, P2 and P3); (b) plume under optimal controls based on perfect conductivity knowledge; (c) plume under ensemble closed-loop controls with EnKF updating using full order modeling; (d) plume under ensemble closed-loop controls with EnKF updating using reduced-order modeling; (e) plume under ensemble open loop controls without EnKF updating using full order modeling.

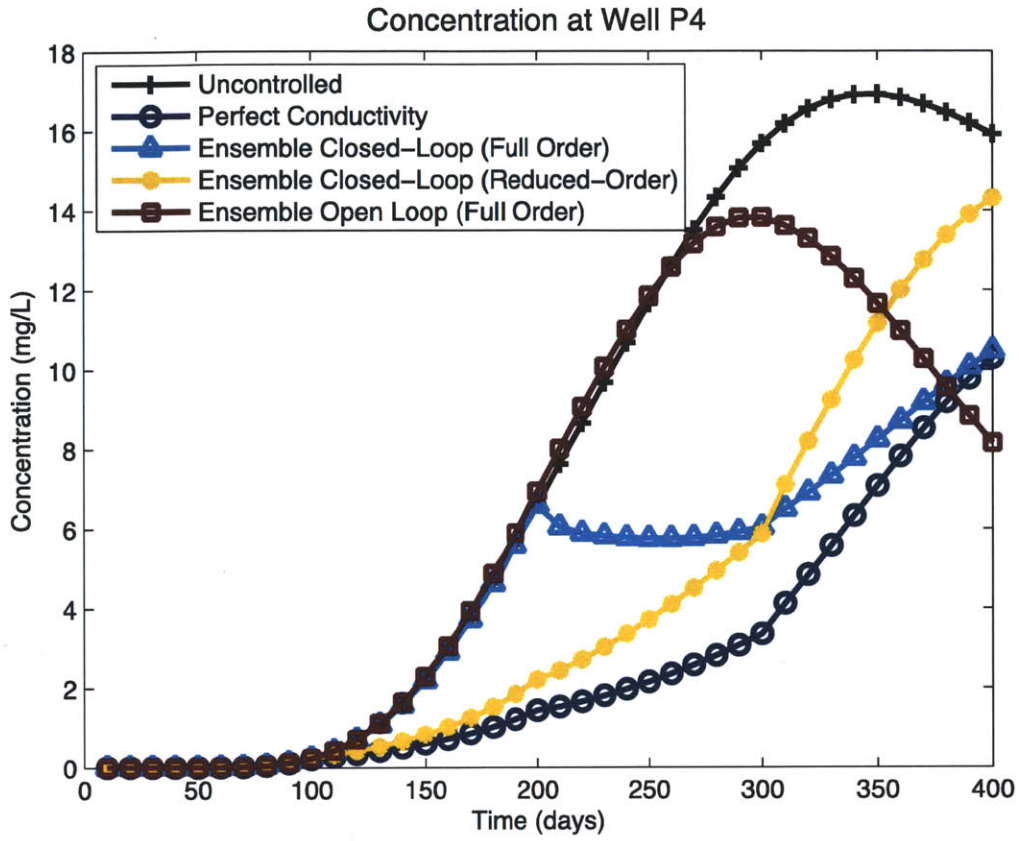

Figure 4-8: Concentration time series at Well P4 under various control strategies.

4.3.5 Estimation Results under Ensemble Closed-Loop Control

In this section the EnKF results of ensemble closed-loop control cases (full order and reduced-order) for estimating grid cell values of head, concentration, and conductivity are presented. The EnKF updating is based on both head and concentration measurements. Two cases are performed to evaluate the performance of the reduced-order model. The first case is the one with the full order model used in the forward simulations of the EnKF as well as the optimization, while the second case is the one with the reduced-order model used in the forward simulations.

Figure 4-9 summarizes the conductivity estimation results. Figure 4-9(a) presents the channelized true conductivity field. The EnKF conductivity ensemble means at different times are shown for the reduced and full-order cases in each row of Figure

4-9(b). The Jaccard distances are presented at the top of each plot to illustrate the dissimilarity between the true conductivity filed and each estimate. From the figure it is clear that the Jaccard distances gradually decrease and the channelized structure of the conductivity field is gradually recovered for both full order and reduced-order cases after the updates on day 100, 200, 300, and 400. The full order case illustrates the ability of the EnKF to identify channelized geological structures. This capability is mainly due to the strong correlations between measurements and uncertain conductivity, which help the EnKF updates converge to the true value, provided that the ensemble is sufficient to characterize the correlation information. The reduced-order case shows that the EnKF can also capture channelized structures in this case, indicating that the reduced-order model is sufficient and accurate enough to provide the information necessary for accurate EnKF updating. This illustrates that the reduced-order is a promising alternative during the forward simulations of the EnKF.

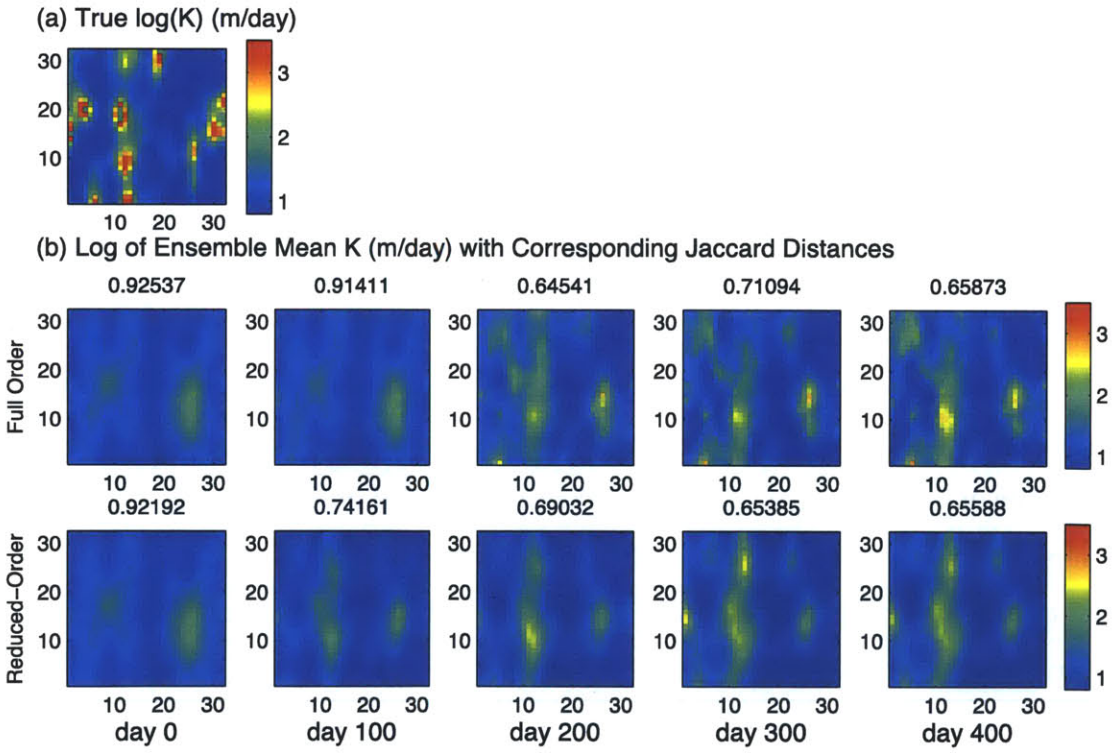

Figure 4-9: Conductivity estimation results: (a) the true log-conductivity field; (b) ensemble mean log-conductivity with corresponding Jaccard distances using the full- and reduced-order models.

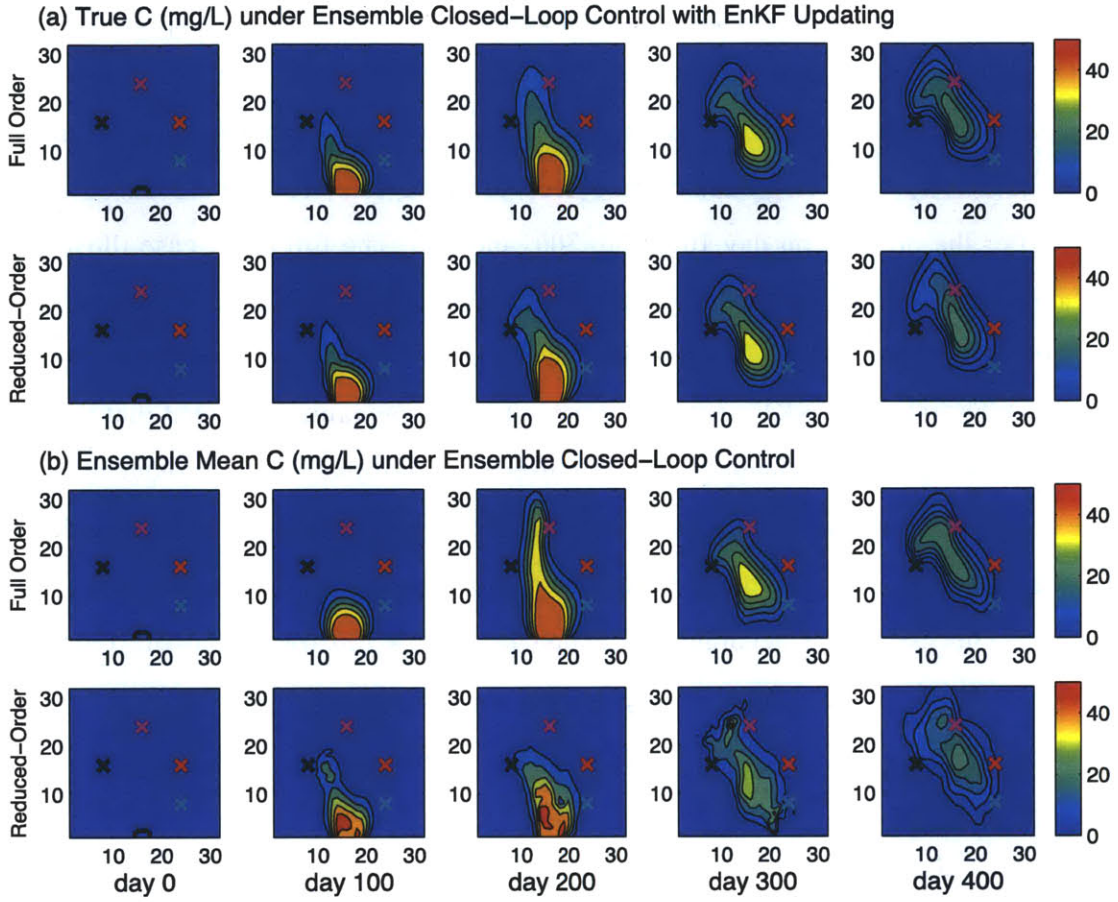

Figure 4-10: Concentration estimation results: (a) true concentration evolutions under ensemble closed-loop control using the full- and reduced- order models with well locations indicated by black (Well P1), red (Well P2), cyan (Well P3), and magenta (Well P4) crosses; (b) ensemble mean concentration under ensemble closed-loop control using the full- and reduced- order models.

It is noticeable that the Jaccard distance of the reduced-order case on day 100 is smaller than that of the full order case. On day 100, the EnKF has already recovered the channelized structure while it is not the case with full order modeling. The reason can be attributed to the fact that in the reduced-order case there are fewer unknowns that need to be updated by the EnKF. The ratio between the number of the states in the reduced-order model and the full order model is about 1 to 10. Since with reduced-order modeling, the EnKF can recover the channelized structure earlier than the full order case, the controller can generated more comparable controls to the deterministic case where the conductivity is known perfectly (cf. Figure 4-5(a)).

A close inspection reveals that it is difficult for the EnKF to capture the high permeable zones at the left and right boundaries of the domain in both cases. This is due to the fact that there is no measurement information near the boundaries. In ideal cases that the ensemble is sufficient to capture the correlations, the head measurements can reveal more conductivity information for those cells near the measurement locations, while the concentration measurements can reveal more information for those cells within solute propagation paths.

Figure 4-10(b) illustrates the ensemble mean concentration snapshots in the full order and reduced-order cases. Compared to Figure 4-10(a), it is clear that in both cases the EnKF can capture the shapes of the plume at different time steps, especially on day 400 when the last update happens. Note that for those two cases, the control strategies are different and thus the shapes of the plume are slightly different. On day 400, the shapes of the plume in both cases are very close to the ones predicted by the true case. This is consistent with the fact that the filter performance improves over time, as more measurements are collected. Note that the front the plume for the full order case on day 100 is quite different from the true case as shown in Figure 4-10(a), where the front has approaches closer to Well P4. This is why the controller determines there should be no pumping during the second control step for the full order case, while for the true field it is not optimal.

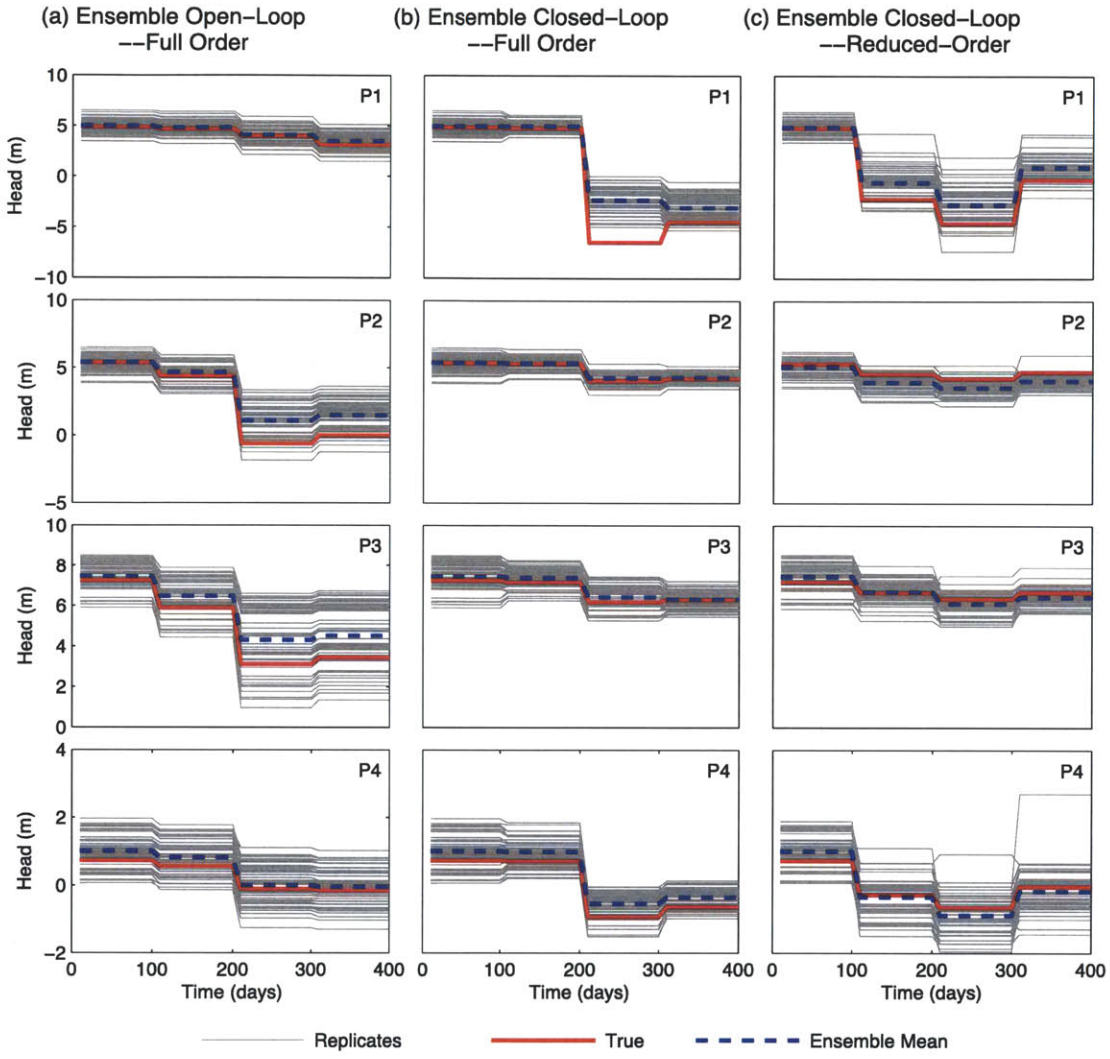

Figure 4-11: Time series of head predictions at the four well locations for replicates (gray lines), the true conductivity field (red lines), and the ensemble mean (blue lines): (a) ensemble open loop predictions using the full order model for replicates in the prior ensemble without EnKF updating; (b) ensemble closed-loop predictions using the full order model for the replicates in the ensemble with the EnKF updating the states and parameters at the end of each control step; (c) ensemble closed-loop predictions using the reduced-order model for the replicates in the ensemble with the EnKF updating.

In this problem head predictions are related to energy consumption of pumping and the concentration predictions are related to water treatment cost in containment transport cases. Figure 4-11 and Figure 4-12 illustrate head and concentration predictions for replicates in the ensemble (gray lines), the controlled true conductivity field

(red lines), the mean over the ensemble members (blue lines), and the uncontrolled true field (magenta lines) at the four pumping wells. Gray lines in Figure 4-11(a) and Figure 4-12(a) show predictions using the full order model under the ensemble open loop control for the prior ensemble without the EnKF updating. The spreads of the gray lines indicate the variability in the prior ensemble. Sufficient variability in the prior ensemble is needed to properly calculate the covariance used in the EnKF updating. In the plots we can also observe significant disparity between the initial estimates (ensemble mean indicated by blue lines) and the true predictions (red lines). However, the true predictions fall inside the spreads of the ensemble. This suggests that the true predictions fall in the space spanned by the replicates.

Gray lines in Figure 4-11(b) and Figure 4-12(b) show ensemble predictions using the full order model with the EnKF updates on day 100, 200, 300, and 400. In the plots the spreads of the ensemble shrinks noticeably over time compared to the unconditional case, indicating decreased variability or uncertainty in the ensemble. The ensemble estimates (blue lines) gradually converge to the true values, indicating the ability of the EnKF to capture the dynamic of the true system.

Similarly, Gray lines in Figure 4-11(c) and Figure 4-12(c) show predictions using the reduced-order model with the EnKF updates on day 100, 200, 300, and 400. We can observe behavior similar to Figure 4-11(b) and Figure 4-12(b), indicating the ability of the reduced-order to predicate system behavior. One noticeable difference between plots in (b) and (c) is that the spreads in (c) can be larger than those in (b) over some control steps. This is primarily due to additional model errors introduced by the reduced-order model. For example, a close inspection of the concentration predictions at Well P3 in Figure 4-12(c) reveals that on day 300, there is a jump in the concentration curves of the replicates. This corresponds to the unsmooth plume in Figure 4-9(c), which are due to predictions errors.

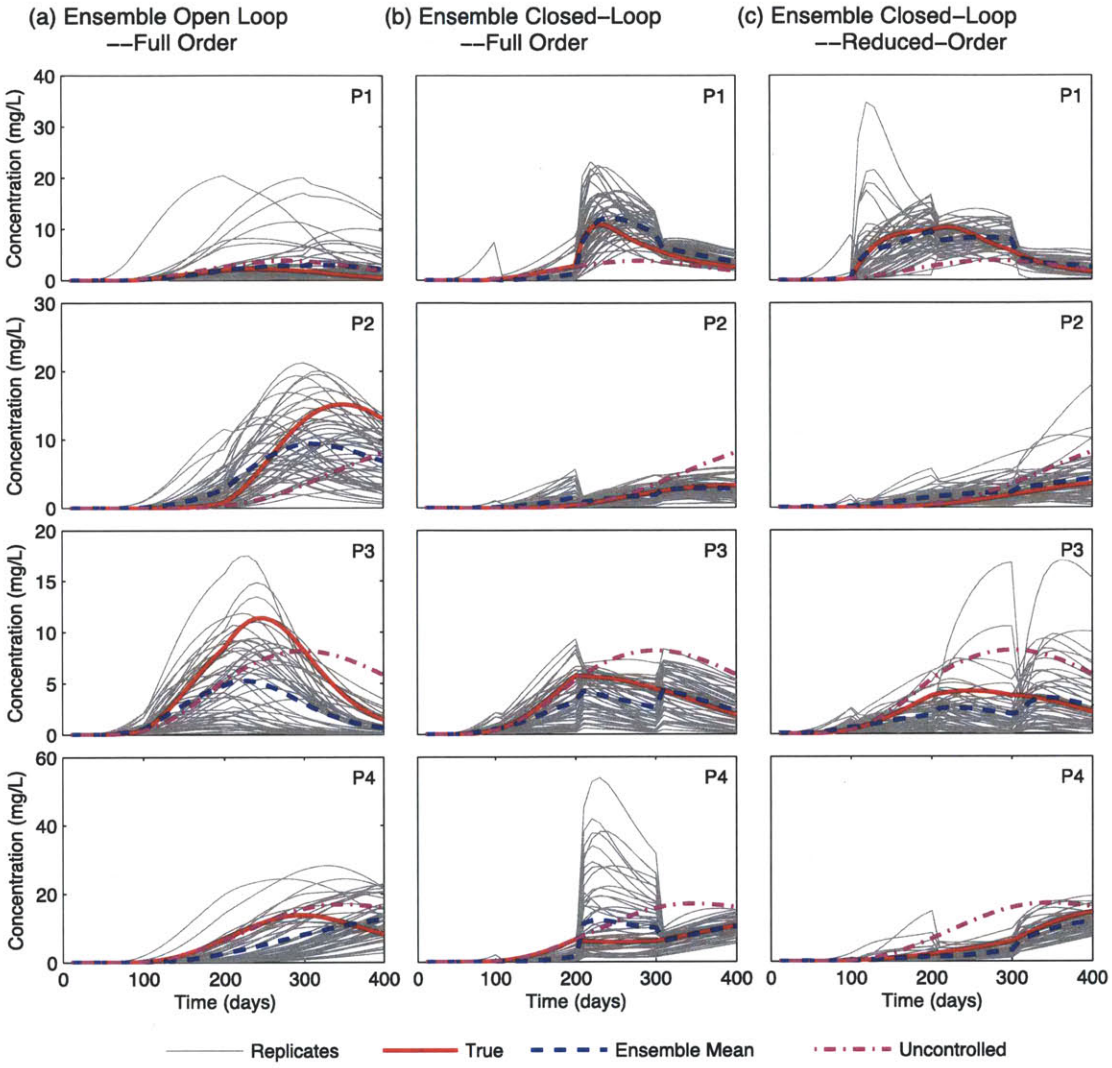

Figure 4-12: Time series of concentration predictions at the four well locations for replicates (gray lines), the controlled true conductivity field (red lines), the ensemble mean (blue lines), and uncontrolled true conductivity field (magenta lines): (a) ensemble open-loop predictions using the full order model for replicates in the prior ensemble without EnKF updating; (b) ensemble closed-loop predictions using the full order model for the replicates in the ensemble with the EnKF updating the states and parameters at the end of each control step; (c) ensemble closed-loop predictions using the reduced-order model for the replicates in the ensemble with the EnKF updating.

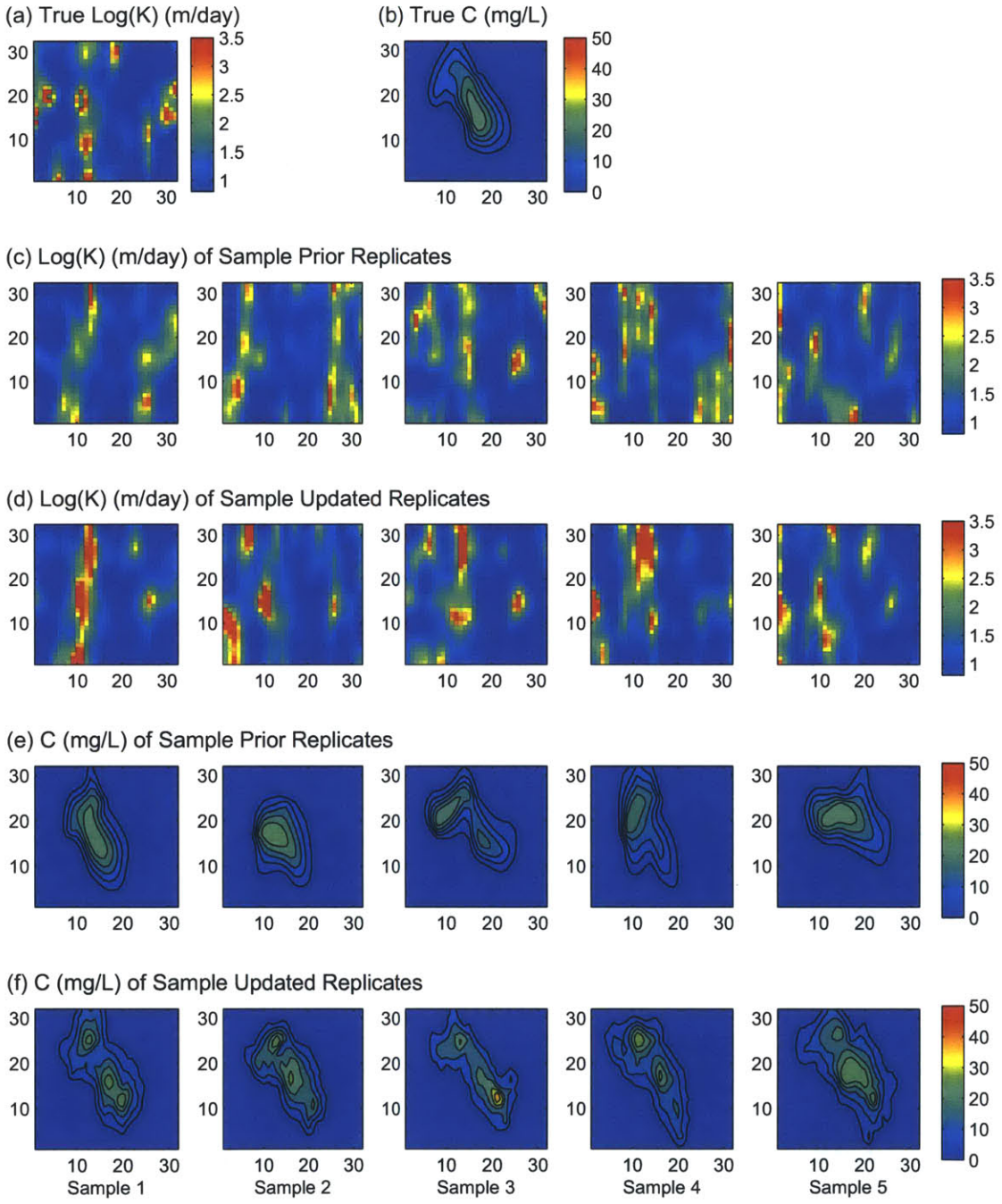

Figure 4-13: Updated conductivity and concentration samples in the ensemble under ensemble closed-loop control with reduced-order modeling: (a) the true log-conductivity field; (b) the snapshot of the concentration filed on day 400; (c) five samples of the conductivity field in the prior ensemble; (d) corresponding updated conductivity samples on day 400; (e) samples of the plume on day 400 corresponding to predictions based on the five sample prior conductivity fields without the EnKF updating; (f) corresponding updated samples of the plume on day 400.

Figure 4-13 illustrates some typical conductivity and concentration updated replicates under ensemble closed-loop control with reduced-order modeling on day 400. Figure 4-13(a) and (b) present the true conductivity field and the true plume shape on day 400. Figure 4-13(c) shows five prior conductivity replicates in the prior ensemble, and the plots in (d) show the corresponding five updated replicates, all on day 400. The updated replicates are more similar than the prior samples. Also, the updates display channels that are more similar to those observed in the true field. This illustrates the EnKF's ability to recover geological features. Similar behavior is shown in Figure 4-13(e) and (f). The update decreases the variability in the plumes displayed in these figures. The updated plumes are generally closer to the true plume of Figure 4-13(b).

From the aforementioned results it is clear that the reduced-order model is an accurate and effective alternative to the full order model during the forward simulations in the ensemble closed-loop control. Another advantage of using the reduced-order model is that the computation time has dropped significantly from about 10000 seconds to about 2000 seconds. In this problem, there are only about 1000 grids in the discretized domain. The speedup could be more dramatic for higher dimensional problems. This indicates the possibility of using a large size of ensemble to calculate necessary statistics such that small sample errors of the EnKF could be reduced. Moreover, it is feasible to perform ensemble-based optimization to obtain optimal controls. The effectiveness and efficiency of the reduced-order model make it a promising alternative for large-scale problems.

4.4 Conclusion

The closed-loop control is a useful tool to steer the system in real time to approach the desired goal under uncertainty. With uncertainty in model parameters, the derived control strategies from model-based optimization often lacks robustness in real applications. The closed-loop control takes the advantage of the feedback from the system and updates model states and parameters such that the uncertainty can be reduced

over time. The controls can be adjusted accordingly in real time to accommodate to parameter changes. The resulting controls are then much more robust than open loop ones.

In this application, an ensemble is generated based on prior information to represent the uncertainty in model parameters. The EnKF is used to update model states and parameters collectively, and robust optimization, which optimizes the expected objective, is used to generate the optimal controls in real time. The ensemble representation is effective for large-scale complex systems. However, normally a large ensemble size is needed for effective representations, and thus this approach is usually computationally prohibitive. To deal with this issue, a robust reduced-order model, which incorporates reduced representations of both states and parameters, is utilized to perform forward forecast in the ensemble closed-loop control framework instead of the high dimensional model. The model parameters are parameterized using the DCT method, which is effective in preserving geological features during statistical inversion. To enrich the reduced-order model such that it is valid during the optimization and the model-updating processes, selected parameter replicates and corresponding optimal controls for the selected replicates are combined to generated snapshots of states for derivation of POD basis vectors. The resulting POD basis vectors can span the space of interest during the ensemble closed-loop procedure.

The ensemble closed-loop control with reduced-order modeling is tested by a synthetic 2D solute transport problem. In this example the control objective is a compromise between energy cost and containment treatment cost. Under conductivity uncertainty, the ensemble open loop control, which disregards feedback from the true system, can improve the performance slightly based on the prior ensemble but lack robustness. The ensemble closed-loop control, which takes advantage of measurements, can adjust the control strategies in real time and thus is much more robust. Compared the performance of the ensemble closed-loop control with full order modeling and reduced-order modeling, it is revealed that the reduced-order model is capable of predicting head and concentration propagations for the ensemble during the optimization

and model-updating processes. Also, the fact that the controls resulted from reduced-order modeling outperforms those resulted from full order modeling suggests the importance of recovering geological features as early as possible. With reduced representations in both state and parameter spaces, the reduced-order model is more effective during the model-updating process. Last but not least, a significant speedup can be achieved by utilizing reduced-order modeling. Although the ratio between the computation time of full order modeling and that of reduced-order modeling is only about five in this example, it is expected that for larger problems, the efficiency can be improved more significantly due to the fact that dimensional reduction will be more dramatically for large-scale problems. Hence, the reduced-order model is a promising and effective alternative to the full order model in applications of closed-loop control.

4.5 References

[1] L. W. Canter and R. C. Knox, *Ground water pollution control.* Chelsea, Mich.: Lewis Publishers, 1986.

[2] J. D. Jansen, "Model-based control of subsurface flow," presented at the 8th International IFAC Symposium on Dynamics and Control of Process Systems, Cancún, Mexico, 2007.

[3] G. Dagan and S. P. Neuman, *Subsurface flow and transport : a stochastic approach.* Cambridge: Cambridge University Press, 1997.

[4] K. J. Åström and R. M. Murray, *Feedback systems : an introduction for scientists and engineers.* Princeton: Princeton University Press, 2008.

[5] J. D. Jansen, O. H. Bosgra, and P. M. J. Van den Hof, "Model-based control of multiphase flow in subsurface oil reservoirs," *Journal of Process Control,* vol. 18, pp. 846-855, Oct 2008.

[6] J. D. Jansen, D. R. Brouwer, G. Naevdal, and C. P. J. W. v. Kruijsdiik, "Closed-loop reservoir management," *First Break,* vol. 23, pp. 43-48, 2005.

[7] J. D. Jansen, L. Durlofsky, K. Aziz, and C. van Kruijsdijk, "Closed-loop reservoir management - Preface," *Computational Geosciences,* vol. 10, pp. 1-2, Mar 2006.

[8] G. A. Birnovskii, "On Optimal-Control of Multiphase Porous Flow in an Oil Bed," *Ussr Computational Mathematics and Mathematical Physics,* vol. 28, pp. 156-163, 1988.

[9] G. A. Virnovsky, "Water flooding Strategy Design Using Optimal Control Theory," in *the 6th European IOR-Symposium*, Stavanger, Norway, 1991.

[10] B. Sudaryanto, "Optimization of Displacement Efficiency of Oil Recovery in Porous Media using Optimal Control Theory," PhD, University of Southern California, 1998.

[11] B. Sudaryanto and Y. C. Yortsos, "Optimization of Fluid Front Dynamics in Porous Media using Rate Control. I Equal Mobility Fluids," *Phys. of Fluids,* vol. 12, pp. 1656-1670, 2000.

[12] B. Sudaryanto and Y. C. Yortsos, "Optimization of Displacements in Porous Media Using Rate Control," in *the 2001 Annual Technical Conference and Exhibition*, New Orleans, Louisiana, 2001.

[13] G. M. van Essen, M. J. Zandvliet, P. M. J. Van den Hof, O. H. Bosgra, and J. D. Jansen, "Robust Waterflooding Optimization of Multiple Geological Scenarios," *Spe Journal,* vol. 14, pp. 202-210, Mar 2009.

[14] Y. Chen, D. S. Oliver, and D. X. Zhang, "Efficient Ensemble-Based Closed-Loop Production Optimization," *Spe Journal,* vol. 14, pp. 634-645, Dec 2009.

[15] C. Chen, G. Li, and A. C. Reynolds, "Robust Constrained Optimization of Short and Long-Term NPV for Closed-Loop Reservoir Management," in *SPE Reservoir Simulation Symposium*, the Woodlands, Texas, 2011.

[16] G. Evensen, "Sequential Data Assimilation with a Nonlinear Quasi-Geostrophic Model Using Monte-Carlo Methods to Forecast Error Statistics," *Journal of Geophysical Research-Oceans,* vol. 99, pp. 10143-10162, May 15 1994.

[17] G. Evensen, "The Ensemble Kalman Filter: theoretical formulation and practical implementation," *Ocean Dynamics,* vol. 53, pp. 343-367, 2003.

[18] G. Evensen, "Sampling strategies and square root analysis schemes for the EnKF," *Ocean Dynamics,* vol. 54, pp. 539-560, Dec 2004.

[19] G. Naevdal, L. M. Johnsen, S. I. Aanonsen, and E. H. Vefring, "Reservoir monitoring and continuous model updating using ensemble Kalman filter," in *the SPE Annual Technical Conference and Exhibition*, Denver, Colorado, 2003, pp. 66-74.

[20] X. H. Wen and W. H. Chen, "Some practical issues on real-time reservoir model updating using ensemble Kalman filter," *Spe Journal,* vol. 12, pp. 156-166, Jun 2007.

[21] X. H. Wen and W. H. Chen, "Real-time reservoir model updating using ensemble Kalman Filter with confirming option," *Spe Journal,* vol. 11, pp. 431-442, Dec 2006.

[22] N. Liu and D. S. Oliver, "Critical evaluation of the ensemble Kalman filter on history matching of geologic facies," *Spe Reservoir Evaluation & Engineering,* vol. 8, pp. 470-477, Dec 2005.

[23] S. I. Aanonsen, G. Naevdal, D. S. Oliver, A. C. Reynolds, and B. Valles, "The Ensemble Kalman Filter in Reservoir Engineering-a Review," *Spe Journal,* vol. 14, pp. 393-412, Sep 2009.

[24] V. Haugen, G. Naevdal, L. J. Natvik, G. Evensen, A. M. Berg, and K. M. Flornes, "History Matching Using the Ensemble Kalman Filter on a North Sea Field Case," *Spe Journal,* vol. 13, pp. 382-391, Dec 2008.

[25] P. Jacquard, "Permeability Distribution From Field Pressure Data," *SPE Journal,* vol. 5, pp. 281-294, 1965.

[26] S. I. Aanonsen, "Efficient history matching using a multiscale technique," *Spe Reservoir Evaluation & Engineering,* vol. 11, pp. 154-164, Feb 2008.

[27] G. R. Gavalas, P. C. Shah, and J. H. Seinfeld, "Reservoir History Matching by Bayesian Estimation," *Society of Petroleum Engineers Journal,* vol. 16, pp. 337-350, 1976.

[28] P. Sarma, L. J. Durlofsky, and K. Aziz, "Kernel principal component analysis for efficient, differentiable parameterization of multipoint geostatistics," *Mathematical Geosciences,* vol. 40, pp. 3-32, Jan 2008.

[29] A. C. Reynolds, N. He, L. Chu, and D. S. Oliver, "Reparameterization Techniques for Generating Reservoir Descriptions Conditioned to Variograms and Well-Test Pressure Data," *SPE Journal,* vol. 1, pp. 413-426, 1996.

[30] B. Jafarpour and D. B. McLaughlin, "Reservoir Characterization With the Discrete Cosine Transform," *Spe Journal,* vol. 14, pp. 182-201, Mar 2009.

[31] B. Jafarpour and D. B. McLaughlin, "History matching with an ensemble Kalman filter and discrete cosine parameterization," *Computational Geosciences,* vol. 12, pp. 227-244, Jun 2008.

[32] R. J. Lorentzen, A. Shafieirad, and G. Nævdal, "Closed Loop Reservoir Management Using the Ensemble Kalman Filter and Sequential Quadratic Programming," in *SPE Reservoir Simulation Symposium*, The Woodlands, Texas, 2009.

[33] H. Gunes and U. Rist, "Proper orthogonal decomposition reconstruction of a transitional boundary layer with and without control," *Physics of Fluids,* vol. 16, pp. 2763-2784, Aug 2004.

[34] B. R. Noack, K. Afanasiev, M. Morzynski, G. Tadmor, and F. Thiele, "A hierarchy of low-dimensional models for the transient and post-transient cylinder wake," *Journal of Fluid Mechanics,* vol. 497, pp. 335-363, Dec 25 2003.

[35] S. S. Ravindran, "Reduced-Order Adaptive Controllers for Fluid Flows Using POD," *Journal of Scientific Computing,* vol. 15, pp. 457-478, 2000.

[36] M. Bergmann, L. Cordier, and J. P. Braucher, "Drag minimization of the cylinder wake by trust-region proper orthogonal decomposition," *Active Flow Control,* vol. 95, pp. 309-324, 2007.

[37] Q. Du, V. Faber, and M. Gunzburger, "Centroidal Voronoi tessellations: Applications and algorithms," *Siam Review,* vol. 41, pp. 637-676, Dec 1999.

[38] S. M. Gorelick, C. I. Voss, P. E. Gill, W. Murray, M. A. Saunders, and M. H. Wright, "Aquifer Reclamation Design - the Use of Contaminant Transport Simulation Combined with Nonlinear-Programming," *Water Resources Research,* vol. 20, pp. 415-427, 1984.

[39] B. J. Wagner and S. M. Gorelick, "Reliable Aquifer Remediation in the Presence of Spatially-Variable Hydraulic Conductivity - from Data to Design," *Water Resources Research,* vol. 25, pp. 2211-2225, Oct 1989.

[40] R. H. Byrd, M. E. Hribar, and J. Nocedal, "An interior point algorithm for large-scale nonlinear programming," *Siam Journal on Optimization,* vol. 9, pp. 877-900, 1999.

[41] R. F. Stengel, *Optimal Control and Estimation*. New York: Dover Publications, 1994.

[42] P. Sarma, L. J. Durlofsky, K. Aziz, and W. H. Chen, "Efficient real-time reservoir management using adjoint-based optimal control and model updating," *Computational Geosciences,* vol. 10, pp. 3-36, Mar 2006.

[43] B. Jafarpour and D. B. McLaughlin, "Estimating Channelized-Reservoir Permeabilities With the Ensemble Kalman Filter: The Importance of Ensemble Design," *Spe Journal,* vol. 14, pp. 374-388, Jun 2009.

Chapter 5

Conclusions and Recommendations

5.1 Conclusions

This thesis addressed the application of reduced-order modeling to the ensemble closed-loop control of subsurface solute transport. The closed-loop control is essentially a combination of the model updating process and optimization process to adjust control strategies in real time with reduction in model uncertainty. The resulting control strategies are then more robust in realistic applications.

However, the closed-loop control requires a large number of evaluations of the complex subsurface model, and thus is usually computationally prohibitive for large-scale problems. Reduced-order modeling is an efficient tool that can replace the original high-dimensional model to predict necessary information with reasonable accuracy, and thus it is promising to combine closed-loop control with reduced-order modeling to open up the possibility of closed-loop control of large-scale problems.

Traditional reduced-order models often lack applicability and robustness in the closed-loop control of subsurface flow due to the facts that: (a) the subsurface model is usually nonlinear and thus it is difficult to derive an efficient reduced-order model based on traditional linear model reduction techniques; (b) the reduced-order model should be able to incorporate model parameter changes explicitly and efficiently, which is crucial for uncertainty quantification in the closed-loop control; and (c) the

reduced-order model should be able to incorporate control changes such that there is no need to update the reduced-order model during online simulations. This thesis attempted to address these issues by developing a robust second order reduced-order model.

The reduced-order model for subsurface solute transport was derived favoring specific characteristics of discretized governing equations. Discretizing the flow equations by the mixed finite element method resulted in a model bilinear in states and parameters, and thus it was then possible to incorporate parameter changes explicitly by expanding the equations around nominal parameters and states. The second-order expansion is crucial to apply reduced-order modeling to uncertainty quantification for it creates the possibility of dimension reduction in both state and parameter spaces. The POD method provides an attractive mechanism to extract low-dimensional basis that contains the key features of model states for complex systems, while the DCT method is an efficient and effective method to project high-dimensional parameters to the low-dimensional DCT coefficient space.

To enrich the POD and DCT basis vectors such that they sufficiently span necessary spaces of interest, the reduced-order model was generated on an ensemble base. This is consistent with the ensemble closed-loop control method proposed here. In the ensemble closed-loop control an ensemble of realizations represents model uncertainty in physical properties. The DCT basis vectors were selected from a constant matrix by ordering the transformed DCT coefficients for each realization in the ensemble. The selected DCT vectors correspond to leading DCT coefficients over the entire ensemble and thus geological features of the random fields can be well captured. It is found by including derivatives of model states with respect to parameters into the snapshots of model states the resulting POD basis vectors are sufficiently robust over the entire ensemble. Significant improvement of model accuracy was observed by comparing the performance of a reduced-order model with derivative information and another one without derivative information.

The efficiency and robustness of the resulting reduced-order model was verified by applying reduced-order modeling to the forecast step of the ensemble Kalman filter to predict state propagations. In the 2D solute transport example the simulation model contained significant uncertainty in hydraulic conductivity. With reduced-order modeling, the high dimensional state and parameter spaces were both reduced to dramatically lower dimensional spaces where only about 3% states and parameters were preserved. The EnKF then updated model states and parameters based on predictions from the reduced-order model as well as measurements from the true system. After several updates the channelized geological features of the true system was well captured. This illustrates that the reduced-order model can provide predictions that are sufficiently accurate and robust for the EnKF updating of the entire ensemble, while the computational burden can be reduced by as much as 95%. Robust reduced-order modeling can then create the possibility of representing uncertainty in large-scale complex systems by a large ensemble size. Small sampling errors, which are normally treated with covariance inflation or location methods, can then be reduced to improve the performance of the EnKF.

Another attractive feature of combining reduced-order modeling with the EnKF for uncertainty quantification is that with reduced representations of both states and parameters, the EnKF can recover the geological features better than full order modeling. This is due to the fact that the DCT can characterize the geological features well and correlations between model states and parameters can be better captured with reduced representations. Hence, the reduced-order model is a promising alternative to the full order model for the EnKF updating not only because it can reduce computation burden for large-scale problems, but also because it can improve the performance of the EnKF by reducing system unknowns while preserving necessary features.

The reduced-order was then extended to incorporate control changes to make it applicable to the ensemble closed-loop control. To enrich the POD basis vectors to incorporate control changes samples of control configurations were generated by optimizing control performance for selected realizations of uncertain model parameters

in the ensemble. With sufficient diversity in control configurations it is hoped that the actual optimal control configurations for the closed-loop control fall inside the neighborhood of the selected configurations. This targeted sampling method is expected to target the actual optimal controls as accurate as possible with as little computation burden as possible for training runs. The numerical example presented in this work has proven this method is effective for generating a robust reduced-order model in the ensemble closed-loop control of 2D solute transport. This numerical example has also proven that the closed-loop control strategies derived by reduced-order modeling are more robust under uncertainty to achieve good performance with reduced computational burden. Hence, the reduced-order model can serve as an effective and efficient tool for robust control of complex systems under uncertainty.

It has been shown that it is crucial to capture geological features as early as possible to improve the performance of closed-loop control strategies. With reduced-order modeling, the geological features can be well captured at early control steps and thus the resulting control strategies have superior performance, provided that the reduced-order model is sufficiently accurate and robust during online simulations. Overall, combining reduced-order modeling with the ensemble closed-loop control can provide an accurate, efficient, robust, and effective option for robust control of large-scale complex systems.

5.2 Thesis Contributions

The original contributions of this thesis can be summarized as follows:

(1) Derivation of an efficient and robust second order reduced-order model for subsurface solute transport. The reduced-order model can incorporate state and parameter changes explicitly, and thus it is possible to utilize reduced representations for model states and parameters simultaneously. The reduced-order can be used to improve computational efficiency to evaluate uncertainty propagation for large-scale so-

lute transport problems. Also, it can facilitate stochastic analysis of uncertain model parameters with reduced representations.

(2) Addressing the aforementioned small sample error problem of the EnKF by improving the efficiency of forward simulations using the reduced-order model. This is the first attempt to address computational burden of the EnKF by reduced-order modeling. Limited ensemble sizes will introduce significant small sample errors and cause divergence of the EnKF updates. Reduced-order modeling creates the possibility to use a large ensemble size for large-scale problems, provided the reduced-order model is sufficiently robust. It has been shown that reduced-order modeling can also improve the performance of the EnKF by reduced representations of states and parameters.

(3) Development of an ensemble closed-loop control framework with reduced-order modeling for robust subsurface transport control under uncertainty. The ensemble closed-loop control adjusts control strategies in real time to account for the EnKF updates. It has been proven to be robust under parameter uncertainty for subsurface solute transport. However, due to computational burden, it is infeasible to apply ensemble closed-loop control to large-scale problems. With reduced-order modeling, the computational burden can be reduced significantly, suggesting possibility of large-scale applications.

5.3 Recommendations

In reduced-order modeling of subsurface solute transport the full order velocity vectors need to be reconstructed during each control step due to the fact that with upwind finite different discretization of the transport equation, the resulting equations are nonlinear in model states, and thus it is infeasible to perform a low order expansion. This procedure will deteriorate the efficiency of the resulting reduced-order model. To overcome this shortcoming, a reduced approximation of nonlinear terms in the equations can be adopted to avoid reconstruction of high-dimensional states. This can be achieved, for example, by the discrete empirical interpolation method (DEIM) [1],

which can be treated as a modification of the traditional POD method with ability to reduce dimensions for general nonlinear equations. With sufficient training of the POD basis, it is possible to reduce the computational burden of the transport equation further by the DEIM while preserving reasonable accuracy for the ensemble closed-loop control.

The resulting discretized flow equation by the mixed finite element method bears a bilinear form, and thus it is possible to reduce dimensions of model states and parameters simultaneously. However, for more complicated multi-phase transport problems the discretized equations usually have higher order nonlinearity and thus additional effort is needed to perform model order reduction in state and parameter spaces. A possible option is to adopt the idea of the piecewise-polynomial representations of nonlinear terms [2] and use a piecewise second-order representation of nonlinear terms in the multiphase model. This is an extension of the trajectory piecewise-linear approximations [3, 4]. The flow equations can still be discretized using the mixed finite element method and the resulting equations have additional dependency on saturation. This approach has the advantage that the velocity can be calculated more accurately for unsmooth permeability fields.

It is noticeable from the numerical examples presented in this work that the reduced-order model adds additional model errors during the EnKF updates. It is mainly due to insufficiency of the POD basis to span necessary spaces in the process of closed-loop control. To reduce model errors the greedy sampling method for selection of snapshots in high-dimensional space proposed by Bui-Thanh [5, 6] can be adopted here. Note that this method requires a number of optimization procedures to search for worst cases in the parameter space and thus the training process is usually computationally extensive. To extend this method to the ensemble closed-loop control a modification must be made to avoid unnecessary computational burden while improved accuracy can be achieved. For example, combinations of samples of control configurations and the ensemble of uncertain model parameters can be proposed to find the worst combinations. The reduced-order model can then be improved by incorporating the snapshots of the selected cases. Note that during this procedure optimization is not necessary, and predicting state propagations for each combination us-

ing a proposed reduced-order model can efficiently approximate the errors between the reduced-order model and full order model.

In the application of reduced-order modeling to the ensemble closed-loop control a relatively small-size example is presented in this work. It is expected for large-scale problems more dramatic speedup can be achieved with reduced-order modeling. However, significant computation burden is required to generate the reduced-order for high-dimensional problems, partly because the POD method requires singular value decomposition of huge snapshot matrices. This issue can be addressed by clustering snapshots to eliminate redundant snapshots that are sufficiently close to each other [7]. Another bottleneck to generate the reduced-order model efficiently is evaluating the Kronecker product of two projection matrices for the second-order term in the expanded equations. However, since the Hessian matrix for the second order term is sparse and constant, it is then possible to avoid calculating the whole matrix of the required Kronecker product [8]. With improved efficiency to generate the reduced-order model, applying reduced-order modeling to more realistic large-scale control problems becomes more promising and feasible.

5.4 References

[1] S. Chaturantabut and D. C. Sorensen, "Nonlinear Model Reduction Via Discrete Empirical Interpolation," *SIAM Journal on Scientific Computing,* vol. 32, pp. 2737-2764, 2010.

[2] N. Dong and J. Roychowdhury, "General-Purpose Nonlinear Model-Order Reduction Using Piecewise-Polynomial Representations," *IEEE Transactions on Computer-Aided Design of Integrated Circuits and Systems,* vol. 27, pp. 249-264, 2008.

[3] M. Rewienski and J. White, "Model order reduction for nonlinear dynamical systems based on trajectory piecewise-linear approximations," *Linear Algebra and its Applications,* vol. 415, pp. 426-454, 2006.

[4] M. J. Rewienski, "A trajectory piecewise-linear approach to model order reduction of nonlinear dynamical systems," Ph D, Massachusetts Institute of Technology, 2003.

[5] T. Bui-Thanh, K. Willcox, and O. Ghattas, "Model Reduction for Large-Scale Systems with High-Dimensional Parametric Input Space," *SIAM Journal on Scientific Computing,* vol. 30, pp. 3270-3288, 2007.

[6] T. Bui-Thanh, K. Willcox, and O. Ghattas, "Parametric Reduced-Order Models for Probabilistic Analysis of Unsteady Aerodynamic Applications," *Aiaa Journal,* vol. 46, pp. 2520-2529, Oct 2008.

[7] M. A. Cardoso and L. Durlofsky, "Development and application of reduced-order modeling procedures for reservoir simulation," Thesis (Ph D), Stanford University, 2009., 2009.

[8] N. Dong and J. Roychowdhury, "Piecewise polynomial model order reduction," in *Proc. IEEE DAC*, Anaheim, California, Jun. 2003, pp. 484–489.